

# Design and Analysis of SmallSat Mission to Venus

A Major Qualifying Project Report  
Submitted to the Faculty of Worcester Polytechnic Institute  
in Partial Fulfillment of the Requirements for the  
Degree of Bachelor of Science  
In Aerospace Engineering

By



Leila Card




Dakota Cross



Paul Golias



Yuvraj Pathania



Daniel Santamaria-Hopkins



Sidney Williams

Date: March 24, 2022

Approved by: Zachary R. Taillefer

Professor Zachary R. Taillefer, Advisor  
Aerospace Engineering Department

WPI

## Abstract

This project details the design and analysis of a SmallSat, the ISS VOPED (Interplanetary Spectroscopy SmallSat for Venus Orbiting Phosphine Existence Detection) on an interplanetary mission to Venus. The satellite is inserted into an interplanetary trajectory to Venus where it transfers to polar orbit at an altitude of 250 km. The spacecraft utilizes a SPIVAC/SOIR Spectrometer to analyze Venus' atmosphere at Phosphine spectral bands. The spacecraft uses an electric propulsion system to complete its transfer, enter the science orbit around Venus and perform station-keeping maneuvers. The BHT-1500 Hall Thruster with a solid iodine propellant is used for compact storage as compared to other propellants like Xenon which require high pressure, cryogenic storage. The propulsion subsystem and other spacecraft components' power requirements are satisfied using multijunction solar arrays, a maximum peak-power tracker distribution unit, and lithium-ion batteries. Systems Tool Kit simulations are used to confirm the power subsystem design. For communication, the spacecraft utilizes the Deep Space Network to communicate with ground stations and transfer data. Multi-layered insulation with varying color surface coating will cover all the internal spacecraft components to maintain the operating temperature ranges. This project also highlights a design of a phase separator and improvements to the thermal vacuum chamber test stand.

## Acknowledgments

The team would like to thank our advisor, Professor Zachary Taillefer for his guidance and support throughout this project. We would additionally like to thank Dr. Adriana Hera for her assistance with COMSOL and ANSYS simulations of the spacecraft.

## Table of Authorship

<b>Section</b>	<b>Author</b>
Introduction	Everyone
Payload	Dakota Cross
Structures	Leila Card
Propulsion	Dakota Cross
Power	Yuvraj Pathania
Attitude Determination and Control	Daniel Santamaria-Hopkins
Communications	Paul Golias
Thermal Control	Sidney Williams
Environment	Paul Golias
Thermal Vacuum Chamber	Leila Card, Dakota Cross, Yuvraj Pathania, and Daniel Santamaria-Hopkins
Conclusion	Everyone
Societal Impact	Sidney Williams

# Table of Contents

Abstract .....	i
Acknowledgments.....	ii
Table of Authorship .....	iii
Table of Contents.....	iv
Table of Figures .....	viii
List of Tables .....	xi
1 Introduction.....	1
1.1 Literature Review .....	2
1.1.1 Venus and Phosphine .....	2
1.1.2 SmallSat Background.....	4
1.1.3 Venus Express Satellite.....	4
1.2 Project Goals .....	5
1.3 Subsystems.....	6
1.3.1 Payload.....	6
1.3.2 Structure and Design.....	7
1.3.4 Power .....	9
1.3.5 Attitude Determination and Control .....	10
1.3.6 Communications .....	11
1.3.7 Thermal Control.....	12
1.3.8 Environment.....	13
1.4 Mission Planning.....	15
1.5 Project Management.....	15
1.6 Thermal Vacuum Chamber .....	16
2 Payload.....	17
2.1 SPICAV/SOIR Spectrometer Properties .....	18
2.2 SOIR and Orientation Requirements.....	20
3 Structures and Design .....	24
3.1 Structures Background .....	24
3.2 Material Selection .....	25
3.3 Primary Structure Design – Iterations .....	26
3.4 Final Design and Sub-System Layout.....	28
3.5 Launch Vehicle Selection and Release .....	32

3.6	Natural Frequencies.....	35
3.7	Random Vibration.....	36
3.8	Power Spectral Density.....	36
3.9	ANSYS Simulations.....	38
3.9.1	External Frame Model.....	39
3.9.2	Populated Model.....	45
3.9.3	Dispenser Ring Connection Model.....	51
4	Propulsion.....	56
4.1	Chemical and Electric Propulsion.....	56
4.2	Thruster Selection.....	57
4.3	Propellant.....	60
4.4	BHT-1500 Information.....	62
4.5	Low Thrust transfer and STK simulation.....	65
5	Power.....	68
5.1	Power Subsystem Background.....	68
5.2	Spacecraft Power Requirements.....	72
5.3	Hardware.....	73
5.4	Power Generation in STK.....	76
6	Attitude Determination and Control.....	82
6.1	Sensor Selection.....	82
6.1.1	Star Tracker.....	82
6.1.2	Sun Sensor.....	84
6.2	Actuator Selection.....	85
6.2.1	Reaction Wheels.....	86
6.2.2	ACS Thrusters.....	87
6.3	Control Algorithm.....	91
6.3.1	Detumbling.....	91
6.3.2	Slew Maneuver.....	93
7.1	Communications Architecture.....	95
7.1.1	Ground Station.....	95
7.1.2	On-Board Computer.....	97
7.1.3	Radio.....	100
7.2	Data and Storage.....	104
7.2.1	Data Rate Equations.....	105

7.2.2	Data Rate Calculations.....	106
8	Thermal Control.....	108
8.1	Thermal Control Background.....	108
8.1.1	Passive Systems .....	109
8.1.2	Active Systems.....	113
8.1.3	Target Temperatures .....	114
8.1.4	Thermal Analysis Tool .....	115
8.2	Thermal Analysis .....	116
8.2.1	Solar Radiation.....	116
8.3	COMSOL Multiphysics Thermal Analysis.....	117
8.3.1	Set Up.....	118
8.3.2	Results.....	122
8.4	Conclusion .....	127
9	Environment.....	129
9.1	Environmental Effects.....	129
9.1.1	Magnetic Fields.....	129
9.1.2	Space Debris .....	130
9.1.3	Thermal Impact.....	130
9.2	Environment Analysis .....	131
10	Thermal Vacuum Chamber.....	135
10.1	TVAC Liquid Nitrogen Assembly & Phase Separator .....	136
10.2	TVAC Test Stand.....	140
11	Conclusions and Recommendations .....	143
11.1	Payload.....	145
11.2	Structures and Design.....	145
11.3	Propulsion.....	146
11.4	Power.....	147
11.5	ACDS .....	148
11.6	Communications.....	148
11.7	Thermal .....	149
11.8	Environment.....	150
11.9	Thermal Vacuum Chamber .....	151
11.9.1	TVac Test Stand.....	151
11.9.2	Liquid Nitrogen Assembly & Phase Separator .....	152

Societal Impact.....	153
References.....	155
Appendix.....	161



## Table of Figures

Figure 1. MQP Gantt Chart.....	16
Figure 2. Infrared Absorption of Phosphine at the 10 $\mu\text{m}$ band. ....	17
Figure 3. Infrared Absorption of Phosphine at the 4.3 $\mu\text{m}$ .....	18
Figure 4. SPICAV/SOIR Spectrometer .....	20
Figure 5. Solar Occultation Technique Diagram .....	21
Figure 6. Diagram of the SOIR spectrometer components and layout.....	22
Figure 7. Final Frame Design .....	28
Figure 8. Initial Design Layout, Cross-Sectional View .....	29
Figure 9. Closed Solar Array Configuration.....	30
Figure 10. 90° Solar Arrays .....	31
Figure 11. Rotated Solar Arrays .....	31
Figure 12. 15” Dispenser Ring Mechanical Interface Volume.....	32
Figure 13. 15” Mechanical Interface Ring (with & without fasteners) .....	33
Figure 14. Dispenser Ring Connection Model .....	34
Figure 15. Allowable Payload Mass and XPL Center of Gravity.....	35
Figure 16. Falcon 9 Random Vibration Maximum Predicted Environment.....	37
Figure 17. External Frame Model in ANSYS.....	39
Figure 18. Total Deformation Occurring at Mode 1 & 4.....	41
Figure 19. Total Deformation Occurring at Mode 2 & 6.....	41
Figure 20. Total Deformation Occurring at Mode 3.....	42
Figure 21. Total Deformation Occurring at Mode 10.....	42
Figure 22. Directional Deformation of External Frame.....	43
Figure 23. Normal Elastic Strain of External Frame .....	44
Figure 24. Von-Mises Stress of External Frame.....	44
Figure 25. Front & Bottom View of Simple Populated Model .....	45
Figure 26. Total Deformation Occurring at Mode 2 & Mode 10 .....	47
Figure 27. Total Deformation Occurring at Mode 4 & Mode 9 .....	48
Figure 28. Total Deformation Occurring at Mode 5.....	48
Figure 29. Directional Deformation for Populated Model.....	49
Figure 30. Normal Elastic Strain for Populated Model .....	50
Figure 31. Von-Mises Stress for Populated Model.....	50
Figure 32. Simplified Dispenser Ring Connection Model.....	51
Figure 33. Total Deformation of Mode’s 3,8 & 10.....	53
Figure 34. Directional Deformation for Dispenser Ring Connection Model .....	54
Figure 35. Strain for Dispenser Ring Connection Model .....	54
Figure 36. Equivalent Stress for Dispenser Ring Connection Model.....	55
Figure 37. Busek BHT-1500 Hall Effect Thruster.....	63
Figure 38. Busek BHT-1500 Hall Effect Thruster Standard Specifications.....	63
Figure 39. ISS VOPED Final Polar Orbit of Venus .....	66
Figure 40. One of three RTGs used on the Cassini Spacecraft.....	69
Figure 41. Block Diagram of EPS .....	72
Figure 42. Cycle Life vs Depth of Discharge .....	76
Figure 43. Blender Render of Simplified Spacecraft Model .....	77
Figure 44. Total Wattage vs. Mission Time .....	78

Figure 45. Modified Satellite Model.....	79
Figure 46. Updated Power Generation vs. Time.....	79
Figure 47. Power Generated in Polar Orbit at Venus .....	80
Figure 48. Battery Capacity vs. Time .....	81
Figure 49. STAR-T3 .....	83
Figure 50. Fine Sensor Photodiode Cell (Boslooper, 2012) .....	84
Figure 51. SSOC-AC Fine Sensor (left) and CoSS-R Coarse Sensor (right) .....	85
Figure 52. Magnitude of Torques Relative to Spacecraft Altitude (Yao,).....	86
Figure 53. ACS Desaturation Maneuver.....	88
Figure 54. ACS Thruster Integration .....	90
Figure 55. Detumble Simulation (Launch Configuration).....	92
Figure 56. Detumble Simulation (Mission Configuration).....	93
Figure 57. 180 degree Slew Maneuver (Mission Configuration) .....	94
Figure 58. Goldstone and Madrid DSN Sites Modeled in STK .....	96
Figure 59. Canberra DSN Site Modeled in STK .....	96
Figure 60. Access Windows from Satellite to DSN Ground Stations .....	97
Figure 61. Kryten-M3 Data Sheet Specifications .....	99
Figure 62. Kryten-M3 Data Sheet Specifications .....	99
Figure 63. Kryten-M3 Dimensions .....	100
Figure 64. Satellite Frequency Bands .....	101
Figure 65. Iris Radio Mass and Power Specifications .....	102
Figure 66. Transponder and Receiver Specification.....	102
Figure 67. Patch Antenna.....	103
Figure 68. Absorbance and Emittance by Wavelength/Color .....	110
Figure 69. Absorbance and Emittance by Material .....	111
Figure 70. Flexible Thermal Straps .....	112
Figure 71. Thermal Louver .....	113
Figure 72. Solar Flux as a Function of Distance.....	117
Figure 73. Spacecraft’s Thermal Mesh.....	120
Figure 74. COMSOL Model setup for Heat Transfer in Solids.....	121
Figure 75. COMSOL Model setup for Surface-to-Surface Radiation .....	122
Figure 76. 2D Thermal Model .....	123
Figure 77. STK SEET Temperature Graph Over 24 Hours.....	124
Figure 78. COMSOL Temperature Model at Earth .....	125
Figure 79. COMSOL Temperature Model at Venus .....	126
Figure 80. Particle Impact Probability with ISS VOPED.....	132
Figure 81. Accumulated Radiation Dose on ISS VOPED .....	133
Figure 82. STK SEET Temperature of ISS VOPED in Orbit Around Venus .....	134
Figure 83. Diagram of the TVAC Liquid Nitrogen System .....	136
Figure 84. Diagram of the Liquid Nitrogen Manifold .....	137
Figure 85. Controller-Valve Configuration .....	138
Figure 86. Isometric View of the Phase Separator .....	139
Figure 87. Internal View of the Phase Separator .....	139
Figure 88. Specimen Holder within TVAC .....	140
Figure 89. Specimen Holder with Flat Plate.....	141
Figure 90. TVACTVAC Test Stand with Dimensions .....	141

Figure 91. Test Stand and Shroud Configurations..... 142

## List of Tables

Table 1. Mission Phases.....	15
Table 2. Table of SPICAV/SOIR Spectrometer Properties .....	19
Table 3. Falcon 9 Random Vibration Maximum Predicted Environment (SpaceX, 2021).....	38
Table 4. External Frame Model Modal Frequencies .....	40
Table 5. Populated Model Modal Analysis Frequencies .....	46
Table 6. <i>Modal Analysis Results for the Dispenser Ring Connection Model</i> .....	52
Table 7. Calculated Propellant Mass and Propellant Mass Fractions for Various Thrusters .....	59
Table 8. Thrust and $I_{sp}$ Values for Various Power Inputs and Firing Modes (Busek, 2021).....	64
Table 9. Spacecraft Maneuvers with Associated Duration and Delta-V Values .....	67
Table 10. Comparison of different power generation methods. ....	70
Table 11. Spacecraft Power Requirements .....	73
Table 12. Star Tracker Decision Matrix .....	83
Table 13. Sun Sensor Specifications.....	85
Table 14. Reaction Wheel Selection Matrix .....	87
Table 15. Hydrazine Thruster Selection Matrix .....	89
Table 16. ACS Thruster pair firing configuration .....	90
Table 17. On-Board Computer Comparison Matrix (Satsearch, nd.).....	98
Table 18. Data rate calculation values .....	106
Table 19. Component Operating and Survival Temperatures .....	115
Table 20. Analysis Points .....	118
Table 21. COMSOL Material List.....	119
Table 22. Solar Radiation .....	120
Table 23. Component Temperatures at Earth .....	125
Table 24. Component Temperatures at Venus.....	127
Table 25. Mass Breakdown of ISS VOPEd .....	144

# 1 Introduction

This project analyzes the design of a small satellite (SmallSat) for an interplanetary mission to Venus, to determine the presence of phosphine in the planet's atmosphere. Phosphine in Venus' atmosphere could indicate some sign of microbial life on the toxic planet. On Earth, trace amounts of phosphine in the atmosphere are due to human or microbial activity (Greaves et.al, 2020). Phosphine has been found in the upper atmospheres of other planets in the solar system, namely gas giants, where phosphine is produced deep in the atmosphere, at high temperature and pressure, and diffuses upward by convection. On rocky planets, such as Earth and Venus, phosphine would be destroyed due to oxidation in the lower atmosphere (Greaves et.al, 2020). This leads to the possibility of biological processes producing phosphine in Venus' upper atmosphere.

The main goal of this project is to conceptually design a 10 kg to 180 kg SmallSat capable of carrying a SPICAV/SOIR Spectrometer as its main payload and reporting the data back to Earth. The SmallSat will be placed in a polar orbit at an altitude where the spectrometer will be able to interrogate Venus' upper atmosphere.

The design of the SmallSat is divided into seven sub-systems: payload, structure and design, propulsion, power, attitude determination and control, communications, and thermal control. Each sub-system works together to support the spacecraft design as a whole and could not be completed without all of them. The objectives of this MQP are to design a SmallSat for an interplanetary mission to Venus, with the goal of interrogating Venus' atmosphere, specifically to detect phosphine, which is an indicator of microbial life.

A secondary goal of the MQP is to improve the design of an existing Thermal Vacuum (TVac) test at WPI (Mayer et al., 2021). The TVac test rig is used to simulate the thermal environment experienced by a spacecraft or component in the vacuum of space. It consists of a

vacuum tank, liquated nitrogen (LN2) cooled thermal shroud and heat lamps. The rig design had several areas which could be improved including the LN2 feed system, device test stand, heat lamp mount and data acquisition system. This project sought to improve all aspects of the test rig design.

## 1.1 Literature Review

### 1.1.1 Venus and Phosphine

Venus is the second planetary object from the Sun, existing as one of the four inner terrestrial bodies. It is the closest planetary neighbor to Earth and is considered Earth's "sister planet" on account of their similarities in mass, size, and bulk composition. However, Venus has many drastic differences when compared to Earth. The main trait of Venus is its dense and toxic atmosphere. Composed primarily of carbon dioxide and sulfuric acid, the atmosphere reaches around 250 km from the surface. The average surface pressure is very high. At 93 bar, Venus' atmospheric pressure is nearly 90 times that of Earth's. Venus also has no magnetic field, meaning there is minimal protection from solar radiation. Due to the high density of the atmosphere and the lack of a magnetic field, Venus' atmosphere traps most of the solar radiation hitting the planet, causing Venus to be the hottest planetary body in our solar system with an average surface temperature of Venus is 475°C (NASA, 2021).

These main characteristics of Venus suggest that life cannot be sustained on the surface of the planet. Current technology would not permit astronauts to safely visit the planet's surface. However, recent studies of the Venusian atmosphere have led some scientists to believe microbial life could exist in the upper atmosphere. There are many trace gases discovered to exist in regions

of Venus' atmosphere including Sulfur Dioxide, Chlorine, and Iron (III) Chloride. These examples do not point to the existence of extraterrestrial life, but another gas could (NASA, 2021).

On September 14th, 2020, Scientists from the James Clerk Maxwell Telescope (JCMT) and Atacama Large Millimeter/submillimeter Array (ALMA) announced the discovery of Phosphine in Venus' atmosphere, where any Phosphorus should exist only in oxidized forms (Greaves, 2021). Phosphine is a colorless, flammable, and toxic gas that exists on Earth. The reason its existence on Venus could mean the potential for extraterrestrial life is that there are few ways for this gas to be created. Currently,  $\text{PH}_3$  can be created industrially, but there is only one other way for a significant amount of it to be produced naturally. Anaerobic bacteria create  $\text{PH}_3$  as a byproduct of some biological processes. Anaerobic bacteria, by their definition, are bacteria that can exist in oxygen-free environments, such as the digestive tract of animals and deep compacted soil (Greaves, 2021). The possible existence of this chemical suggests that there may be bacterial or microbial life in Venus' upper atmosphere.

The experiments conducted by JCMT and ALMA reported they detected a Phosphine composition of around 20ppb, which is a significant amount for the vast atmosphere of Venus. Due to this concentration level, scientists were able to determine Phosphine was not generated by surface volcanoes or geological activity, as these would not produce Phosphine to the level that was detected (Greaves, 2021). However, there were errors detected in the data collection process that the ALMA telescope used, which resulted in debate amongst scientists, suggesting that the detection of Phosphine was an error and is not conclusive. Thus, the difficulty of accurately measuring phosphine concentrations remotely necessitated a spacecraft mission to measure it directly.

### 1.1.2 SmallSat Background

The first SmallSat was launched on October 4<sup>th</sup>, 1957, from the Soviet Union, also known as Sputnik. Sputnik weighed approximately 84 kg, and operated for nearly three weeks before its batteries died, later falling back into Earth's atmosphere on January 4<sup>th</sup>, 1958. The implementation of CubeSats and SmallSats have increased the opportunities for not only companies, governments, and private organizations to build and launch their own satellites, but also students and universities. The CubeSat standard was developed by California Polytechnic State University in San Luis Obispo and Stanford University's Space Systems Development Lab in 1999 by Jordi Puig-Suari and Bob Twiggs. The creation of the CubeSat model provided students with the potential to design, build and test low-cost space systems.

### 1.1.3 Venus Express Satellite

The Venus Express Satellite (VEX) was the first Venus exploration mission of the European Space Agency. The spacecraft launched in November 2005 and arrived at Venus in April 2006. The spacecraft entered a polar orbit around Venus and continuously sent back science data. The mission concluded in December of 2014.

Equipped with seven scientific instruments, the main objective of the Venus Express mission was the long-term observation of the Venusian atmosphere. More specifically, Venus Express studied the Venusian atmosphere and clouds in detail, the plasma environment, and the surface characteristics of Venus from orbit. It also made global maps of the Venusian surface temperatures (ESA, 2021). Since observation over such long periods of time had never been done in previous missions to Venus, the data collected was key to a better understanding of the atmospheric dynamics.



The VEX satellite was rather large, with dimensions of 1.5 x 1.8 x 1.4 m and a gross mass of 1,270 kg on launch. The satellite reached speeds of up to 29,000 km/h with a periapsis of 250 km and an apoapsis of 66,000 km. Since Venus' atmosphere extends to nearly 250 km, the periapsis of the satellite orbit was designed to be as close to the atmosphere as possible to provide more accurate measurements (ESA, 2021). There were many different observation phases for the mission. One was using the SPICAV/SOIR spectrometer, detailed in the Payload section of this report, to use solar occultation techniques to study the composition of the atmosphere.

## 1.2 Project Goals

The goals of the spacecraft design aspect of this project were to:

- Determine a payload capable of detecting phosphine in Venus' atmosphere.
- Design a structure capable of supporting all necessary components while maintaining a wet mass below 180 kg.
- Determine a propulsion system capable of providing a sufficient  $\Delta V$ .
- Design a power system capable of sufficiently powering the spacecraft for the length of the mission.
- Design an attitude control system to determine and manage the spacecraft's position and orientation.
- Design a thermal system to keep all components of the satellite within their operating temperatures.
- Design a communication system capable of relaying information to and from Earth.

## 1.3 Subsystems

### 1.3.1 Payload

The primary project goal is to design an interplanetary SmallSat that will be able to reach Venus, enter its orbit, and use a payload that will be able to detect Phosphine in the upper atmosphere. The Payload subsystem is arguably the most important part of the satellite. The payload encapsulates the main sensors or components that will achieve the desired mission objectives and drives the mission requirements. The specific payload of a satellite or spacecraft is dependent on the mission. For missions such as the Moon landings or future Mars exploration, the main payload will be the humans aboard the spacecraft. For satellites, there is a much larger range of payloads present.

Satellites exist in a few different places; Low Earth Orbit (LEO), Geocentric Orbit (GEO), Interplanetary travel, etc. LEO satellites tend to have communication or navigation-based payloads that assist with the technology down on the surface of Earth. The most notable LEO satellites and payloads involve the Global Positioning System (GPS) that most humans have used at some point. In GEO, satellites orbit at the same speed as the rotation of Earth, meaning that they are essentially locked on to a specific place on Earth's surface. The satellites existing in this location have many useful payloads, but the most notable could be that of weather detection or military application.

Satellites in the interplanetary travel class focus less on improving technology or the function of life back on Earth, but rather the investigation of our solar system and beyond. These satellites also include imaging telescopes such as the Hubble Space Telescope or the James Webb Space Telescope. The payloads for interplanetary probes or satellites with fly-by missions can vary

greatly, but all essentially study the bodies in the solar system and beyond. The satellite designed for this project and described in this report has a payload dedicated to examining the Venusian atmosphere, its composition, and mainly to detect the presence of Phosphine.

**Objectives:**

- Determine a suitable payload, capable of examining Venus' upper atmosphere and detecting the existence of Phosphine.
- Determine the properties and requirements of the selected payload.

### 1.3.2 Structure and Design

The objective of the structure and design subsystem was to ensure structural integrity throughout the SmallSat for mobilization for interplanetary travel. All the subsystems are attached to the main framework of the satellite or installed within it. The main constraint for the successful creation of the SmallSat frame were conserving mass while increasing internal volume, durability, high temperature tolerance, and potential for design configuration of internal subsystems.

For the structure to function as a complete system, it needed to contain the propulsion, ADCS, power, thermal, data acquisition and payload components. While mobilizing these systems without damage occurring from launch and environmental factors. The mission is successful when the SmallSat collects and sends the detected phosphine levels in Venus' atmosphere back to the ground base where the information can be analyzed.

**Objectives:**

- Design a primary structure capable of successfully carrying subsystem components for interplanetary travel to Venus
- Maximize internal volume
- Conserve primary structural mass
- Design ideal layout for subsystem components to increase compactness at specified internal volume
- Ensure center of mass to simplify ADCS model and calculations
- Meet launch vehicle requirements including PSD G Acceleration environment, center of mass and natural frequencies
- 1.3.3 Propulsion

The primary role of the propulsion system is to deliver the satellite to the desired location and complete all required maneuvers during the transfer to Venus. These required maneuvers consist of the escape from Earth, interplanetary low-thrust orbit transfer, and an orbit capture at Venus. To meet the mission maneuvers, the propulsion system must meet the required  $\Delta V$ . This  $\Delta V$  value can be determined through calculations or simulations.

To meet the  $\Delta V$  requirement, two types of propulsion systems can be considered. One being a chemical propulsion system, and the other being an electrical propulsion system. Chemical propulsion systems are currently the most common for spacecraft due to its relative simplicity and high thrust capability. Thrust is generated by chemical reactions with fuels and oxidizers to release energy and accelerate the gasses producing thrust. The disadvantage of this propulsion type is the specific impulse ( $I_{sp}$ ) is relatively low. The specific impulse tends to be within the range of 200-500s (NASA, 2021). The specific impulse is a measure of how efficiently an engine can generate thrust.

The second option for a propulsion system is an electric propulsion system. This technology is rather new and less common than chemical propulsion. However, many smaller satellites have been using it as their main propulsion system due to many beneficial properties. Electric propulsion operates by using combinations of electric and magnetic fields to generate and accelerate charge particles, or ions. This option has a very low thrust when compared to the chemical counterpart, however, the  $I_{sp}$  is significantly higher. The typical  $I_{sp}$  for electric propulsion is between the 600-4000s, with some options going higher (NASA, 2021). Many other properties of these two propulsion types are also taken into account when determining a suitable propulsion system.

**Objectives:**

- Determine the required  $\Delta V$  to transfer to Venus' orbit.
- Determine a suitable propulsion system type.
- Determine a suitable thruster, based on the  $\Delta V$  requirement and orbit maneuvers.

### 1.3.4 Power

The primary objective of the power subsystem is to design and manage the supply and distribution of power to all spacecraft subsystems. The power subsystem is also responsible for storing power and disseminating it even during eclipses and periods of high demand. In order for the power subsystem to complete its primary objective, it is necessary to determine methods of generating, distributing, conditioning, and storing power. The components' power requirements, mission destination, and physical storage requirements are crucial to finding an optimal source of power. The spacecraft also requires a method to store generated energy, which is typically dictated by the

mission time, as the spacecraft will degrade over the course of the mission. This information will allow the team to evaluate the optimal hardware for our mission.

**Objectives:**

- Determine power requirements for each component
  - Create a power budget matrix
- Determine power source and storage
  - Create comparison matrices
- Determine distribution and conditioning methods

### 1.3.5 Attitude Determination and Control

The attitude determination and control system (ADCS) is used to detect the spacecraft's attitude and control its orientation. Small adjustments help maintain the spacecrafts' attitude to a fixed orientation, which prevents external forces from inducing an undesired rotation in the system. Thus, the ADC system can be divided into sensors and actuators. Where the sensors determine the attitude, and the actuators reorient the spacecraft toward the desired attitude. The four main phases the ADC system will focus on are: initial detumble, attitude acquisition, orbital maintenance and scientific maneuvers.

The initial detumble is performed after decoupling from the launch vehicle, where the spacecraft experiences an initial rotation induced by the separation. Gyroscope sensors are used to determine the rotation which will send feedback to the actuator control system that applies a counter torque to stabilize the satellite. Attitude acquisition is performed by sensors such as GPS or star trackers, sun sensors and gyroscopes. Most of the mission will fall under the orbital

maintenance phase, where the satellite performs and maintains the desired orientation to fulfill the orbital maneuvers. Last data acquisition phase is tasked with pointing the payload's spectrometer towards the desired location in Venus's atmosphere to acquire spectroscopic measurements of the atmosphere.

**Objectives:**

- Determine the necessary attitude maneuvers carried out by the system to fulfill the mission.
- Select optimal sensors based on the outlined requirements.
- Study potential disturbance torques and estimate their magnitude
- Determine the respective actuator torques needed to counteract disturbances
- Design and model control system to detumble spacecraft

### 1.3.6 Communications

The objective of the communications subsystem is to manage and control the spacecraft's communication with the ground. The communications subsystem consists of a communication architecture which is a network of satellites and ground stations interconnected by communication links. The term ground station is synonymous to Earth station, ground terminal, and Earth terminal, including land mobile, airborne, and shipborne terminals. All these names refer to the same thing: the antenna, transmitter, receiver, and control equipment required to communicate with the satellite. On the satellite, an on-board computer with pre-installed flight software will be used to pass on commands received from the ground.

For this mission, the satellite will transmit and receive data over long distances. Only a few ground stations are capable of reliably receiving signals from beyond Earth orbit, therefore when choosing which ground station will be used to communicate with the satellite, there are not many options to choose from. Additionally, transmitting and receiving data over large distances increases the power usage of the communication architecture, so the data budget for the satellite will be limited.

**Objectives:**

- Select the communications subsystem architecture that satisfies the mission's communication, command, and control requirements.
- Investigate the use of NASA's Deep Space Network as the primary ground station.
- Calculate the satellites functional downlink and uplink data transfer budget.

### 1.3.7 Thermal Control

The primary objective of the spacecraft's thermal control system is to ensure all the spacecraft's components are kept within their respective operating temperatures while in operation and their survival temperatures while they are not in operation. In addition, the thermal control system manages temperature gradients across the spacecraft and its components. The battery and electrical components are the most sensitive to temperature, having differences of 10-35°C between both their operational and survival temperature ranges. Satellite design allocates little mass and power to the thermal control system due to larger requirements from other systems. This



can be more critical in SmallSats design since they have even less volume, mass, and power. The preferred thermal control system of a satellite is generally a passive system.

The design of the thermal control system for a SmallSat is limited by four factors: low thermal mass, limited surface area, limited volume, and limited power. To maximize efficiency while minimizing mass and power, the structure of the SmallSat will be used to absorb and radiate solar flux. Thermal equilibrium can be achieved through effectively generating and dissipating heat.

**Objectives:**

- Identify operating and survival temperature ranges for all spacecraft components
- Determine environment of the spacecraft for the duration of the mission
- Simulate the spacecraft in the thermal environments
- Determine the required thermal control system(s) for the spacecraft
  - Passive
  - Active, if necessary

### 1.3.8 Environment

Spacecraft encounter many different conditions in the vacuum of space. The effects include but are not limited to thermal loading, radiation, and space debris. To ensure that a spacecraft can survive in these environmental conditions, it must be capable of mitigating these effects to avoid a catastrophic failure. The conditions of interplanetary space are different than the conditions of a spacecraft orbiting near Earth. Even though the mission is interplanetary, the spacecraft does orbit Earth for some of its mission life, so the environment around Earth must still be considered. Low Earth Orbit (LEO) contains additional hazards such as drag, magnetic fields, plasma, and space

debris which are not as prevalent in deep space. It is the responsibility of the environment subsystem to consider the conditions the spacecraft will encounter during its mission life and propose countermeasures to ensure that the spacecraft can successfully carry out its mission.

**Objectives:**

- Identify hazardous space conditions and their effect on the spacecraft
- Create a model of radiation absorption across the lifespan of the spacecraft
- Provide recommendations to Thermal, Communications, and ADC subsystems

## 1.4 Mission Planning

The final destination of the ISS VOPEd is the planet, Venus. The mission has been divided into three main phases of operations based on the proximity to planetary bodies and their respective gravity wells. Table 1 outlines the order of events in which the SmallSat will operate.

Table 1. Mission Phases

<b>Mission Phase</b>	<b>Operation Segment</b>	<b>Description</b>
Earth Operations	Rideshare Launch/Deployment	ISS VOPEd launched onboard Falcon 9 launch vehicle and deployed near GEO
	Launch Vehicle Separation	Initialize automated systems and detumble spacecraft
	Mission Configuration Deployment	Deploy solar arrays, and commence departure burn positioning
	Earth Departure Burn	Spiral out of Earth's sphere of influence
Interplanetary Operations	Inclination Burn	Adjust inclination to align with Venus' orbit
	Venus Transfer Burn	Reduce perihelion to intersect with Venus
Venus Operations	Planetary Capture Burn	Orbit insertion around Venus
	Venus Circularization Burn	Reach target altitude
	Inclination Burn	Complete Venus polar orbit
	Venus Mission	Detect atmospheric readings and transmit data to ground station
	Orbit Maintenance	Apply any orbital maintenance or station-keeping burns

## 1.5 Project Management

The importance of a project management lead is to help the team stay on track throughout the duration of the Major Qualifying Project. The Gantt chart, shown in Figure 1, was the primary tool the team used to allocate responsibilities and keep track of how long each task took throughout the time period. Gantt charts are very useful, as they are easy to update and extremely intuitive. A new project manager was decided every three weeks and their responsibilities included setting team meetings, updating the Gantt chart, presenting during weekly meetings with the advisor and creating an agenda.

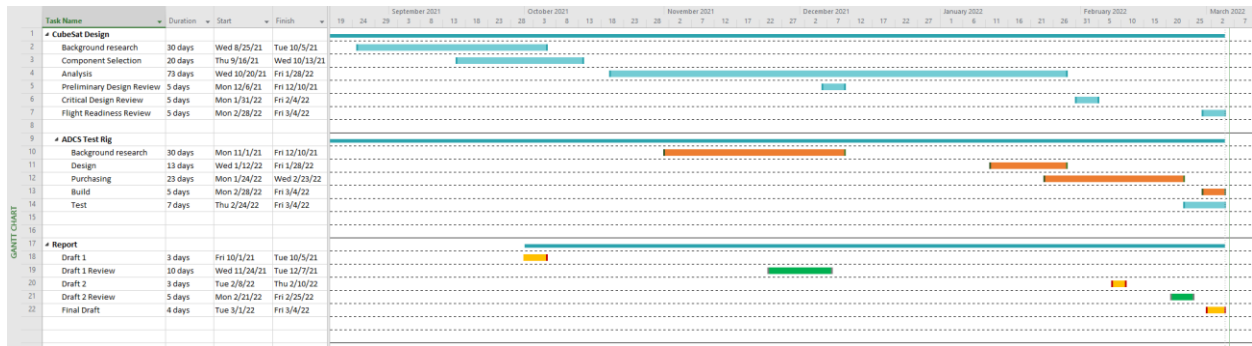


Figure 1. MQP Gantt Chart

## 1.6 Thermal Vacuum Chamber

The responsibility of a vacuum chamber is to reduce the level of residual gases and vapors to an acceptable level (Science Direct, 2007). The importance of testing the spacecraft in the thermal vacuum chamber or TVac, is to validate the spacecraft in a space-like environment by simulating the vacuum of space and thermal environment (heating and cooling) to resemble environment behavior during a spacecraft mission.

### Objectives:

- Research similar Thermal Vacuum Chamber designs
- Design a test stand to support the device under test (DUT) within the shroud while mitigating unwanted thermal effects
- Conduct demonstration test of the TVac

## 2 Payload

When determining a suitable payload, the starting grounds exist around the overall mission. Since a payload capable of detecting a chemical within an atmosphere is necessary, the type of payload required is reduced to a spectrometer. Spectrometers are scientific instruments that separate and measure spectral components from a sample space. For the case of the mission, the sample space is Venus' atmosphere, and the light passing through it is emitted from the sun. The electromagnetic spectrum is broad, going from Gamma waves, under 100 picometers, to Radio waves, 1mm to 100km (NASA, 2020) A spectrometer that covers the entire magnetic spectrum range would be too inaccurate to detect the trace composition of Phosphine. The spectrometer would need to be able to detect in only one or two ranges of the electromagnetic spectrum.

To determine what range is necessary, the location of the spectral bands when light is emitted in a sample space with just Phosphine is required. It is observed that the spectral absorption bands of Phosphine exist between 0.9 and 3.7 $\mu\text{m}$  (Butler, 2006). The Infrared radiation from the electromagnetic spectrum has a wavelength range of 0.78 $\mu\text{m}$  to 1mm. This deduces the payload selection to an Infrared Spectrometer. Figure 2 and Figure 3 below show the measured infrared absorption of Phosphine, observed during an experiment at the University of Michigan.

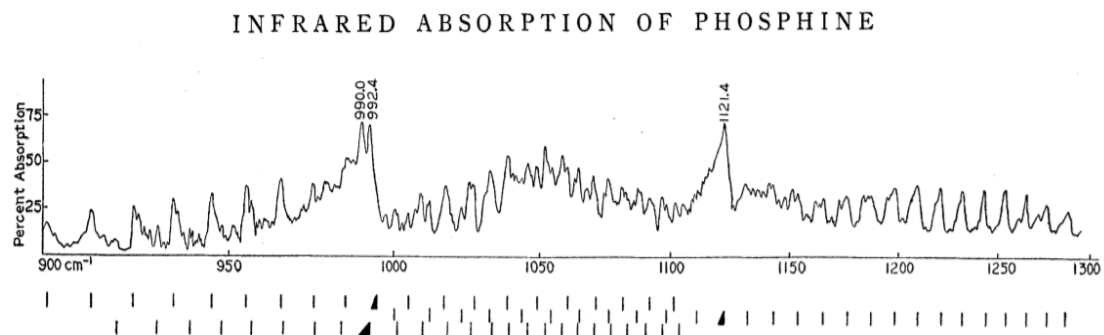


Figure 2. Infrared Absorption of Phosphine at the 10  $\mu\text{m}$  band (Butler, 2006)

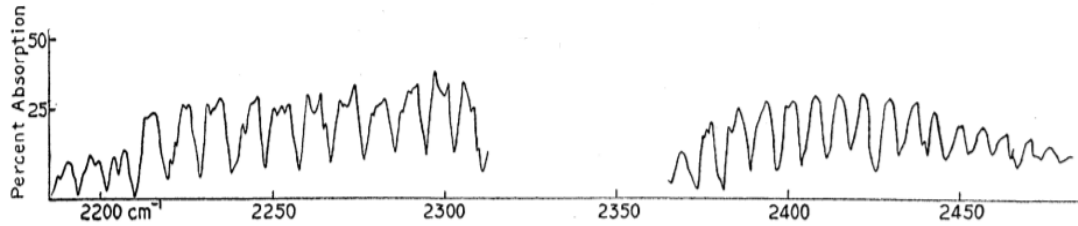


Figure 3. Infrared Absorption of Phosphine at the 4.3  $\mu\text{m}$  (Butler, 2006)

The next step into determining a payload is based upon the other subsystem requirements of the satellite. There are power, mass, data, volume, thermal, and orientation requirements for any spectrometer. Since the design is a SmallSat, all the requirements listed above are very limited. This creates a requirement that the spectrometer must be rather small, energy efficient, light in mass, and operable in the space environment around Venus. From all these requirements, research led to the SPICAV/SOIR Spectrometer from the Venus Express Satellite.

## 2.1 SPICAV/SOIR Spectrometer Properties

The Spectroscopy for the Investigation of the Characteristics of the Atmosphere of Venus Solar Occultation Infrared (SPICAV/SOIR) spectrometer was developed specifically to investigate the composition of the Venus atmosphere, even the most trace gases present. This spectrometer covers the optical range required to detect phosphine, while maintaining a low mass, volume and power. The specifications of the SPICAV/SOIR are listed in Table 2.

Table 2. Table of SPICAV/SOIR Spectrometer Properties

<b>Property</b>	<b>Value</b>
Modes	UV, IR, and SOIR
Mass	13.915 kg
Dimensions	504 x 400 x 350 mm
Operating Temperature	-20 to +40°C
Power	17.6 - 51.4 W
Data Rate	9 - 66 kbits/s
Data Volume	100 - 400 Mbits/day

The mass range for the entire satellite is 10 - 180kg. The chosen spectrometer has a very reasonable mass, at 13.915kg, which allows the extra mass for the satellite to be allocated to other systems or structures (Berteaux, 2007). The dimensions, however, are rather large for a SmallSat, if more than one payload is necessary. This is due to the entire spectrometer being composed of three smaller spectrometers: UV, IR, and SOIR. All which can be very useful when examining Venus' atmosphere. The power usage of this device can vary from 17.6 - 51.4 W. This is because the spectrometer is capable of running all three channels at once, at the cost of more power. The operating temperature of this spectrometer is between -20 and +40°C. This means that the thermal subsystem must regulate the temperatures around the spectrometer to stay within this range (Berteaux, 2007). If not done correctly, either the performance of the spectrometer could be hindered, or permanent damage could occur. Within the spectrometer exists a detector made of Mercury Cadmium Telluride (HgCdTe). This detector houses the camera that records all the filtered and grated light passing through Venus' atmosphere. This detector has an operating temperature of -163.15°C. However, the spectrometer has a built-in cooling system that uses Stirling Cycles to remove the heat from the spectrometer to the other side of the satellite (Berteaux,

2007). The data rate and volume also vary based upon the same idea of the power requirements. If all three spectrometers are running, then more data will be collected at a time. This spectrometer is depicted in the figure below.



Figure 4. SPICAV/SOIR Spectrometer (Berteaux, 2007)

## 2.2 SOIR and Orientation Requirements

The main spectrometer channel that would be used during the mission is the SOIR channel. Solar Occultation is a technique where the transmission of sunlight through a planet's atmosphere is measured and ratioed to control conditions, with no atmosphere. It allows measurements to be taken through various altitudes of Venus' atmosphere. This process will allow us to retrieve continuous data acquisition at varying altitudes in Venus' atmosphere. Figure 5 displays the motion and process of the solar occultation technique.



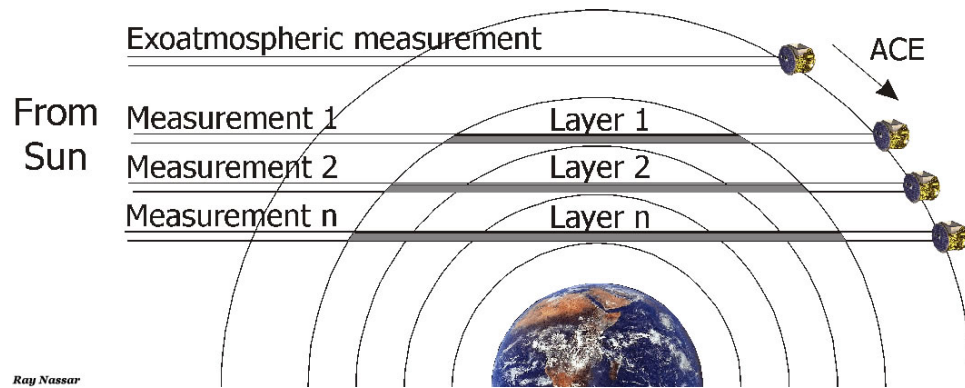


Figure 5. Solar Occultation Technique Diagram (Nassar, 2010)

This technique imposes many orientation requirements for the satellite. The spectrometer lens will be mounted off the front face of the satellite. This means that when in orbit, this plane must be pointed at the sun. The SOIR spectrometer is very accurate due to the acousto-optical tunable filter, so we must have the lens pointed at the solar center of the Sun during the entirety of the data collection process. The spectrometer will start by acquiring data at an exoatmospheric point, where no atmosphere is between the satellite and the Sun. This will allow a control to be measured and used later in during data processing to be ratioed from alternate data samples (Berteaux, 2007). As the satellite orbits to the back side of Venus, relative to the Sun, data acquisition will continue. The light being emitted from the Sun will pass through Venus' Atmosphere and be collected by the spectrometer. Since Venus' atmosphere will refract the light passing through it, it is suggested that the spectrometer be angled +10 arcmin above the solar center to counteract the refraction (Berteaux, 2007).

As the satellite continues along its orbit. The plane from the spectrometer to the solar center will intersect parts of Venus' atmosphere. It will start at the very edge of the atmosphere and move its way closer to the surface as the satellite dips behind the horizon of Venus. The SOIR spectrometer will be able to collect readings and detect solar radiation until the plane's altitude is

roughly 80 km (Berteaux, 2007). The atmosphere below this point is too dense for the spectrometer to accurately collect data that is usable. The need for the satellite to be pointed in one direction during its orbit creates less work for the ADCS subsystem. Once in orbit, the satellite's direction can be locked onto the solar center and then only adjusted by very small amounts to account for the refraction of light, or other minor adjustments. Since Venus is on average 108.89 million km away from the Sun, we will not have to adjust for any angle change during the data collection process. At the perihelion of our orbit, the angle from the Sun to the satellite and then the center of Venus is only  $0.003^\circ$ . The FOV of the spectrometer allows variability up to  $0.5-1^\circ$  in the satellite's orientation. This is due to the entrance slit being able to change size for different wavelength ranges to be observed (Berteaux, 2007). Since the angle between the satellite, the Sun, and Venus' center is miniscule compared to the variability expressed above, the satellite will not need any reorientation during its orbit.

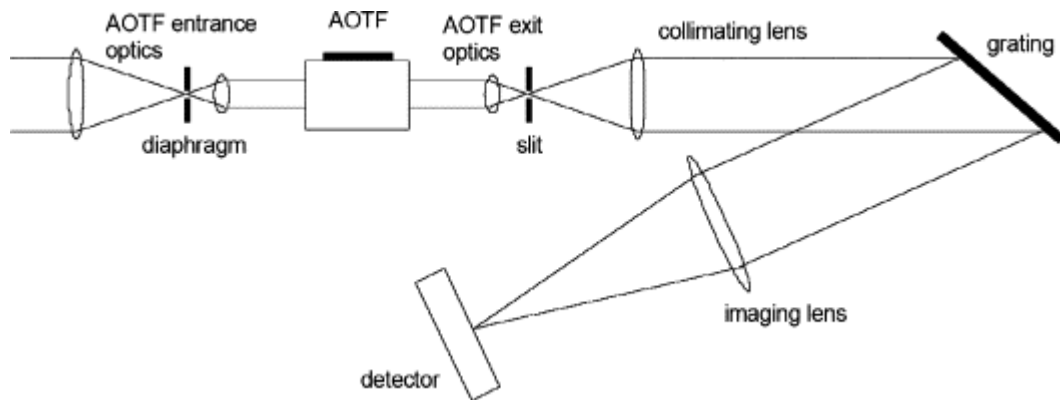


Figure 6. Diagram of the SOIR spectrometer components and layout (Berteaux, 2007)

Figure 6 above shows the layout of the SOIR spectrometers components. At the front entrance, light passes through the acousto-optical tunable filter (AOTF). The AOTF is able to reduce diameter so that light passing through the lens can be compatible with the size of the

selected aperture. After the AOTF exists a diaphragm to reduce the FOV slightly to ensure that no unwanted light is entering and interfering with the spectrometer. The light then is directed to an echelle grating to provide a higher resolution and dispersion. This light is then reflected off the echelle grating, through the imaging lens and onto the HgCdTe detector. In all, the SOIR spectrometer is able to detect a wavelength range between 2.325 and 4.25 $\mu\text{m}$  (Berteaux, 2007). This makes up a large portion of the Phosphine absorption range, meaning that it will be capable of detecting Phosphine at varying altitudes of the atmosphere, if it exists there. The other two channels UV and IR will be able to detect in ranges of 0.118 - 0.32  $\mu\text{m}$  and 0.65 - 1.7  $\mu\text{m}$ , respectively (Berteaux, 2007). The combination of these three spectrometers encompasses the entire Phosphine absorption range, while also being able to detect and rule out other chemical compositions that exist in the atmosphere. The data collected will be transferred via our communication subsystem and then compared to synthetic test data of Phosphine that was conducted back on Earth.

Other data collection methods exist with the SPICAV/SOIR spectrometer. The general UV and IR channels are capable of standard spectrometry of various locations on Venus' atmosphere. There is also a Nadir mode for the spectrometers collection method. Nadir is the point on a celestial surface directly below the observer. The spectrometer could be angled to the nadir point below allowing for continuous data acquisition of the upper atmosphere along the circumference of Venus. These data collection methods, allowable by the chosen spectrometer, prove to be a capable way to detect or rule out the existence of Phosphine on Venus.

## 3 Structures and Design

### 3.1 Structures Background

There are two main potential designs that are being used as inspiration, a modular frame and a monocoque frame. NanoAvionics developed a generic modular frame design that has the ability for configurations from 1U to 12U manufactured from Al 7075-T7351. The modular design allows for “building block” construction that provides flexible integration, broad use of components, and ease of manufacturability while also being simplistic in design. This is ideal for the possibility of components having to be replaced or updated to cater to each mission (NanoAvionics, 2022). Pumpkin developed a monocoque frame from sheet metal which increased the strength to weight ratio. Monocoque frames are known for their “external skin” and chassis design complexity. The design allows for a variety of components to be mounted on the outside of the frame, increasing the internal volume for specific components (Pumpkin Inc, 2015).

The parameters of consideration, which are maximizing internal volume and conserving primary structural mass, factor in when choosing which design route to take. The overall spacecraft mass constraints are between 10 kg and 180 kg and the design needs to have enough internal volume to carry the SOIR Spectrometer, OBC, power distribution unit, fuel tank and many other components. The advantage to conserving the structure mass is the difference in which propulsion system is chosen.

## 3.2 Material Selection

There are three potential materials that could be applied to the spacecraft design, Al 6061-T6, Al 5052-H32, and Al 7075-T6. The parameters of consideration for material determination are:

- Machinability
- Tensile Strength
- Low Cost
- Lightweight - Low Density
- Weldability

The importance of material weldability - is because it decreases the demand for fasteners, which in turn, increases structural reliability. When fasteners are needed, hex head cap screws will be used because they have many advantages. Some advantages of hex head cap screws are:

- Higher grip strength
- Larger bearing surface area
- Higher clamping pressure
- Less debris build-up
- Allow for greater torque

A comparison was conducted of the three Aluminum Alloys in consideration. The initial material of choice was Al 6061-T6 because it has an ultimate tensile strength of 310 MPa, yield tensile strength of 276 MPa and a fatigue strength of 96.5 MPa. As well as, a thermal

conductivity value of 167 W/m-K, a melting point between 582-651.7 ° C, a density of 2.7 g/cm<sup>3</sup>, highly weldable and high resistance to corrosion (Matweb, 2022).

Next material considered was Al 5052-H32, which has an ultimate tensile strength of 228 MPa, tensile yield strength of 193 MPa and fatigue strength of 117 MPa. Al 5052-H32 has moderate strength, high weldability, high resistance to corrosion, thermal conductivity value of 138 W/m-K, a melting point between 607.2-649.0 degrees Celsius and a density of 2.68 g/cm<sup>3</sup> (Matweb, 2022).

Finally, the last material in consideration was Al 7075-T6 which has an ultimate tensile strength of 572 MPa, yield tensile strength of 503 MPa and a fatigue strength of 159 MPa. The material has a density of 2.81 g/cm<sup>3</sup>, a thermal conductivity value of 130 W/m-K, melting point between 477 degrees Celsius and 635 degrees Celsius. This material is generally used for highly stressed structural parts and is stress-corrosion cracking resistant (Matweb, 2022).

The material chosen for this mission was Al 6061-T6 because it is lightweight, low-cost, has a high yield and ultimate tensile strength. The density falls between the two other options making it ideal when compared to the overall strength of the material. Al 6061-T6 has been used in a variety of aerospace applications like aircraft fittings, brake pistons, marine's fittings and hardware, valves and many more.

### 3.3 Primary Structure Design – Iterations

The design process for the main structure of the satellite was determined through comparative analysis of two different frame shapes, hexagonal and rectangular. Each frame had

two iterative phases that were altered to increase the structural soundness. Taking into consideration a SmallSat allowable mass of 10 kg to 180 kg, a generous portion of the overall mass was allocated to the frame to obtain an internal volume that would hold all subsystem components. The driving factors in the design process were conserving mass while increasing internal volume.

Phase I of the hexagonal frame was very basic and was used to gauge deformation and stress behavior. Phase II involved the addition of a top panel as well as a center support pole. The static stability analysis showed that the support pole increased the overall strength of the frame, as well as the mass. Phase I of the rectangular frame started with the creation of a simple cube that could be stacked to increase internal volume. Phase II was a rectangular structure constructed of two units of the original design. The static stability analysis showed minimal deformation when put under the environment within the fairing.

An advantage to the hexagonal frame was the high moment of inertia which helped with the initial detumbling, unlike the rectangular frame. An advantage to the rectangular frame was the potential for a modular platform, with a variety of organized installments. The rectangular frame was chosen because of the ability to maximize internal volume while minimizing mass. While also having a myriad of layout options for the components, and the organizational ability of storing payload components in the upper cube and propulsion in the bottom cube. Another parameter that had to be ensured was the maximum allowable dimensions for the spacecraft to guarantee it corresponds to the specific dispenser ring. As well as being able to be stored comfortably within the launch vehicle fairing.

### 3.4 Final Design and Sub-System Layout

The final design was constructed to ensure compactness of internal components and conservation of mass. The rectangular frame, shown in Figure 7, is the subsystem components within the structure. It has the ability for a modular platform as well as high internal volume, minimizing mass while increasing structural soundness and conserving the center of mass. All iterations of the frame were designed using SolidWorks, a solid modeling computer aided design software.

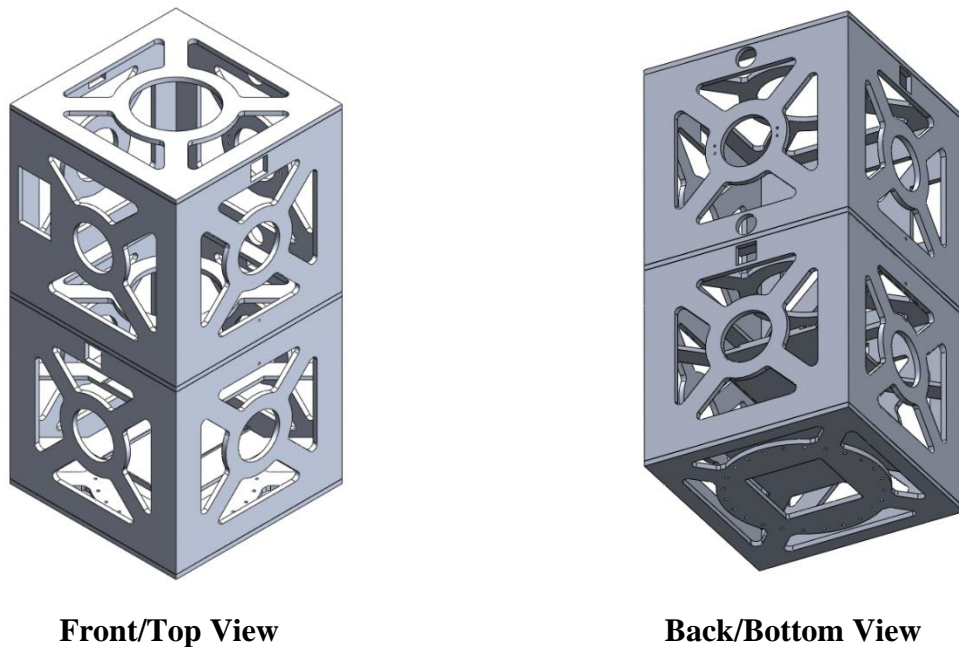


Figure 7. Final Frame Design

As shown in Figure 7, the entire structure is composed of cross-sectional bars. This design was implemented to increase the structural integrity of the spacecraft while decreasing the overall mass of the frame. Each side panel is the same, with the exception of the front panel where the spectrometer is housed. The purpose of this was to conserve the center of mass as best as possible. The bottom plane was designed to hold the thruster and attach to the dispenser ring



within the fairing. The connection consists of a 0.318-meter diameter ring with 24, 0.0069-meter diameter holes.

The layout design, shown in Figure 8, for the subsystem components was decided based on the necessity of each part. For example, the T3 Star Trackers are sensitive to light and the SOIR Spectrometer needs to face the sun. Therefore, they will be located on opposite faces of the spacecraft. The upper cube was designed to house the payload, communications, and power components. The lower cube was designed to hold the propulsion system and some excess components from other subsystems.

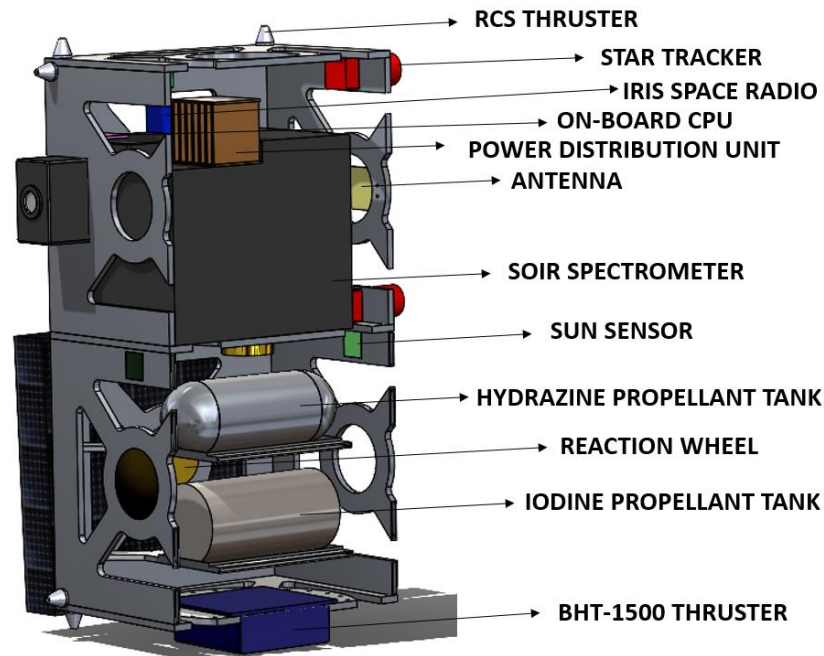


Figure 8. Initial Design Layout, Cross-Sectional View

The only component not pictured in Figure 8 is the propulsion power unit. The PPU is housed in the bottom unit of the spacecraft, near the thruster and iodine propellant tank. This layout provides a center of mass of (0, -0.31, -0.24) meters. As seen from the center of mass position, the

spacecraft is not perfectly centered. This is due to the placement of the spectrometer, although this is a downside to its placement, it allowed the external structure to be more symmetric.

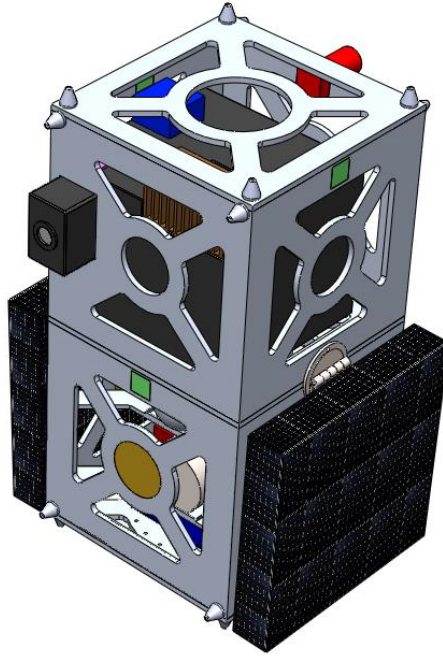


Figure 9. Closed Solar Array Configuration

As shown in Figure 9, the solar arrays are displayed in a closed state. The deployed dimensions of those arrays are 2.2098 x 0.889 x 0.0127 meters each. Since it is crucial for the solar arrays to be facing the sun, they are connected to a hinge that is connected to a rotating mechanism. The hinge can move 90 °, while the rotator can move 180 °. Figure 10 shows the spacecraft with the solar arrays in their first state of deployment.



Figure 10. 90° Solar Arrays

While Figure 11. Rotated Solar Arrays, shows the spacecraft with the solar arrays in their rotated view. This view would be presented during the transfer orbit when both the spectrometer and the solar arrays are pointed at the sun.

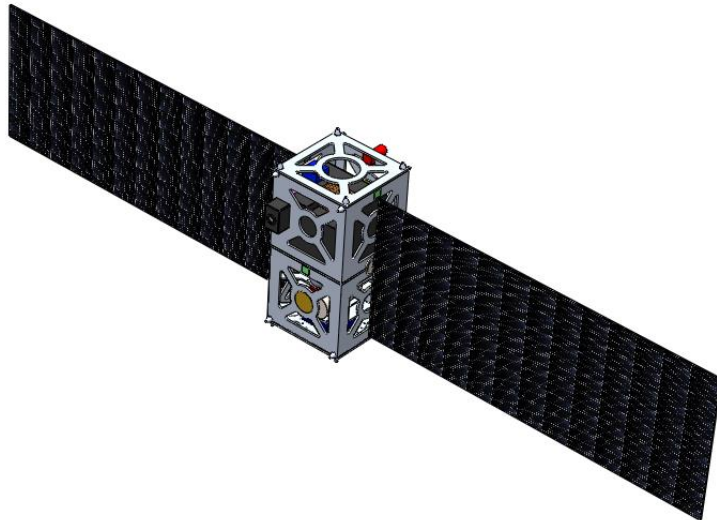


Figure 11. Rotated Solar Arrays

The solar array's ability to move and rotate is very important to the design. Without this ability, the solar arrays would be unable to achieve the amount of power storage needed to complete the mission.

### 3.5 Launch Vehicle Selection and Release

The launch vehicle was chosen as the Falcon 9 due to a variety of parameters. First, the Falcon 9 is a reliable launch vehicle, having 141 successful total launches and 101 total landings (SpaceX, 2022). It also has the ability for injection into LEO, GEO or Mars, increasing its versatility. Most importantly, the Falcon 9 has the ability for rideshare with a variety of configurations, like dispenser rings or the Starlink adapters. Specifically for this mission, the 0.381-meter dispenser ring will be utilized. This payload configuration has a vast amount of previous data for the payload environment dependent on the size of the spacecraft. The 0.381-meter dispenser ring has the potential to hold six rideshare payloads at once. With allowable dimensions of 1.4224 x 0.8382 x 0.8638 meters in the x,y,z directions, in a 60° cone shape as shown in Figure 12 (SpaceX, 2020).

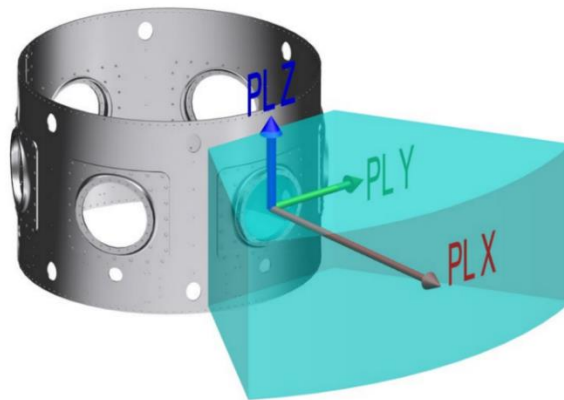


Figure 12. Dispenser Ring Mechanical Interface Volume  
(SpaceX, 2020)

Initially the payload fairing breaks off, exposing the dispenser ring and the connected spacecraft. The spacecraft is connected to the dispenser ring by a mechanical interface ring, shown in Figure 13. Both the spacecraft and the dispenser ring connected to the launch vehicle have a mechanical interface ring installed. Those rings are connected by twenty-four 28 TPI fasteners and the locking system is deactivated when the launch vehicle reaches a certain height. The separation of rings occurs when the propulsion system of the spacecraft is initiated.



Figure 13. Mechanical Interface Ring (with & without fasteners)  
(SpaceX, 2020)

The rings are connected by twenty-four 28 TPI fasteners and the locking system is deactivated when the launch vehicle reaches a certain height. The separation of rings occurs when the propulsion system of the spacecraft is initiated. The satellite connects to the dispenser ring through the mechanical interface ring, as shown in Figure 14.

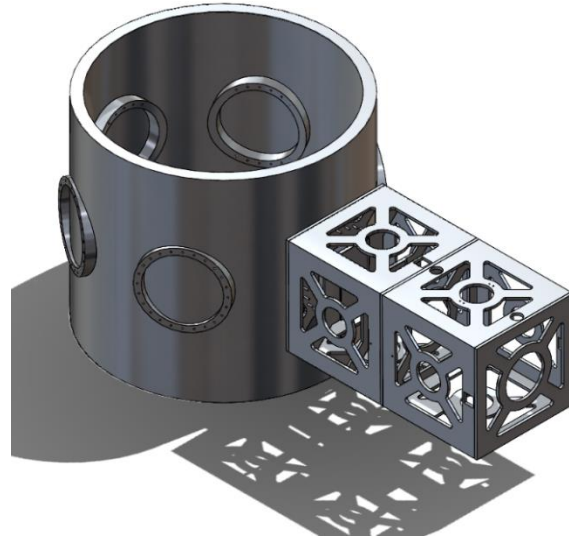


Figure 14. Dispenser Ring Connection Model

The dispenser ring allows for five other spacecraft to be attached, but for our purposes we will conduct analysis with just one. The focus of the analysis will be on the connection between rings where the stress and strain will be examined. To ensure accurate results, the center of gravity must first be verified. The maximum center of gravity offset from the mechanical interface on top of the second stage payload adapter is 3.048-meters. Since the ISS VOPED is significantly smaller than the largest possible, data must be extrapolated from Figure 15.

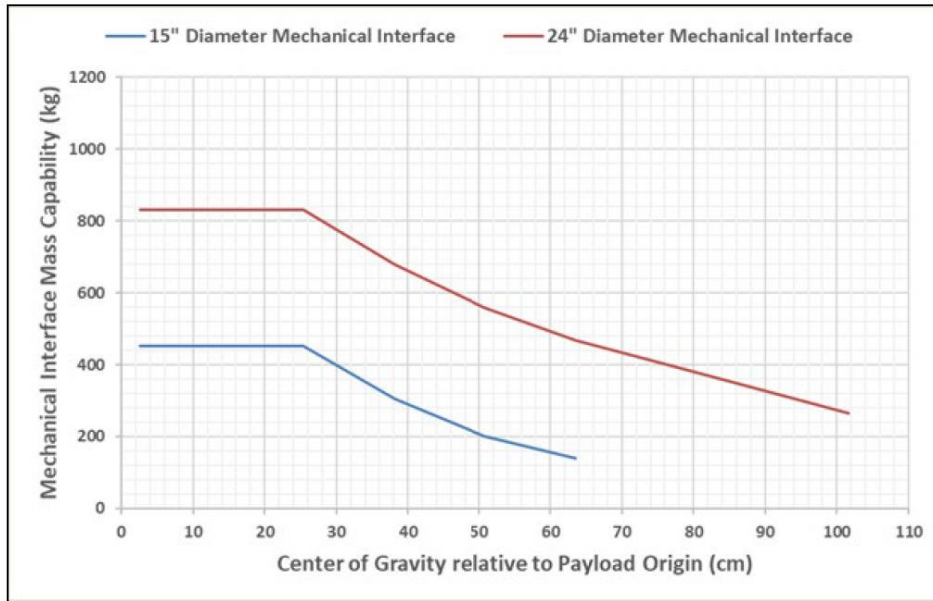


Figure 15. Allowable Payload Mass and XPL Center of Gravity  
(SpaceX, 2021)

From SolidWorks, the center of gravity in the x direction is 10 cm, which corresponds to about a Mechanical Interface Mass Capability of about 440 kg. The mass of ISS VOPED is 185.43 kg, meaning the center of gravity to interface mass is within an acceptable range and analysis can continue.

### 3.6 Natural Frequencies

The natural frequency of a system refers to the oscillations it undergoes when there is no driving or damping force. When a system is being driven at its natural frequencies, it is known to be resonating. The natural frequency is a function of the material's mechanical properties. The spacecraft will undergo oscillation within the fairing during launch. If the structure reaches

resonance, it has the potential to lead to mechanical failure. If the spacecraft fails within the failure, the mission would be unsuccessful.

Modal analysis computes any desired number of natural frequencies within a structure. In order to conserve the structural integrity of the spacecraft, the outputted natural frequencies from the structure are compared to the ones it would experience in the flight environment. From the Falcon Payload User's Guide, the allowable minimum frequency of 100 Hz, a minimum of 5 Hz under 0.5 gees of acceleration in the axial and lateral directions. It is also stated that the secondary structure should maintain a minimum resonant frequency above 35 Hz. This is to ensure no potential interaction with launch vehicle dynamics (SpaceX, 2009).

### 3.7 Random Vibration

Random vibration simulates an array of forcing frequencies that simultaneously excites the system's resonance. The difference between random vibration analysis and modal analysis is that modal analysis is a linear frequency input analysis. Meaning, it calculates through a summation of damped sinusoidal waves, where each wave is known as a Mode, to find the natural frequencies within the system. While random vibration is the analysis of nonlinear vibration, usually through Power Spectral Density, to test the failure of a system. Random vibration analysis is more realistic in general because not all frequencies are going to be damped sinusoidal waves.

### 3.8 Power Spectral Density

Power Spectral Density (PSD) is a type of frequency analysis where a system is exposed to a theoretical spectrum of harmonic loading. Within an analysis, the spectrum can be confined



by maximum and minimum bounds. The purpose of random vibration testing is to detect failure in your system when the desired PSD input is applied. For clarification, PSD does not take into consideration the variable of measurement. For our purposes, the system will be simulated under Acceleration PSD of the Falcon 9.

In order to simulate the random vibration analysis and achieve accurate results, specific PSD data needs to be inputted that correlates with the chosen launch vehicle. The PSD G environment that corresponds to the Falcon 9 is shown in

Figure 16, with specific values shown in Table 3

. The frequency and acceleration data can be manually inputted in ANSYS, PSD G Acceleration input.

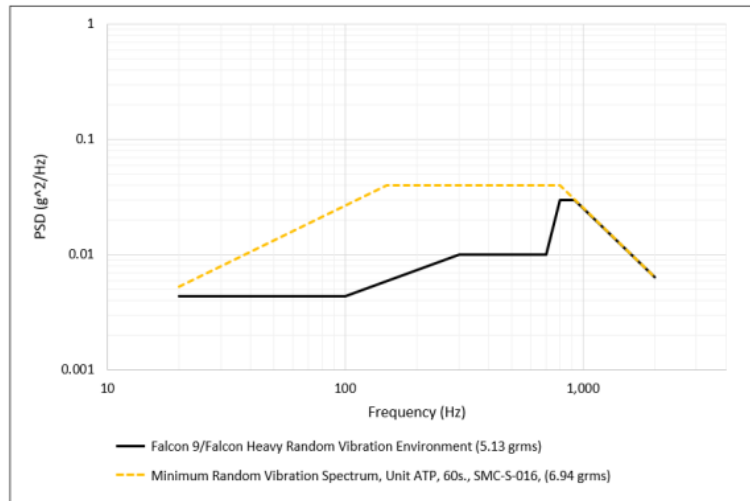


Figure 16. Falcon 9 Random Vibration Maximum Predicted Environment (SpaceX, 2021)

Table 3. Falcon 9 Random Vibration Maximum Predicted Environment (SpaceX, 2021)

<b>Frequency (Hz)</b>	<b>Random Vibration MPE (P95/50), All Axes</b>
20	0.0044
100	0.0044
300	0.01
300	0.01
300	0.01
700	0.01
800	0.03
925	0.03
2000	0.00644
<b>GRMS</b>	<b>5.13</b>

In order to use this data, the mass of all components must be less than 22.68 kg (50 lbs.), according to the General Environment Verification Standard (GEV) (NASA,2021). Since all our components are less than the allowable value and random vibration analysis can be conducted with this specific environment.

### 3.9 ANSYS Simulations

A series of analysis was conducted on the spacecraft in order to simulate the flight environment. A modal analysis that revealed the natural frequencies of the structure and displayed where the structure has potential for failure. The random vibration builds off the modal analysis by presenting a more complex series of frequencies. This analysis presents any deformities, stresses, or strains on the spacecraft. Analysis was done on three different configurations of the system: the external frame of the satellite, the frame populated with components, and the external frame connected to the dispenser ring.

### 3.9.1 External Frame Model

An analysis was conducted on a model of the external frame in ANSYS for modal and random vibration analysis, as shown in Figure 17. The external frame model entails the basic structure with no internal components. The purpose of this analysis was to test the stability of the frame while validating that the external structure can withstand the frequencies that will be applied in the fairing environment.

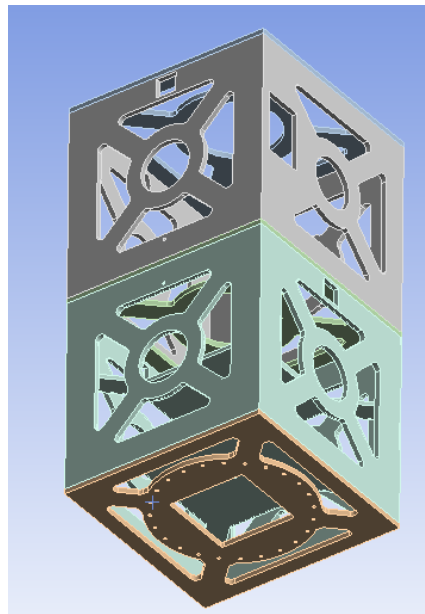


Figure 17. External Frame Model in ANSYS

#### 3.9.1a Modal Analysis Results

*The conditions that were set for the modal analysis were a fixed support at the bottom panel of the spacecraft where the thruster lies. Once the modal simulation is connected the results would ideally generate frequency values greater than 100 Hertz. From this analysis, the ten modes ranged from 118.07 to 255.21 Hertz, as shown in*

. These results fall within the acceptable values stated in the Falcon 9 Payload User Guide (SpaceX, 2009).

Table 4. External Frame Model Modal Frequencies

<b>Mode</b>	<b>Frequency [Hz]</b>
1	118.07
2	126.03
3	141.20
4	141.88
5	211.34
6	219.38
7	235.46
8	238.35
9	245.4
10	255.21

After the modal analysis was conducted, the total deformation was examined. The range of frequencies within the fairing for this analysis, did not lead to any crucial damage of the structure. This tells us we can move forward with the population of internal components and then run tests on the final system. Below, the ten modes with their corresponding deformations is displayed.

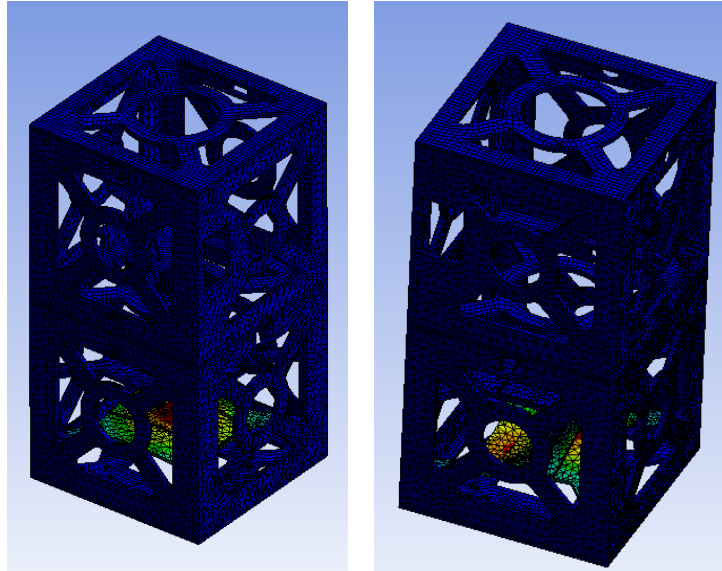


Figure 18. Total Deformation Occurring at Mode 1 & 4

The total deformation at Mode 1 and 4 falls within a range of 0 to 0.1696 m from a frequency of 118.07 Hz and 141.88 Hz, as shown in Figure 18. The damage occurs at the panel that holds the iodine propellant tank. Mode 7 also produces similar results to 2 and 6.

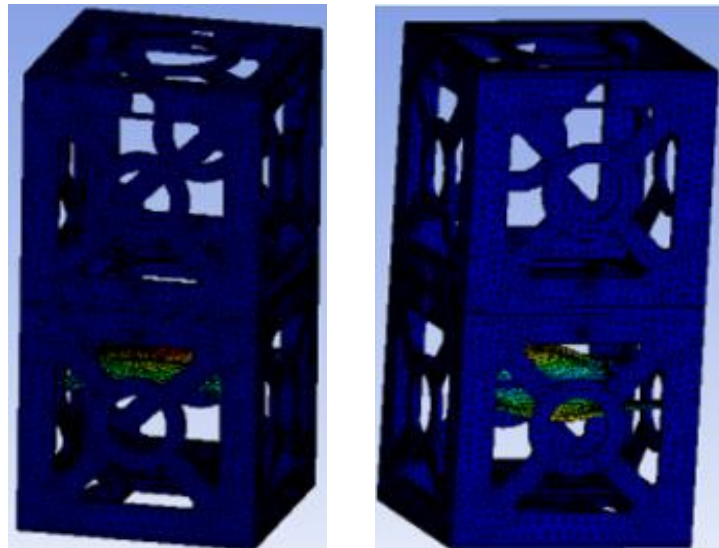


Figure 19. Total Deformation Occurring at Mode 2 & 6

The total deformation at Mode 2 and 6 fall within a range of 0 to 0.17532 m from a frequency of 126.03 Hz and 219.38 Hz, as shown in Figure 19. The damage occurs at the panel that holds the hydrazine propellant tank. Mode 8 also produces similar results to 2 and 6.



Figure 20. Total Deformation Occurring at Mode 3

The total deformation at Mode 3 falls within a range of 0 to 0.2535 m from a frequency of 141.20 Hz, as shown in Figure 20. The damage occurs throughout the top cube of the structure but is most concentrated around the cross-sectional bars. Mode 4 and 9 produce similar results to Mode 3.

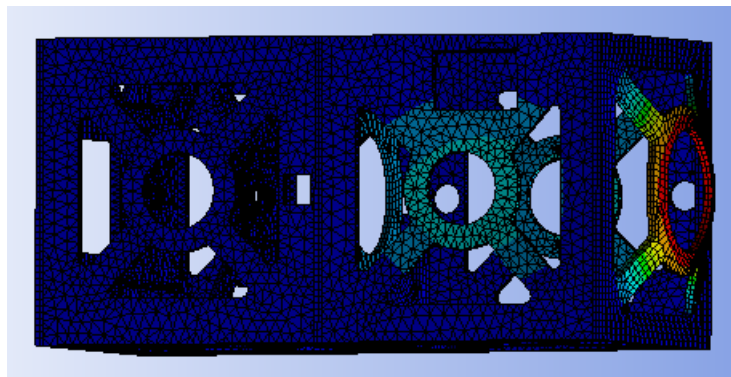


Figure 21. Total Deformation Occurring at Mode 10

The total deformation at Mode 10 falls within 0 and 0.95157 m from a frequency of 255.21 Hz, as shown in Figure 21. The damage occurs mainly at the topmost panel of the satellite, causing a

convex of the cross-sectional structure. Although most modes lead to deformation, the most concerning one is Mode 10. Nevertheless, all ten modes are at an acceptable range of frequencies, making the deformation caused by a frequency of 255.21 Hz disregarded.

### 3.9.1b Random Vibration Analysis Results

*The random vibration analysis was conducted by applying the conditions stated in Section 3.8 from*

into the PSD G Acceleration option of the analysis. The results from the random vibration analysis consist of directional deformation, strain, and von-mises stress. Figure 22, displays the directional deformation of the system.

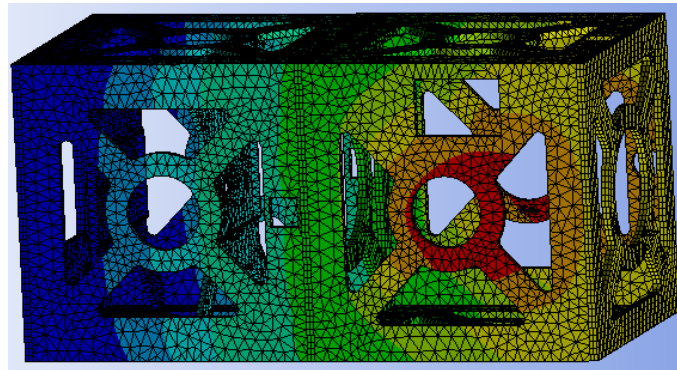


Figure 22. Directional Deformation of External Frame

The directional deformation occurring from the PSD G Acceleration falls within a range of 0 to 0.00015378 m, where the maximum deformation occurs at the cross-sectional structure of the top cube (red area).

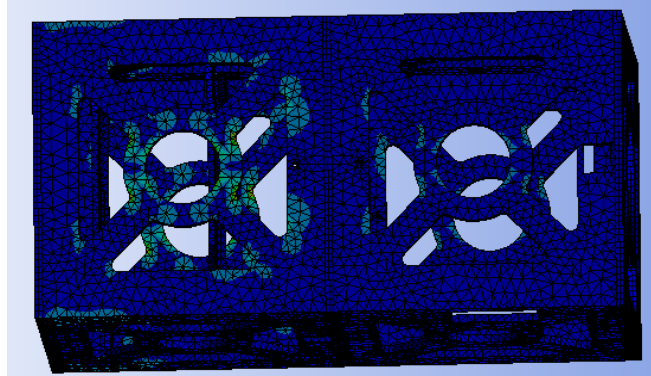


Figure 23. Normal Elastic Strain of External Frame

The normal elastic strain occurring from the PSD G Acceleration falls within a range of  $4.513 \times 10^{-17}$  to  $0.00014082$  m/m. Most of the strain shown in the image is about  $1.567 \times 10^{-5}$  to  $6.2588 \times 10^{-5}$  m/m, as shown in Figure 23. From this analysis, the strain on our system is not a concerning factor and validates the design of the structure.

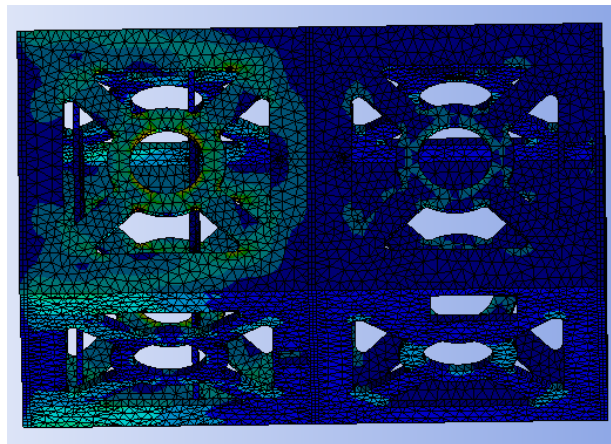


Figure 24. Von-Mises Stress of External Frame

The Von-Mises stress occurring from the PSD G Acceleration falls within a range of  $0.00013315$  to  $1.1245 \times 10^7$  Pa. However, most of the stress shown in Figure 24 falls within a range of  $0.00013315$  to  $4.9977 \times 10^6$  Pa. The highest points of stress are found within the fillets of the cross-sectional



structure. The maximum stress on the external frame does not exceed the yield strength of Al 6061 T6 of  $2.76 \times 10^8$  Pa.

### 3.9.2 Populated Model

In order to successfully run an ANSYS simulation for the populated model of the satellite it had to be slightly simplified. The simplified version contains any component that contributes largely to accurate mass allocation and purpose. Any component that was lightweight and small was suppressed for this simulation. Figure 25, shows the front and bottom view of the spacecraft within ANSYS.

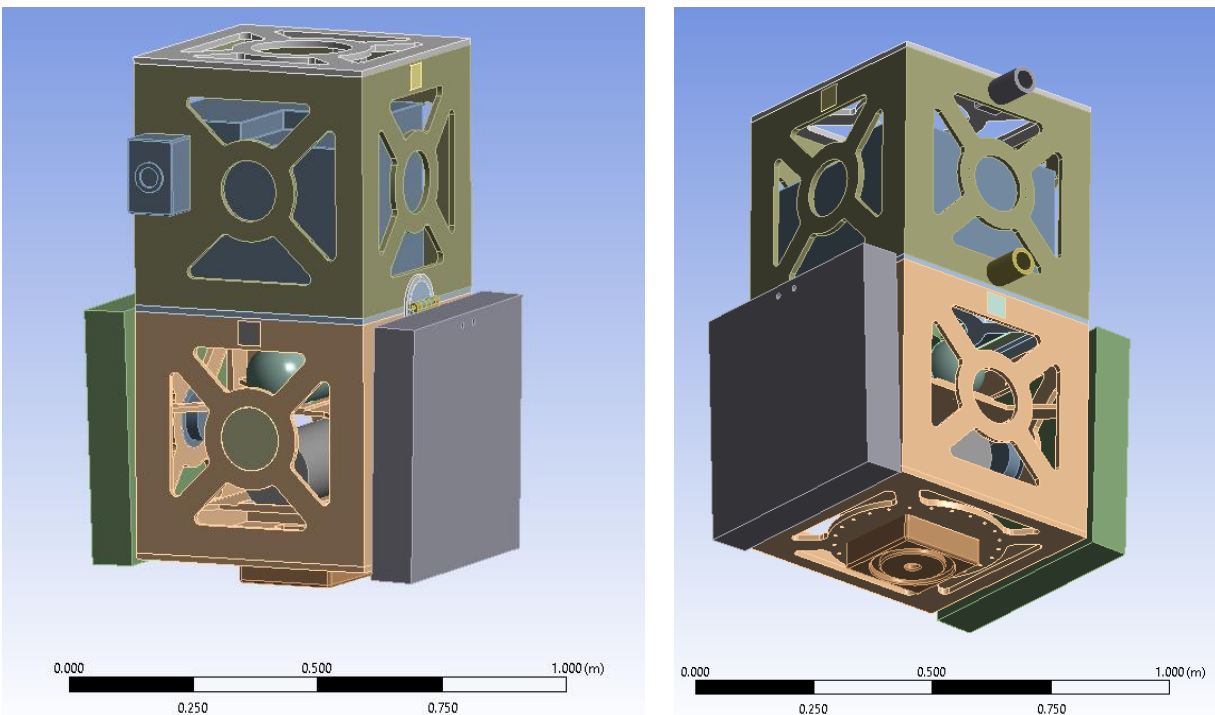


Figure 25. Front & Bottom View of Simple Populated Model

### 3.9.2a Modal Analysis Results

*As previously stated, the results of this analysis would ideally generate frequencies greater than 100 Hz. The conditions that were set for the modal analysis were a fixed support at the bottom panel of the spacecraft where the thruster lies. The purpose of choosing this panel was to mimic the dispenser ring connection. From this analysis, the ten modes ranged from 105.93 to 237.91 Hertz, as shown in*

. These results fall within the acceptable values stated in the Falcon 9 Payload User Guide.

Table 5. Populated Model Modal Analysis Frequencies

<b>Mode</b>	<b>Frequency [Hz]</b>
1	106.04
2	118.25
3	142.45
4	143.47
5	144.95
6	152.94
7	153.45
8	154.01
9	156.04
10	198.14

Since the modal analysis resulted in frequencies greater than 100 Hz, the total deformation that corresponds to each mode can be investigated. Mode 1 did not result in any deformation. The total deformation caused by Mode 2 and Mod 10 are shown in Figure 26.

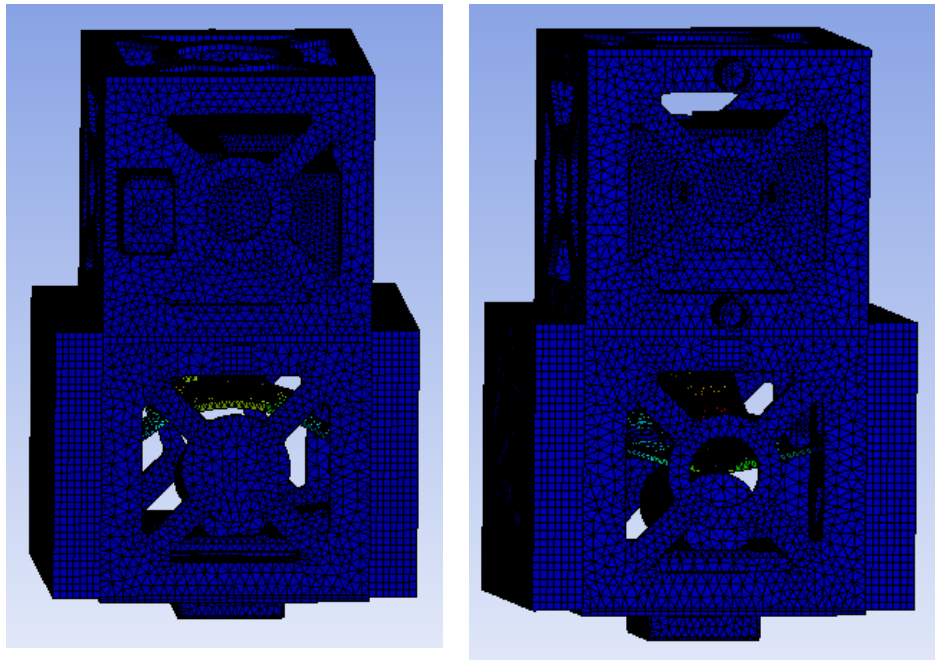


Figure 26. Total Deformation Occurring at Mode 2 & Mode 10

A frequency of 106.04 and 198.14 Hz causes deformation on the hydrazine propellant tank, as well as the cross-sectional structuring that is holding it. The average deformation is about 0.18917 m where the minimum occurs at the bottom panel and the maximum occurs at the hydrazine tank. Mode 3 did not lead to any deformation. Mode 4 and 9 are shown in Figure 27.

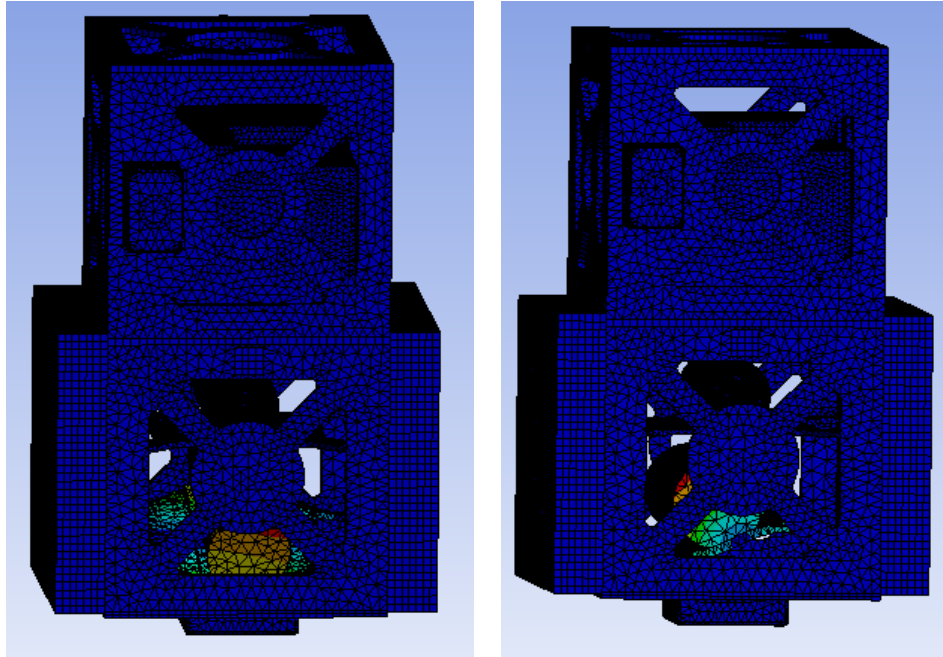


Figure 27. Total Deformation Occurring at Mode 4 & Mode 9

The deformation occurring at both modes affects the iodine propellant tank as well as the cross-sectional structure that is housing it. The tank is more affected by the frequency, causing an average deformation of  $2.8353e-2$  m, where the minimum occurs at the bottom panel and the maximum occurs at the iodine propellant tank. Mode 5 led to minimal deformation throughout the spacecraft, as shown in Figure 28.

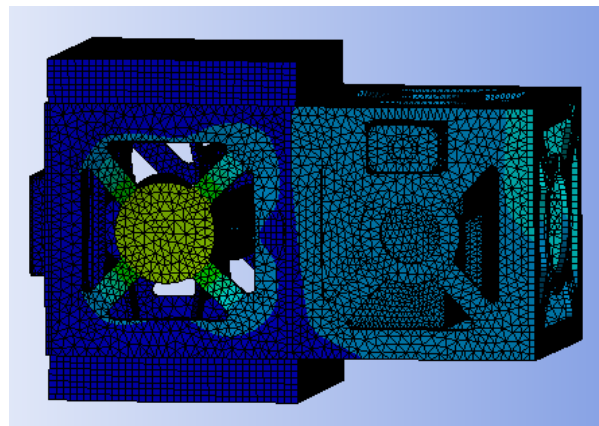


Figure 28. Total Deformation Occurring at Mode 5

The deformation occurring at Mode 5 has an average deformation of  $3.457e-2$  m, with the minimum occurring at the bottom panel and the maximum occurring at the Hydrazine propellant tank. Mode 6, 7 and 8 did not lead to any deformation. Most of the deformation caused by the natural frequencies is concentrated on the two propellant tanks. Increasing the thickness of the housing panel for the propellant tanks would ideally lead to a smaller potential of deformation.

### 3.9.2b Random Vibration Analysis Results

*The conditions for the random vibrational analysis were imposing a fixed support at the bottom plane of the spacecraft and creating the PSD G Acceleration environment, stated in*

. As well as implementing the previously calculated modal analysis. The results from the random vibration analysis consist of directional deformation, strain, and von-mises stress. Figure 29, displays the directional deformation of the system.

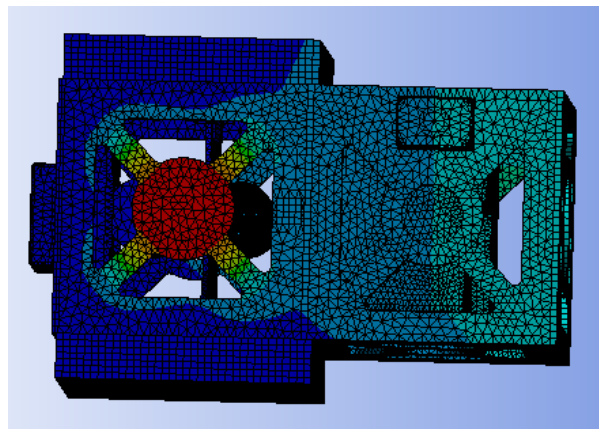


Figure 29. Directional Deformation for Populated Model

The overall directional deformation is quite small and falls within a range of 0 to  $0.0004$  m with an average deformation of  $5.497e-5$  m. The minimum occurs at the bottom panel and the maximum

occurs at the reaction wheel. This analysis presents results that will not lead to failures among the system, but the reaction wheel is concerning. Next, the normal elastic strain was examined, as shown in Figure 30.

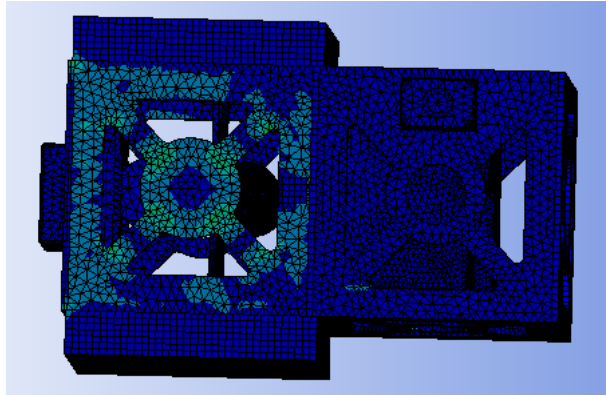


Figure 30. Normal Elastic Strain for Populated Model

The strain is only seen in the bottom unit of the system on the wall shown in Figure 30. The strain falls within a range of 0 to  $2.5379 \times 10^{-5}$  m/m, with an average of  $5.11 \times 10^{-6}$  m/m. The minimum occurs at the bottom panel while the maximum occurs at the SOIR Spectrometer. Finally, the equivalent von-Mises stresses were analyzed, as shown in Figure 31.

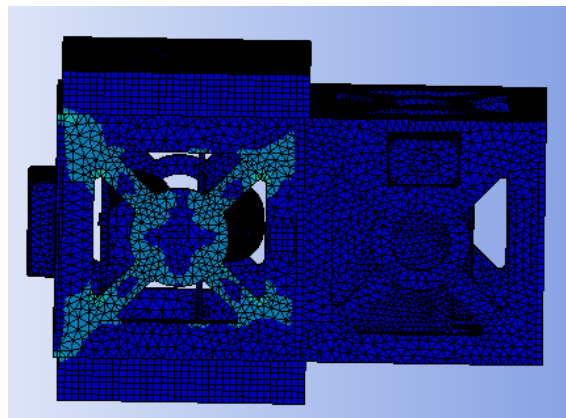


Figure 31. Von-Mises Stress for Populated Model

The result of this analysis shows the stress throughout the structure is mainly occurring on the corners of the external frame. The stress parameters fall within a range of  $1.7497 \times 10^{-3}$  to  $7.1703 \times 10^7$  Pa, with an average of  $1.349 \times 10^6$  Pa. The yield strength of Al 6061 T6 is 276 MPa ( $2.76 \times 10^8$  Pa), so the maximum stress occurring on the spacecraft would not lead to any yield of the external structure. The minimum occurs at the BHT-1500 Thruster and the maximum occurs at the SOIR Spectrometer. Although it does not lead the system to any catastrophic failure, the spectrometer is the prioritized payload for this mission. A recommendation on the design is to find a layout configuration to decrease the stress on the spectrometer.

### 3.9.3 Dispenser Ring Connection Model

The dispenser ring connection model consists of the 15-inch diameter dispenser ring, the empty satellite frame and twenty-four fasteners. This analysis was conducted to prove that the weight distribution of the satellite would be able to withstand the force from takeoff. The importance of this analysis was to display how the satellite is affected differently when connected to the ring rather than having the bottom panel as the main fixed support surface. A simplified version of the dispenser ring connection is shown in Figure 32. The model was modified to one connection port instead of five for the purpose of simplification within the software.

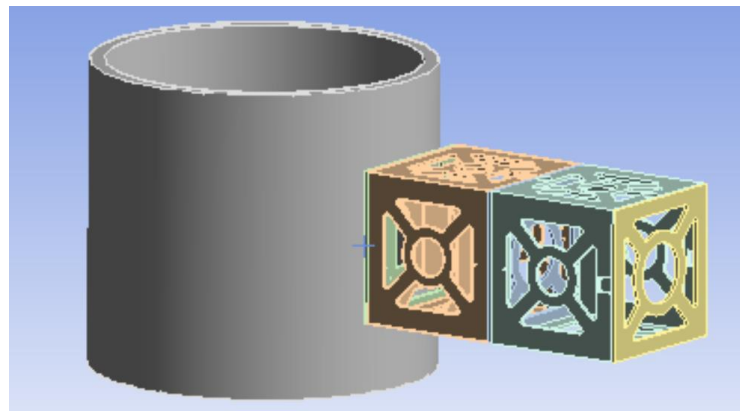


Figure 32. Simplified Dispenser Ring Connection Model

### 3.9.3a Modal Analysis Results

*As previously stated, since the environment the analysis was being conducted in was to simulate the Falcon 9 fairing. The results should be above 100 Hz for the system to have the least potential for failure during launch. The modal analysis results between the external frame and the dispenser ring are shown in*

Table 6. *Modal Analysis Results for the Dispenser Ring Connection Model*

<b>Mode</b>	<b>Frequency [Hz]</b>
1	121.09
2	132.28
3	169.44
4	214.43
5	223.57
6	238.14
7	250.43
8	261.85
9	264.26
10	279.67

Next, the total deformation caused by the modal environment was examined. The majority of the modes cause deformation where the spacecraft is connected to the dispenser ring. However, Mode's 3, 8 and 10 affect the spacecraft external and internal cross-sectional bars, as shown in



Figure 33. The maximum deformation (shown in red) for each of the modes are 0.12853 m, 0.45973 m, and 0.47601 m.

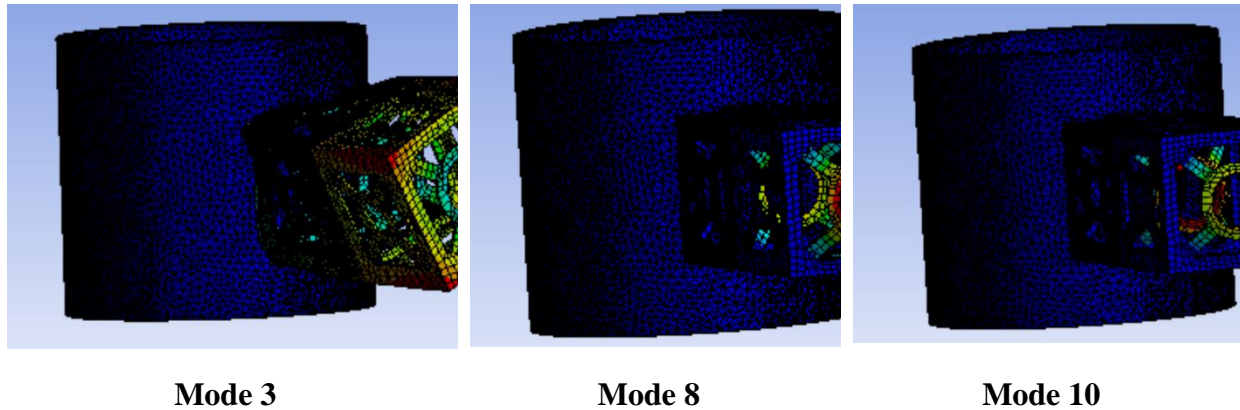


Figure 33. Total Deformation of Mode's 3,8 & 10

### 3.9.3b Random Vibration Analysis Results

The Random Analysis environment contains the same parameters used in the external frame model. This analysis only affects the portion of the model where the spacecraft and the dispenser ring are connected. The directional deformation is shown in Figure 34, with a deformation range of 0 to 1.1381e-6 m. This result is very attractive from an analysis point of view. The damage is very small when both the PSD G Acceleration and the previously simulated modal analysis is applied to the system.

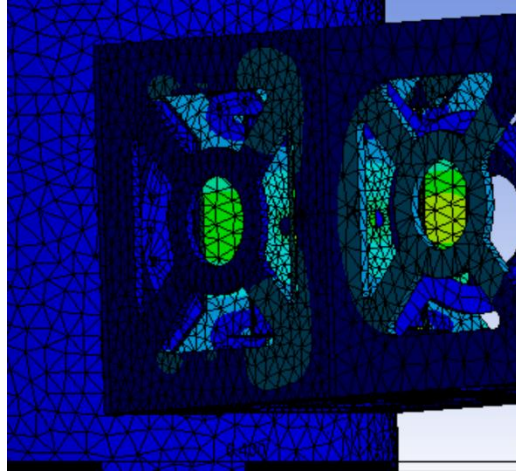


Figure 34. Directional Deformation for Dispenser Ring Connection Model

The normal elastic strain is shown in Figure 35, with a range of 0 to  $1.0357e-5$  m/m. The majority of the strain measurements fall within the magnitude of  $e-6$ . These results do not present any concerning elements or failures within the model.

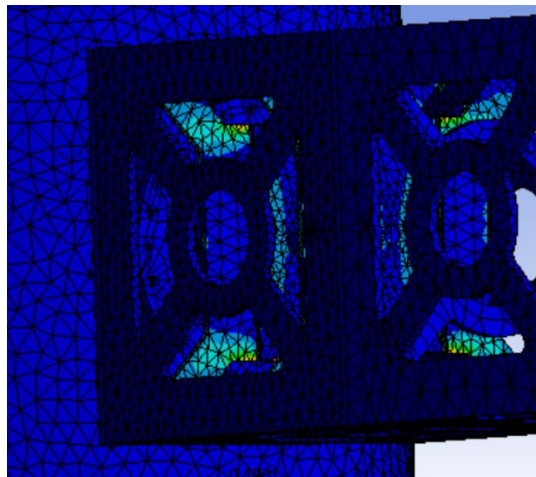


Figure 35. Strain for Dispenser Ring Connection Model

The Von-Mises Stress is shown in Figure 36, with a range of 0 to  $3.3492e6$  Pa. As previously stated, the maximum stress on the model is below the yield strength of the material of the frame. This is ideal because it won't lead to any extreme damage in terms of stress.

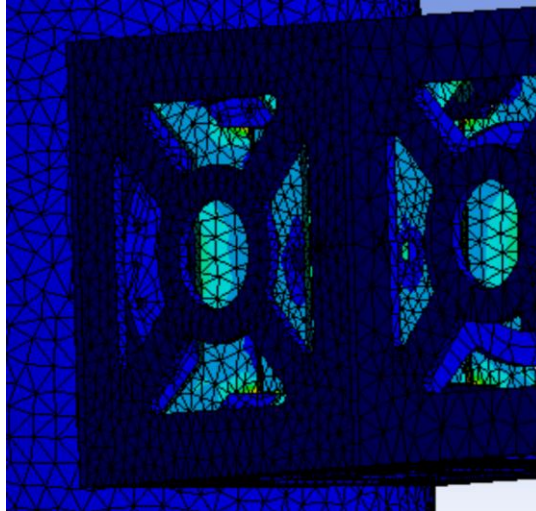


Figure 36. Equivalent Stress for Dispenser Ring Connection Model

From this analysis, the loading in the complex environment will not cause the material to yield in any direction. Meaning the connection between the spacecraft and the rideshare apparatus will not fail while in the launch environment.

## 4 Propulsion

As stated previously, the primary role of the propulsion system is to perform all major maneuvers for the spacecraft during its mission. This can consist of escaping Earth's orbit, interplanetary orbit transfers, and capturing a new orbit. The section below will describe the necessary background information to understand the selection process for the proper propulsion system

### 4.1 Chemical and Electric Propulsion

The two types of propulsion systems are chemical and electrical. Each type of propulsion system generates thrust in a unique way. In the case of the chemical propulsion system, thrust is generated through chemical reactions. Chemical propulsion systems can use liquid, solid, or hybrid propellants. For liquid propellants, it exists as either a monopropellant or a bi-propellant. These would be the cases of having just a singular uniform propellant to use as fuel, or by using a fuel and an oxidizer to generate the chemical reaction to provide thrust. In the case of solid propellant, the fuel and oxidizer are typically molded and casted together so that when the solid propellant sublimates, both parts of the propellant will react. Hybrid systems will involve a solid propellant that is kept separate from a liquid or gas propellant that is required to create a reaction (NASA, 2021). However, this last option is uncommon, and most spacecraft will use monopropellant or bipropellant.

Three types of electric propulsion exist based on their method of thrust generation. These types are electrostatic, electrothermal, and electromagnetic. The most common form is electrostatic, which comes in two forms: Ion thrusters and Hall effect thrusters (HETs). Ion thrusters generate thrust by accelerating ions through a series of charged grids. Hall effect thrusters

use a magnetic field to limit the electrons' axial motion within the propellant gas. This ionizes the propellant, generating plasma, that ejects out and away from the propulsion system. This ionized gas and plasma then neutralizes within the plume of the thruster (NASA, 2021). These electric propulsion types typically use gas propellants such as Xenon or Krypton. However, solid Iodine propellant has emerged and recently been researched and tested. Electric propulsion systems provide much higher Specific Impulse capabilities at the cost of a lower thrust, when compared to chemical propulsion.

## 4.2 Thruster Selection

The mission consists of several parameters and constraints that determine the optimal spacecraft propulsion system. The first is the requirement of having a total spacecraft mass of 180 kg. This is due to the launch vehicle requirements, and to keep the ISS VOPEd defined as a SmallSat. The propulsion system can compose a large percentage of the spacecraft if the propellant mass fraction ( $\zeta$ ) is high. One of the main determining factors of the propellant mass fraction is the propulsion system's specific impulse ( $I_{sp}$ ).

$$\zeta = \frac{m_p}{m_0} \quad \text{Eq. 1}$$

The propellant mass fraction is determined by Eq. 1. The propellant mass fraction is equal to the mass of the propellant ( $m_p$ ) divided by the initial wet mass ( $m_0$ ). This provides a decimal value, which can be multiplied by 100 to determine the percent of total mass used by the propellant.

$$m_p = m_0 - m_f \quad \text{Eq. 2}$$

The propellant mass can be calculated by the difference of the initial wet mass and the dry mass ( $m_f$ ) of the spacecraft, as show in equation 2Eq. 2.

$$c = I_{sp}g \quad \text{Eq. 3}$$

$$m_f = m_0 e^{-\frac{\Delta V}{c}} \quad \text{Eq. 4}$$

Eq. 4 is defined as the rocket equation. The effective exhaust velocity ( $c$ ) is determined by the specific impulse ( $I_{sp}$ ) of the propulsion device. The variable  $g$  stands for gravity, which causes the variable to be constant at  $9.81 \frac{m}{s^2}$ , in Earth-like conditions. Having a high  $I_{sp}$  value will decrease the propellant mass fraction, ultimately lowering the amount of propellant required to complete the mission or  $\Delta V$ . The  $\Delta V$  of the mission is  $7.131 \frac{km}{s}$ . This points to the use of electric propulsion systems due to a much higher  $I_{sp}$  compared to chemical propulsion options.

The second major property which effects the total spacecraft mass is the power requirement of the propulsion system. This directly effects the overall size and mass of the solar arrays. Electric propulsion systems require significantly more power than chemical propulsion options.

Table 7 shows propellant mass and propellant mass fraction data for various thrusters and firing modes. An average chemical propulsion system was used as a basic way to rule out that choice of propulsion method. At the bottom of Table 6, an assumption was made that a generic thruster will have an  $I_{sp}$  around 300s and a low power input of around 10 W. Although there are options with higher  $I_{sp}$  values, chemical thrusters cannot provide a sufficient specific impulse to keep the propellant mass low. The example in table size calculates to propellant mass fraction of 91.13%. This means that 91.13% of the spacecraft's mass would need to be comprised of propellant.

Table 7. Calculated Propellant Mass and Propellant Mass Fractions for Various Thrusters

<b>Thruster Option</b>	<b><math>I_{sp}</math> (s)</b>	<b>Power Input (W)</b>	<b><math>m_p</math> (kg)</b>	<b><math>\zeta</math></b>
Busek BHT-600	1500	600	58.797	37.85%
Busek BHT-1500 (High $I_{sp}$ Mode)	1860	1000	49.488	31.86%
Busek BHT-1500 (High Thrust Mode)	1615	1000	55.471	35.71%
PPS-1350	1660	1500	54.268	34.94%
NSTAR (High $I_{sp}$ Mode)	3300	2700	30.202	19.44%
NSTAR (High Thrust Mode)	1700	2300	53.241	34.28%
Average Chemical Propulsion System	300	10	139.418	91.13%

Three types of HETs and one type of Ion thrusters were investigated. The HET thrusters were the BHT-600, BHT-1500, and the PPS-1350. The Ion thruster was the NSTAR option. In Table 7, there are two different firing modes for the BHT-1500 and NSTAR thrusters. These firing modes are either a high thrust or high  $I_{sp}$  mode. A high thrust mode will offer more thrust at the cost of lower  $I_{sp}$ . This will provide a higher acceleration for the spacecraft. A higher  $I_{sp}$  mode will offer more  $I_{sp}$  at the cost of lower thrust. It allows for a lower propellant mass. From Table 7, two thrusters stand out for different reasons. The first is the high firing mode of the NSTAR thruster.

This thruster has a very high  $I_{sp}$  of 3300 s. This results in a much lower propellant mass when calculated. This also causes the propellant mass fraction to be lower. The propellant mass fraction for the NSTAR thruster was 19.44%. This is significantly lower than all other options. The downside of this choice is the high-power requirement of 2700 W. This will result in a much larger solar array size and mass. The lower propellant mass is counteracted by the increase in mass by the solar array.

The other notable thruster choice is the high  $I_{sp}$  BHT-1500 thruster. This thruster has the second lowest propellant mass fraction and the second lowest power requirement. The propellant mass is relatively low, and the power requirement allows for a relatively small solar array. This results in the lowest mass contribution. The propellant mass fraction of this option is 31.87%. The power requirement of this option is only 1000 W. This makes the BHT-1500 propulsion device a great choice for a SmallSat (Szabo, 2017).

### 4.3 Propellant

There are three types of propellants that the BHT-1500 thruster is compatible with Xenon, Krypton, and Iodine are the compatible propellants. Xenon and Krypton propellants are stored as gasses, and Iodine propellant is stored as a solid. Xenon is one of the most common propellant types for HETs. This is due to its reliability and high amount of testing hours. Krypton has similar test data when compared to Xenon. The differences between the two come with the available  $I_{sp}$  and the efficiency. (Welle, 2007). Tests from Busek have shown that Krypton propellant would increase the  $I_{sp}$  by 140-190s. However, Xenon was around 8% more efficient when it came to fuel usage (Busek, 2021). The storage properties for these propellants are as stated. Xenon and Krypton can be stored as either a very high pressurized supercritical gas, or as a cryogenic liquid. This



requires either a spherical tank or a cylindrical tank with spherical end caps to allow an internal pressure between 75 – 300 bar (Welle, 2007). The intense pressure also requires a strong tank material, to prevent ruptures of the tank. This all is accompanied by a very high cost to obtain these two propellant gasses. Overall, Xenon and Krypton will provide very good  $I_{sp}$  values along with high efficiencies. However, they come with many drawbacks, that of being an overall increase to spacecraft mass and volume usage due to the storage properties. This can be difficult in a SmallSat, where every kilogram and square centimeter counts.

Iodine is the third option for the propellant. Iodine has significantly less in-flight tests when compared to Xenon or Krypton. However, in-lab testing, and recent in-flight test have shown that Iodine has very comparable  $I_{sp}$  and efficiency values to Xenon. Since Iodine is very similar to Xenon with its performance, there are other properties that separate the two. Iodine has a much simpler storage device. Iodine is stored in a tank as a solid, either in the form of small pellets or as a casted block. This also allows the pressure in the tank to be very low compared to Xenon. An inherent state of solid matter is that the density is much higher compared to gas and liquid. This means that Iodine propellant has a higher packing factor, and therefore a smaller tank volume. The density of Iodine is 4930 kg/m<sup>3</sup>. (Rafalskyi, 2021). Iodine is capable of sublimating at very low temperatures, allowing for Iodine gas to easily be created and used in the HET.

The major drawback of Iodine is that it can be corrosive to many metals. This prevents the use of many steel and titanium materials in components that contact the Iodine. Some of these components are able to be changed to ceramic or ceramic-composite materials, in order to prevent corrosion. The corrosion can cause a significant decrease to thruster performance or lifespan, therefore, it must be treated to allow for optimal thruster performance. Iodine storage tanks must

be comprised of materials that will not corrode. Recent in-orbit testing of Iodine propulsion systems have used solid Iodine propellant. A solid block of Iodine is able to be formed by casting.

The storage tank is comprised of a thin anodized aluminum outer layer and a porous aluminum oxide ceramic block with a porosity of 95% (Rafalskyi, 2021). This is to prevent any breaking of the Iodine block from vibrations during launch. This will allow for better thermal contact during the heating process. This ceramic housing will also prevent any corrosion. The tank will operate between the temperature range of 80-100 °C. This will prevent the Iodine propellant from changing states, while also keeping the propellant temperature just below the sublimation point to allow for quick and easy access to Iodine gas (Rafalskyi, 2021). The heat generated from the thrust is able to be conducted back to propellant tank to keep it in the temperature range. Ultimately, Iodine propellant will be ideal for the ISS VOPED. This is due to the high storage density, high  $I_{sp}$  values, and high efficiency.

#### 4.4 BHT-1500 Information

The Busek BHT-1500 is the ideal thruster for the ISS VOPED. This thruster has a center-mounted cathode design to improve overall performance and have a more efficient cathode-plume coupling. This center-mounted cathode design also exhibits less plume divergence when firing. The center-mounted cathode can be seen in the figure below.

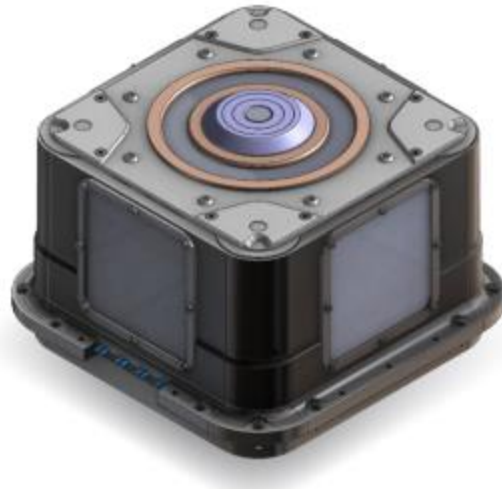


Figure 37. Busek BHT-1500 Hall Effect Thruster (Busek, 2021)

<b>Discharge Power:</b>	1500 W	<b>Thruster Mass:</b>	6.3 kg
<b>Throttle Range:</b>	1000 W - 2700 W	<b>Cathode Mass:</b>	0.3 kg
<b>Nominal Thrust:</b>	101 mN	<b>Demonstrated Impulse:</b>	Pending
<b>Nominal Specific Impulse:</b>	1710 seconds	<b>Predicted Total Impulse:</b>	> 6.5 MN-s
<b>Propellants:</b>	Xenon, Krypton, Iodine		

Figure 38. Busek BHT-1500 Hall Effect Thruster Standard Specifications (Busek, 2021)

The standard specifications of the BHT-1500 thruster are shown in Figure 38. This shows the mass of the overall thruster, as well as the mass of the center-mounted cathode. The standard discharge power of this thruster is 1500W. However, there is a throttleable range for various firing modes. This ranges from 1000-2700W. These alternate firing modes are accompanied by different  $I_{sp}$ , power, and thrust values (Busek, 2021).

Table 8. Thrust and  $I_{sp}$  Values for Various Power Inputs and Firing Modes (Busek, 2021)

Power (W)	High Thrust Mode		High $I_{sp}$ Mode	
	Thrust (mN)	Total $I_{sp}$ (s)	Thrust (mN)	Total $I_{sp}$ (s)
1000	68	1615	58	1860
1500	101	1710	87	1895
1800	120	1740	103	1940
2000	134	1700	118	1915
2400	158	1735	143	2045
2700	179	1865	154	2035

Table 8 was adapted from data by Busek, and it provides the thrust and  $I_{sp}$  for various power inputs, based on the firing mode. There are two firing modes, a high thrust mode and a high  $I_{sp}$  mode. The high  $I_{sp}$  mode is ideal for ISS VOPED as it will allow for a lower propellant mass and propellant tank volume. The ISS VOPED will use a low power throttle instead of the nominal values in order to reduce the size of the solar arrays. This is a 1000 W high  $I_{sp}$  firing mode with a thrust of 58 mN and an  $I_{sp}$  of 1860 seconds. The BHT-1500 thruster also provides an efficiency of around 50% (Busek, 2021). This is average for a Hall Effect thruster. This thruster will operate with the same compact power processing unit (PPU) that the Busek BHT-600 uses. This operates and controls the thruster by regulating the power inputs and propellant supply. The propulsion system also contains many other components such as wiring, tubing, thermal components, flow feed mechanisms, and fixtures (Busek, 2021). An assumption was made that all these extra components will have a correlated mass of 20% of the final propulsion system mass. This assumption was made to provide an even more accurate mass breakdown for the propulsion subsystem.

## 4.5 Low Thrust transfer and STK simulation

The final component of the propulsion system design consists of a mission analysis from Systems Tool Kit (STK). STK is an engineering application for aerospace, defense, and telecommunication industries. It is comprised of various programs, capable of simulating and analyzing things such as thermal/radiation environments, communication systems, solar environments, and more. STK has a program called Astrogator, which allows a spacecraft propulsion system to be simulated and analyzed. The propulsion system and orbital maneuvers of the ISS VOPED were simulated using STK and its accompanying programs to develop final flight times and Delta-V requirements.

Since the ISS VOPED uses an electric propulsion system, a low-thrust orbit transfer is required. Most orbit transfers consist of a Hohmann Transfer; however, electric propulsion systems are unable to produce enough thrust to provide the acceleration to complete a Hohmann Transfer. A low-thrust orbit transfer consists of a spiraling motion of the spacecraft. The orbit radius will increase gradually, until the destination is reached. The radius of the orbit will increase faster as time goes on, as the spacecraft will be constantly accelerating. Three major maneuvers were simulated with the STK Astrogator program. The first maneuver is a  $23.4^\circ$  inclination change. This is a plane change, which accounts for the axial tilt of the Earth. The plane change will place the spacecraft on an orbital plane parallel to that of Venus'. This is a circular orbit of 300 km above the surface. This orbit change will take around 3 complete orbits to obtain. The second maneuver is the largest, the low thrust orbit transfer. This is a transfer from a circular 300 km altitude orbit around Earth to a circular 250 km altitude orbit around Venus. The maneuver requires the most amount of propellant to complete as it is the longest and largest maneuver that the ISS VOPED will complete.

The third and final maneuver will be a 90° inclination change to place the ISS VOPED on a polar orbit path.

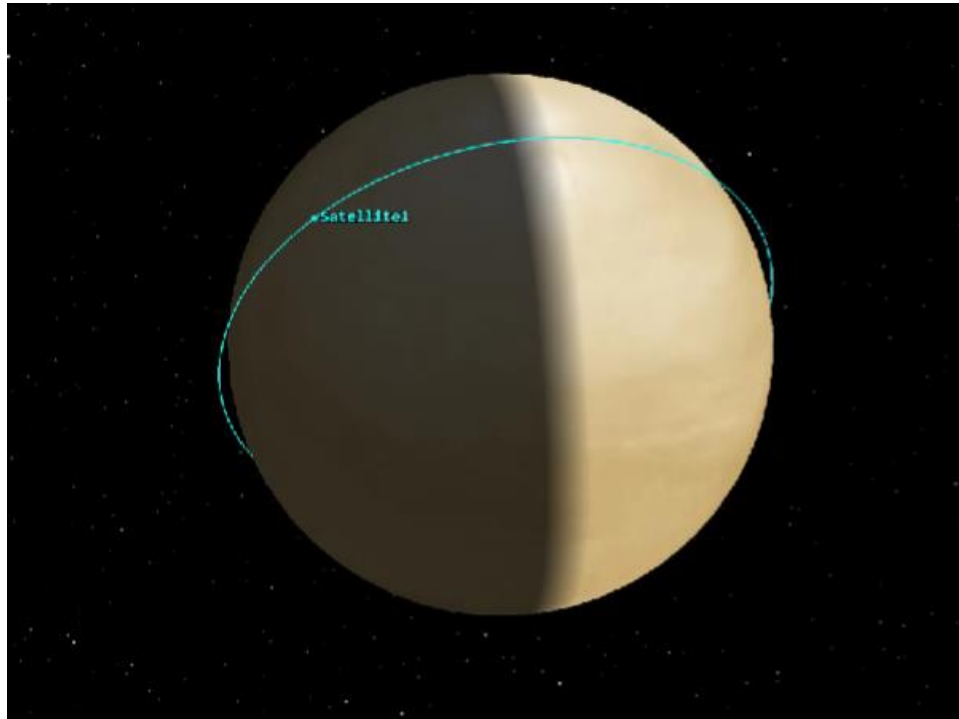


Figure 39. ISS VOPED Final Polar Orbit of Venus

This final orbit can be explained as a counterclockwise orbit, if the viewer is looking at the orbit from the same direction as shown in Figure 39. In other words, the satellite will be moving away from the Sun when at the northern part of Venus and then moving towards the Sun when at the southern part of Venus.

Table 9. Spacecraft Maneuvers with Associated Duration and Delta-V Values

<b>Mission Phase</b>	<b>Description</b>	<b>Duration (days)</b>	<b>Delta-V (km/s)</b>
<b>Near Earth</b>	23.4° maneuver to get on orbit plane	74.5	0.598
<b>Orbit Transfer</b>	Low Thrust	392.3	5.327
<b>Near Venus</b>	90° maneuver to obtain a polar orbit	115.7	1.206
<b>Summary</b>		582.5	7.131

Table 9 provides the calculated duration of each maneuver and the Delta-V requirement of each maneuver. The total trip will take around 583 days to reach the final desired orbit around Venus. This mission has a total Delta-V requirement of  $7.131 \frac{km}{s}$ . These values were determined by inputting thruster and propellant information, and then creating target sequence maneuvers in the Astrogator program. There were some assumptions made for this data to be collected. The first assumption was that the interplanetary transfer consisted of constant thruster firing with no change in thrust or impulse. However, this does not include the use of any coast periods. All spacecraft maneuvers will use a series of coast periods to allow for more efficient use of the propellant.

## 5 Power

The power subsystem is responsible for ensuring that the spacecraft has the required amount of power to complete its mission and that this power is properly managed to avoid power-related hardware failures. The subsystem is also responsible for storing extra power if the spacecraft can't generate power, or if any component requires more than nominal generated power. This section discusses methods of power generation, storage, and distribution, as well as the design and analysis of the power subsystem on the ISS VOPED.

### 5.1 Power Subsystem Background

A spacecraft must be capable of generating, storing, and distributing power to each component of the spacecraft for the duration of the mission. The most common form of spacecraft power generation is through photovoltaic (PV) solar cells. These cells convert solar radiation to electrical energy that can be utilized by the spacecraft's components. Another method is to use a solar thermal power source. The main difference between photovoltaic panels and solar thermal panels is that the latter uses solar radiation to heat a fluid and uses a thermodynamic process, such as a Brayton or Rankine cycle to generate useful electrical power (Larson & Wertz, 1992). Some less common sources are radioisotope thermoelectric generators (RTG) and fuel cells. RTGs, shown in Figure 40, rely on the heat released by a naturally decaying isotope, typically plutonium-238, and thermocouples to generate electricity (Dept. of Energy, 2021). The Cassini mission and the Curiosity Rover are two high profile cases where RTGs were used to generate power and heat. RTGs are extremely useful in environments where solar radiation is not viable as the sole source for power generation. Fuel cells, typically hydrogen, are another way of generating power and rely on converting chemical energy from a redox reaction to generate power. Because a fuel cell is



essentially a chemical reaction, it requires reactant tanks which can take up a considerable amount of volume (Larson & Wertz, 1992).



Figure 40. One of three RTGs used on the Cassini Spacecraft  
(Nasa, 2018)

Table 10 shows a comparison matrix between these technologies. RTGs and Fuel Cells are not suitable for this mission as the former would be impossible to realistically implement in a SmallSat, leaving the photovoltaic and thermal solar cells. From the table, it is clear that PV cells provide more power per unit weight and have more information due to their popularity. Because of these reasons, PV solar cells were selected.

Table 10. Comparison of different power generation methods.

(Adapted from Larson & Wertz, 1992)

<b>Power Generation Method</b>	<b>Solar Photovoltaic</b>	<b>Solar Thermal</b>	<b>Radioisotope Thermoelectric Generator</b>	<b>Fuel Cells</b>
<b>Fuel Availability</b>	Unlimited	Unlimited	Low	Medium
<b>Commercial Availability</b>	Very High	N/A	Very Low	N/A
<b>Mounting</b>	Can be mounted or folded during launch	N/A	Mounted	N/A
<b>Power Range (kW)</b>	0.2 – 300	5-300	0.2-10	0.2 – 50
<b>Specific Power (W/kg)</b>	25-200	9-15	5-20	275
<b>Specific Cost (\$/W)</b>	800-3000	1000 - 2000	16K – 200K	N/A

The spacecraft also needs a way to store energy that can be accessed when solar panels cannot harness solar radiation or during peak-power demands. This energy can be stored using batteries. Lithium-ion batteries, the same batteries used in many portable home electronics, can be used as back-up to the solar arrays. There are other options for battery technology such as Nickel Cadmium, which have been used extensively in spacecraft, but have a much lower specific energy density, making lithium-ion the ideal choice (Larson & Wertz, 1992).

Power generated by the solar arrays will be virtually useless if it isn't properly conditioned and distributed to our components. This process is managed by an electrical power system (EPS). The EPS is responsible for converting the optimal amount of energy for the solar arrays and making sure that power supplied to a component is the correct voltage and current. Figure 41 showcases how power travels from the arrays to the battery and then to the main bus where it is distributed out to different voltages. Controlling this power is essential to preventing overcharging and overheating inside the spacecraft. The two widely used methods of controlling this power are maximum peak-power trackers (MPPT) and direct-energy transfer (DET). An MPPT is essentially a DC-DC converter that changes the high voltage from the solar array to a lower voltage that can be used by a battery, while maintaining the array's maximum power output (Larson & Wertz, 1992). A DET system would use shunt regulators to direct excess current towards resistor banks or shunt the current at the array. Both systems are extremely efficient, but the MPPT is more preferable in missions that last less than 5 years and require higher power at beginning of life (BOL) (Larson & Wertz, 1992).

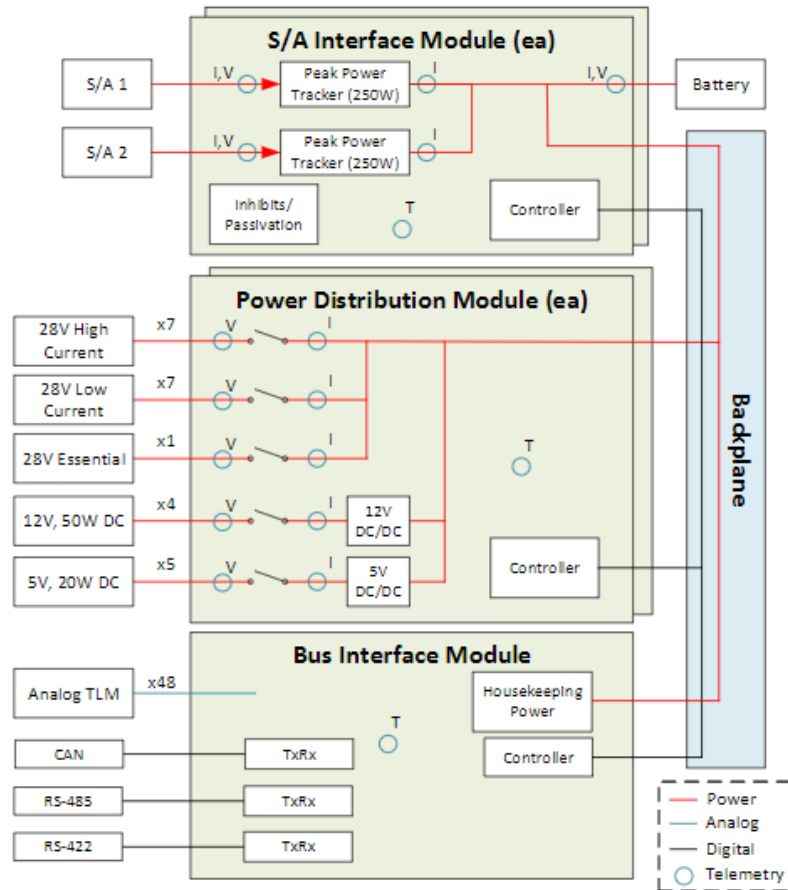


Figure 41. Block Diagram of EPS

(Standard Products, nd.)

## 5.2 Spacecraft Power Requirements

To determine the optimal hardware for our mission, it is necessary to determine how much power the spacecraft will require. A power budget contains the list of the power requirements for every component in the spacecraft. This will allow tracking of each subsystem's power needs and change hardware, such as array size, or dismiss any component changes if there are conflicts with other subsystems. The table below shows the power budget for the SmallSat, as well as detailed power specifications for each component. It is evident that the propulsion subsystem is responsible

for almost 90% of the spacecraft’s power requirements making it the most influential driver in the power subsystem design. The total maximum required power for the spacecraft was determined to be 1212.7 W with a 10% contingency factor. It should be noted that many component datasheets do not provide information on nominal current or voltage. For this reason, this analysis assumes that these components will be compatible with the EPS.

Table 11. Spacecraft Power Requirements

<b>Subsystem</b>	<b>Name</b>	<b>Nominal Wattage (W)</b>	<b>Max Wattage (W)</b>	<b>Voltage (V)</b>
<b>Propulsion</b>	BHT-1500	1500  (Operated at 1000)		28
<b>Payload</b>	SOIR Spectrometer	17	51.4	24
<b>ADCS</b>	Sun Sensor	< 0.036	0.036	3.3 - 5
	Star Tracker	4	-	5- 12
	Reaction Wheels	4.2	15	12-24
<b>Comms.</b>	IRIS Radio	0.5	35	12-28
	Kryten-M3 OBC	0.4	1	N/A

### 5.3 Hardware

This spacecraft will be using photovoltaic (PV) solar cells to generate power. PV solar cells are composed of layers of semiconductors, and when light strikes the cells, the energy is absorbed by the electrons in the material. These energized electrons now begin to flow through the material, forming an electrical current, which is extracted by conducting metal contacts on the panels. A

panel's efficiency is determined by how much of the available power it is able to extract (Dept. of Energy, n.d.). This available power per unit area is known as the solar flux, which is a function of distance away from the sun, as shown in Eq. 5:

$$S = \frac{L}{4\pi d^2} \quad \text{Eq. 5}$$

Where L is solar luminosity constant, and d is the distance away from the sun. This equation shows that the solar flux is higher the closer one is to the sun, meaning more power can be generated. This also means that the minimum amount of power the spacecraft can generate will be at Earth. At Earth, the solar flux is 1367 W/m<sup>2</sup>. A solar panel's efficiency is determined by how much of the solar flux it can actually use, which depends on the type of semiconductor used in the panel. Modern panels use layers of different semiconductors to greatly improve efficiencies. These panels are called multijunction panels and can have efficiencies of up to 30%, much higher than the maximum 20%, offered by a single-junction silicon panel (Larson & Wertz, 1992). As a result, a multijunction ZTJ solar array was selected for this mission. It is also important to consider the optimal array size, as to not carry unnecessary weight on the mission, while still delivering enough power for the spacecraft's components. To find the optimal array size, following equations were used:

$$P_0 = n \cdot S \quad \text{Eq. 6}$$

$$P_{BOL} = P_0 \cdot I_D \cdot \cos(\theta) \quad \text{Eq. 7}$$

$$A_{sa} = \frac{P_{sa}}{P_{BOL}} \quad \text{Eq. 8}$$

In order to perform some of these calculations, various assumptions were made about the panel and panel orientation. First, it was assumed that the panel outputted power,  $P_0$  with an efficiency,  $n$ , of 29.5% and would be directly facing the sun, meaning that the solar incidence angle,  $\theta$  was 0 degrees. Our beginning of life power ( $P_{BOL}$ ), as a result, was just the output power multiplied by the nominal inherent degradation, which was assumed to be 77% (Larson & Wertz, 1992). To determine the optimal array size, the last required variable was the power required by the spacecraft which was calculated from Table 11. With a 10% contingency factor, the mission required an array of size 3.92 m<sup>2</sup> to power the spacecraft. Using the array size with the array specific mass, the mass was determined to be 11.75 kg.

Lithium-ion batteries were chosen for energy storage. Their high energy density and extensive use in other spacecraft made them the clear candidate for this mission. The following equations were used to calculate the optimal size and mass of the batteries:

$$C_r = \frac{P_e \cdot T_e}{n \cdot N \cdot DOD} \quad \text{Eq. 9}$$

$$M_b = \frac{C_r}{E} \quad \text{Eq. 10}$$

Where,

$C_r$  Battery Capacity

$P_e$  Power Required in Eclipse

$T_e$  Time in Eclipse

$n$  Transmission Efficiency

$DOD$  Depth of Discharge

$N$  Number of Batteries

$M_b$  Battery Mass

$E$  Energy Density

The energy density and transmission efficiency were determined to be 175 W-hr and 0.9, respectively (Larson & Wertz, 1992). The time in eclipse was determined by inserting a satellite into a polar orbit at Venus and using the report function in STK to extract the eclipse time. From the eclipse times, the number of eclipse cycles per year was calculated, and this number was used in conjunction with Figure 42 to determine the depth of discharge. Since the BHT-1500 wasn't used during the orbit, the power requirements decreased dramatically. As a result, the battery capacity was 175 W-hr and weighed 1 kg.

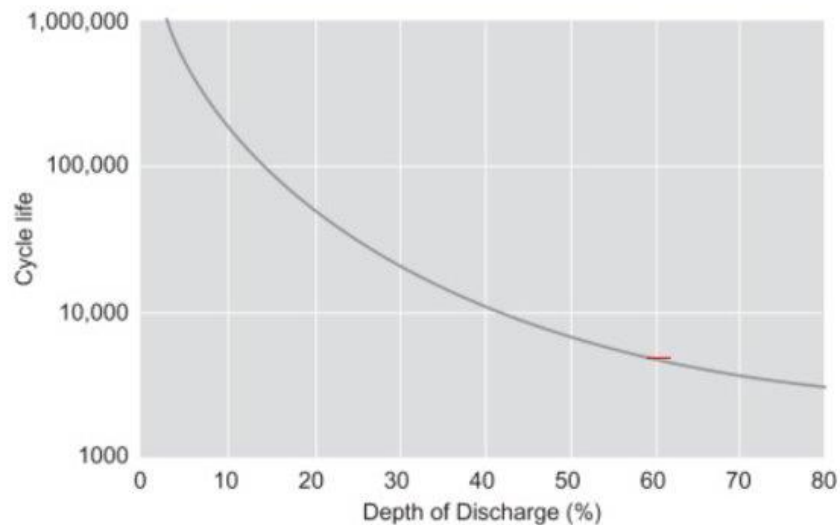


Figure 42. Cycle Life vs Depth of Discharge

(Kalogirou, 2018)

#### 5.4 Power Generation in STK

To ensure the selected components perform as expected, STK was used to simulate the orbit to Venus and calculate the power generation during that period. STK provides basic satellite models for analysis, but a power subsystem analysis is mostly dependent on the size of the solar arrays. Since STK does not allow the user to edit the default models, these calculations were



performed by first creating a simplified model of the spacecraft in Blender, and adding this model into STK. The model is shown in Figure 43. The black rectangular prism represents the main spacecraft bus and the two blue layers to its side represent the solar cells.

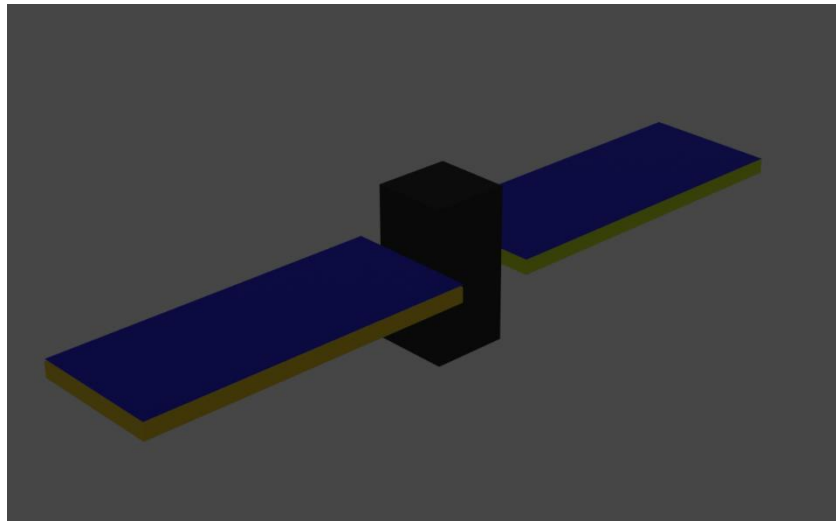


Figure 43. Blender Render of Simplified Spacecraft Model

This model was then exported as a COLLADA file (.dae). This file format allowed STK to read and display the model. This, however, did not give sufficient information to STK for it to use the Solar Panel Tool. An ancillary (.anc) file had to be included to detail the panel and body articulations. To maximize power generation, the panels had to point towards the sun at all times. This was done by adding a pointing node in the ancillary file, for the panels. With the pointing node created, STK was able to have the panel vectors face the sun. Figure 44 shows the total power generation for the mission.

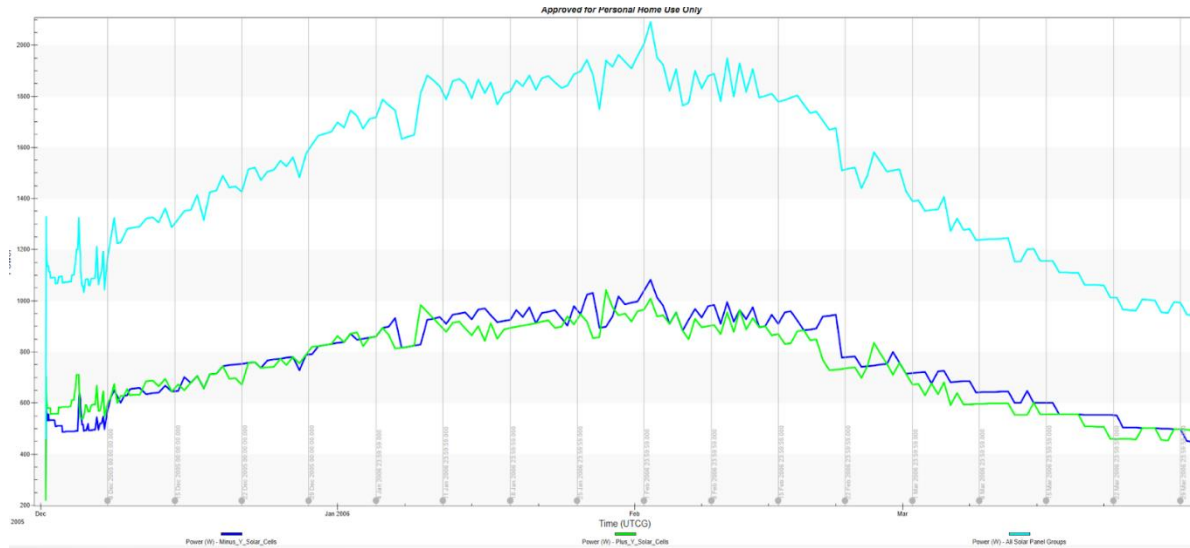


Figure 44. Total Wattage vs. Mission Time

Immediately, it was clear that the STK model was not producing the correct results. Generally, the total power generation would increase as the spacecraft gets closer to Venus. The sharp discontinuities are also unexpected and as a result, the spacecraft is unable to produce the necessary power from start to finish. After some troubleshooting it became clear that the model was not properly tracking the sun. This issue was resolved by modifying a Blender model, shown in Figure 45, made available from STK to match the desired solar panel size and then using the Solar Panel Tool.

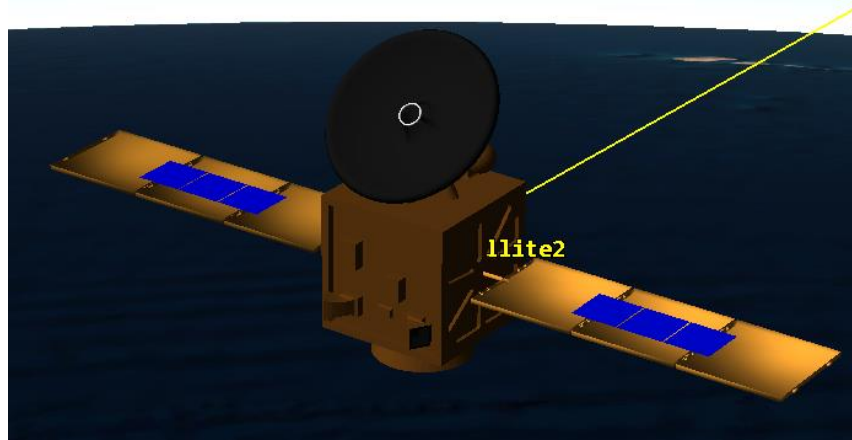


Figure 45. Modified Satellite Model

The power generated by this model is shown below in Figure 46. This is more aligned with what was expected; the plot is smooth, and the power generated increases as the satellite approaches Venus. This model also validates the mission’s design choices since the power generated is always greater than the maximum power required.

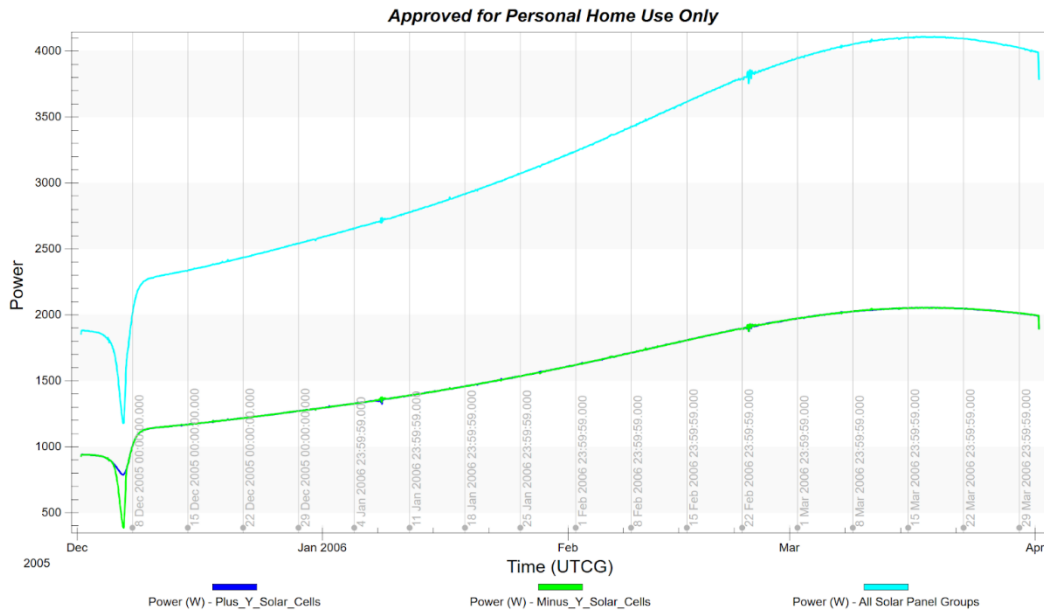


Figure 46. Updated Power Generation vs. Time

After verifying the solar panel design, it was essential to ensure that the battery would be able to provide enough power for the satellite's equipment while in eclipse. This was done by simulating a polar orbit around Venus at an altitude of 250 km in STK. The figure below shows the power generated at Venus. Since the period of the orbit is approximately 90 minutes, the satellite goes into eclipse 16 times in a 24 hour scenario.

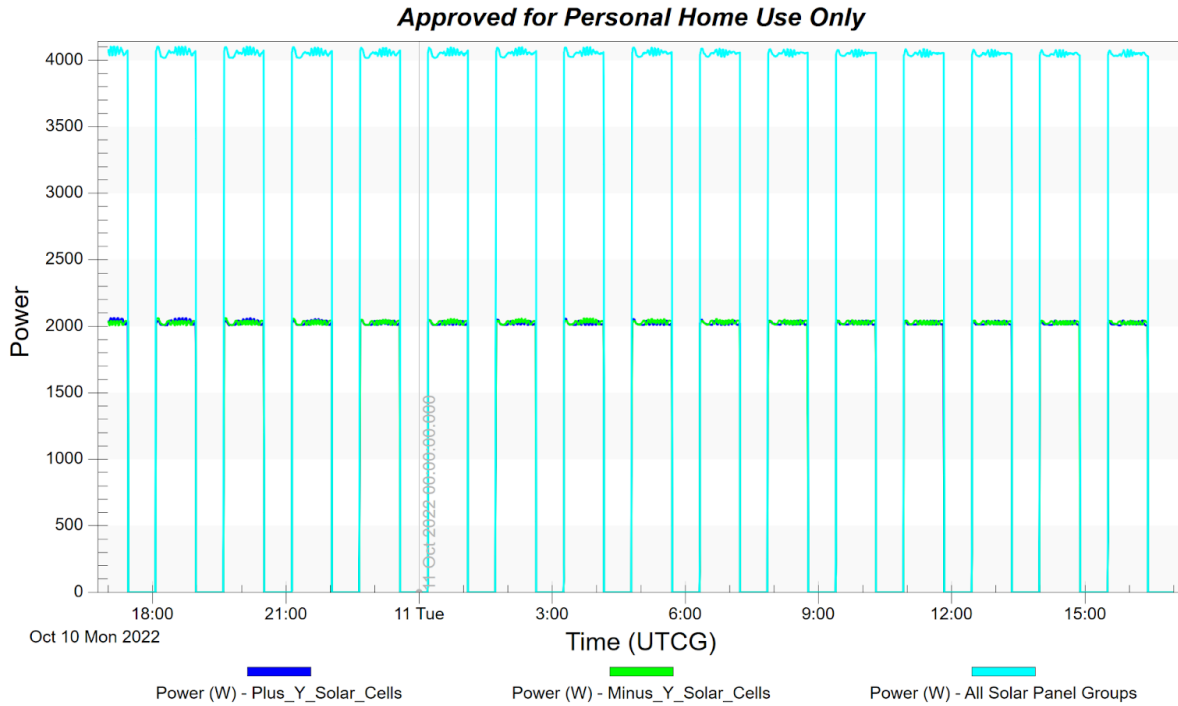


Figure 47. Power Generated in Polar Orbit at Venus

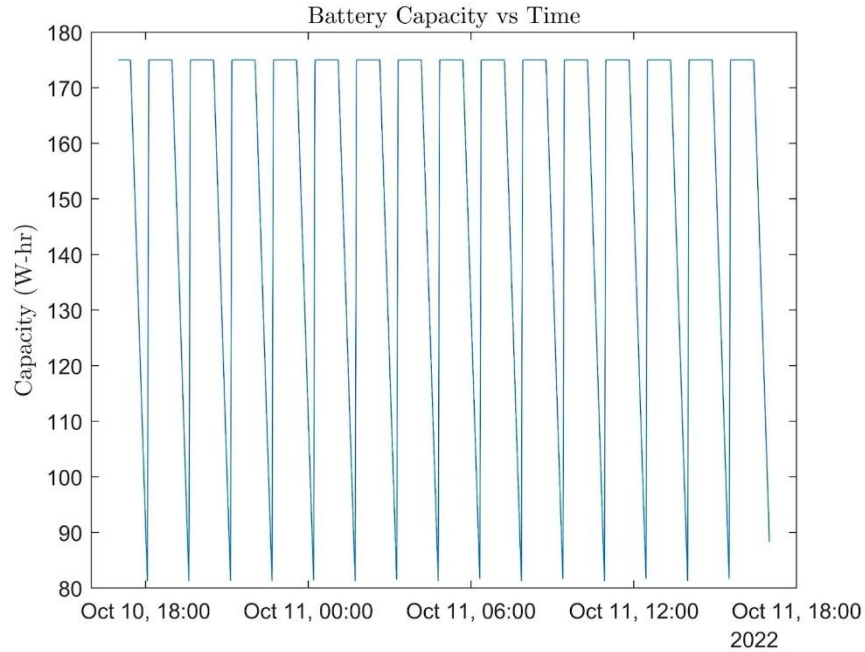


Figure 48. Battery Capacity vs. Time

The results of the battery discharge simulations for this scenario can be seen in Figure 48. The code used to create this plot can be found in Appendix A. The battery initially starts out with the maximum capacity of 175 W-hrs., and then as the spacecraft goes into eclipse, the spacecraft components are powered using the battery, decreasing its capacity. The plot above was calculated by implementing the following equation into MATLAB:

$$C_r = C_r(i - 1) + P_{net}(i) \frac{dt}{60} \quad \text{Eq. 11}$$

The equation finds the capacity at the current time step using the capacity at a previous time step and the net power at that time step multiplied by the time step in hours. The net power is the difference between power generated and the required power in orbit, which was determined to be 150 W.

## 6 Attitude Determination and Control

### 6.1 Sensor Selection

The ADC system requires the conjunction of a variety of sensors and actuators to operate correctly. Some of the most commonly used components are star trackers, Global Position System (GPS), sun sensors, horizon sensors, magnetometers, gyroscopes, reaction wheels, and magnetic torquers. Some of these serve the same purpose yet only function in certain environments. For example, magnetic torquers require an external magnetic field to create torque. Venus does not possess a magnetic field necessary to operate this specific actuator. Likewise, GPS relies on a constellation of satellites to determine the position. These vehicles only orbit around Earth, most of our mission will take place outside of the effective range of this positioning system. Consequently, the mission environments and component limitations have been considered in order to determine the following sensor selection.

#### 6.1.1 Star Tracker

This component is a digital camera which is capable of determining the position of the ISS VOPED. It relies on tracking star clusters and autonomously matching them with known stars in an internal catalog. A positioning algorithm computes the star tracker's attitude with respect to a celestial reference frame. A couple of the specifications to evaluate while comparing different star trackers are field of view (FOV) and accuracy which is measured in arcseconds. The score is weighted in favor of accuracy (60%), followed by volume (20%), mass (20%), and power (10%). The component selection is based on the highest score.

Table 12. Star Tracker Decision Matrix

Component	Mass (Kg)	Volume (m <sup>3</sup> )	Power (W)	Accuracy (arcsec)	Score
CT-2020	3	1.02E02	8	1.5	0.22
ST 400	0.28	2.62E04	0.7	10	0.24
STAR-T3	0.35	3.17E04	2	2	0.76
Kairospace S	0.197	3.12E04	0.7	5	0.60

The STAR-T3, shown in Figure 49, is the best option based on the selection. It has the best accuracy for a reasonable amount of mass and volume. The sensors are susceptible to space light from the Sun and the Earth albedo, this interference results in a loss of accuracy. As a safety measure, the SmallSat employs star trackers which are positioned in locations opposing the sunny side. While, the spectrometer takes measurements facing the Sun, the two star trackers are placed on the opposite face, limiting sunlight exposure.



Figure 49. STAR-T3

## 6.1.2 Sun Sensor

Sun sensors fall into two categories, coarse Sun sensors (CSS) and fine or digital Sun sensors (DSS). Where coarse sensors are less accurate but usually have larger FOVs. The following figure represents the sunlight entering the rectangular aperture of a fine sun sensor.

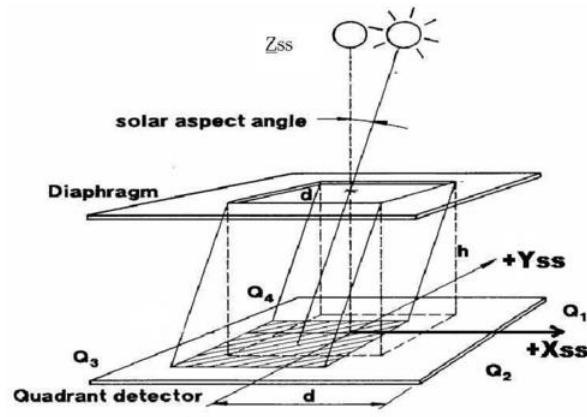


Figure 50. Fine Sensor Photodiode Cell (Boslooper, 2012)

The ADC system is tasked with pointing the solar array cells directly at the Sun to maximize solar power generation. To accomplish the task one fine sun sensor will be pointed at the Sun, this sensor is mounted next to the spectrometer, this side will be facing the sun for most of the mission. If at any point of the mission the Sun leaves the fine sensor's FOV, the satellite will not be able to determine the direction of the sun. To remedy this, four coarse sun sensors have been selected, one per face except the thruster side. The main fine Sun sensor chosen is the SSOC with an accuracy of 0.3 degrees. The four secondary coarse CoSS Sun sensors have an accuracy of three degrees.



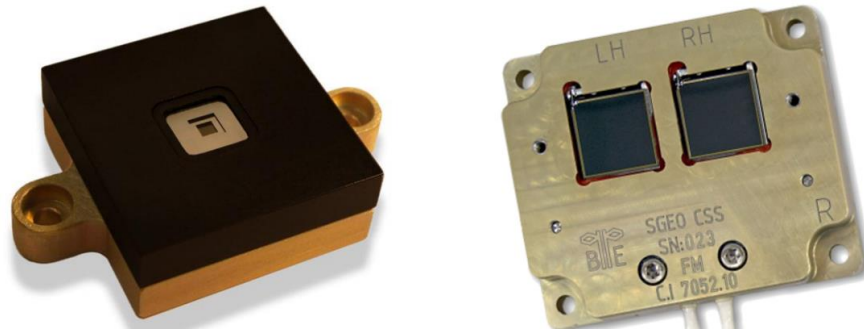


Figure 51. SSOC-AC Fine Sensor (left) and CoSS-R Coarse Sensor (right)

Table 13. Sun Sensor Specifications

	SSOC-AC	CoSS-R
FOV	60 deg	180 deg
Average Consumption	0.01 W	0 W
Supply Voltage	3.3/5 V	0 V
Mass	0.025 kg	0.015
Operating Temperature	-45 °C to 85 °C	-55 °C to 115 °C

## 6.2 Actuator Selection

Actuators are components that perform orientation changes upon the spacecraft. Our ADC system will focus on reaction wheels because magnetic torquers are unable to function in a Venus mission. The environmental disturbances that the spacecraft will experiment within an orbit around Earth are represented in the Figure 52. The ISS VOPED's size and final 250 km polar orbit around Venus make these disturbances negligible.

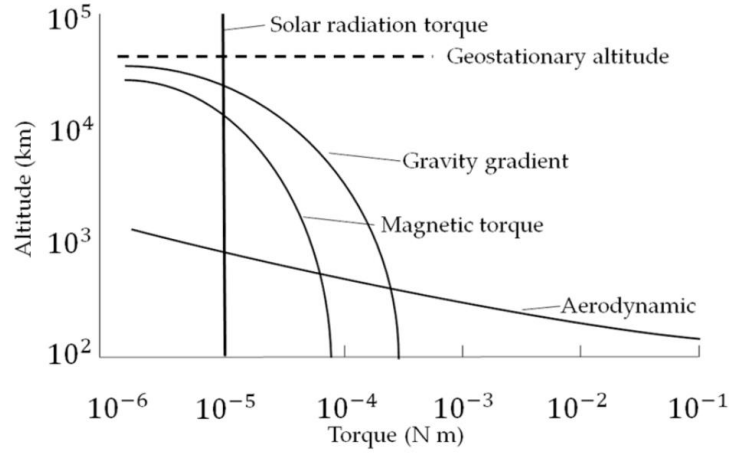


Figure 52. Magnitude of Torques Relative to Spacecraft Altitude (Yao, 2021)

### 6.2.1 Reaction Wheels

Reaction wheels are the primary attitude actuators for most spacecraft. At least three reaction wheels are needed for full three axis control. For simplicity, only three reaction wheels are used, even though adding more reaction wheels prevents the system from losing an axis of rotation if a wheel were to fail. On the other hand, failure from one reaction wheel usually is followed by other failing components of the same model (Markley, 2014).

The total spacecraft angular momentum is given by

$$H_{Total} = H_{SC} + H_w \quad \text{Eq. 12}$$

$$H_{Total} = J_{SC}\omega_{SC} + J_w\omega_w \quad \text{Eq. 13}$$

Where  $H_{SC}$  is the angular momentum of the spacecraft, and  $H_w$  is the angular momentum of the reaction wheels. If we consider the angular momentum to be constant, then the total change in angular momentum depends upon the angular momentum of the reaction wheels. Thus, by

modifying the angular speed of the reaction wheels ( $\omega_w$ ) we will be able to change the total angular speed of the spacecraft.

Reaction wheels offer an accurate and reliable approach towards stabilizing and reorienting a spacecraft without the necessity of fuel consumption. The main limiting factor is that these wheels reach a speed limit when building up momentum, this speed ceiling is considered the maximum momentum that a reaction wheel can store.

Table 14. Reaction Wheel Selection Matrix

Model	Mass (kg)	Volume (m <sup>3</sup> )	Power (W)	Max Power (W)	Momentum Storage (Nms)	Max Torque (Nm)
Tensor Tech RS100	0.25	-	0.7	1	1.00E-02	1.00E-03
CubeWheel Large	0.2	1.02E-04	0.18	-	3.00E-02	2.30E-03
Flywheel	3	3.07E-03	10	70	2.00E+00	5.00E-02
MWA-50	10.5	6.65E-02	20	100	67.8	7.00E-02
RW 35	0.5	3.61E-04	1.4	5	1.00E-01	1.90E-04
RSI 01-5/28i	0.7	7.23E-04	2	4	1.20E-01	5.00E-02

The amount of torque needed will depend on the settling time of the detumbling phase as well as angular momentum storage. The chosen wheel is the RW 35 due to its high momentum storage and sufficient torque. Its only downside is the mass and power consumption.

### 6.2.2 ACS Thrusters

To remedy the limitation on reaction wheel storage, the spacecraft will employ ACS thrusters to routinely dump the excess momentum stored within the reaction wheels. This procedure is called desaturation. This mission will employ low impulse monopropellant thrusters to dump the momentum with precision. To select the most ideal thruster we will choose one that requires the least amount of wet mass.

The efficiency of a thruster is measured in specific impulse ( $I_{sp}$ ), which is governed by the following equation:

$$I_{sp} = \frac{T}{g_0 \dot{m}} \quad \text{Eq. 14}$$

Eq. 14 describes how much fuel is needed (mass flow rate) to propel a spacecraft at a specific thrust of an engine (T). Where  $g_0$  is the standard acceleration due to gravity on Earth's surface. The fuel consumed can be calculated by multiplying the burn time and the mass flow rate. A higher  $I_{sp}$  is ideal because less fuel is used per desaturation burn. There are trade-offs when reaching a higher  $I_{sp}$ , these compromises can also influence thruster choice.

When desaturating spacecraft, the thrusters are generally actuated in thruster couples. This coupled configuration ensures that the rotation is stable around an axis of rotation of our choosing. Ideally, intersecting with the center of mass. Figure 53 demonstrates a coupled thrust inducing a rotation over the X axis.

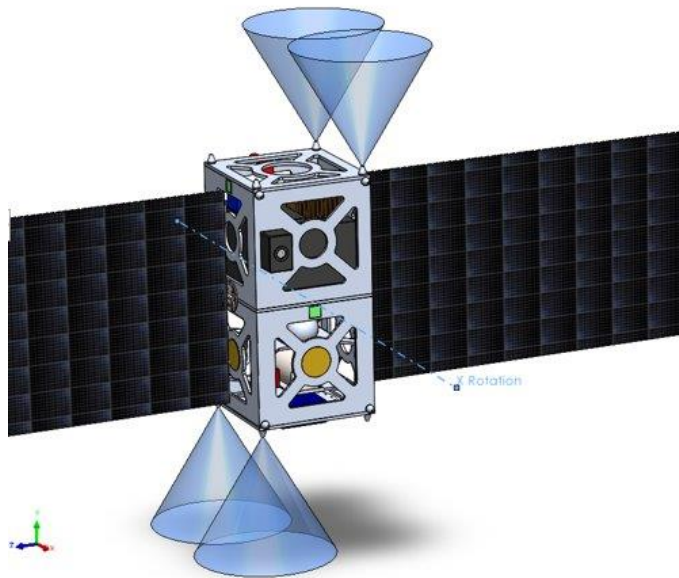


Figure 53. ACS Desaturation Maneuver

The total moment of inertia of the RCS configuration is described in the following equation:

$$h_{saturation} = T L t_b \quad \text{Eq. 15}$$

Where L is the moment arm and  $t_b$  is the burn time. Both Thrust and L are constant, we can calculate the burn time if we know how much momentum ( $h$ ) we want to dump. Consequently, the propellant mass can also be determined.

Following this logic, the total wet mass can be found for each individual monopropellant thruster. The following table presents the results of this comparison.

Table 15. Hydrazine Thruster Selection Matrix

Model	Propellant	Thrust (N)	Mass (kg)	Flow Rate (g/sec)	Isp (s)	Desaturation Time (s)	Propellant Mass (kg)	Total Wet Mass (kg)
MR-103M	Hydrazine	0.99	0.16	0.45	221	61.52	3.37	3.53
MR-103D	Hydrazine	1.02	0.33	0.5	224	59.71	3.33	3.66
MR-111C	Hydrazine	5.3	0.33	2.4	229	11.49	3.25	3.58
MR-106E	Hydrazine	24.1	0.635	13.1	235	2.53	3.17	3.81

For the sake of simplicity, only thrusters that use hydrazine as propellant have been selected. The total mass propellant is determined by assuming that an individual reaction wheel has been desaturated a total of 100 times. The desaturation time represents the total amount of time necessary to desaturate a reaction wheel during a single continuous burn. Given these assumptions, the thruster that requires the least amount of wet mass is the MR-103M, even though its  $I_{sp}$  is lower to the other thrusters (consuming more propellant).

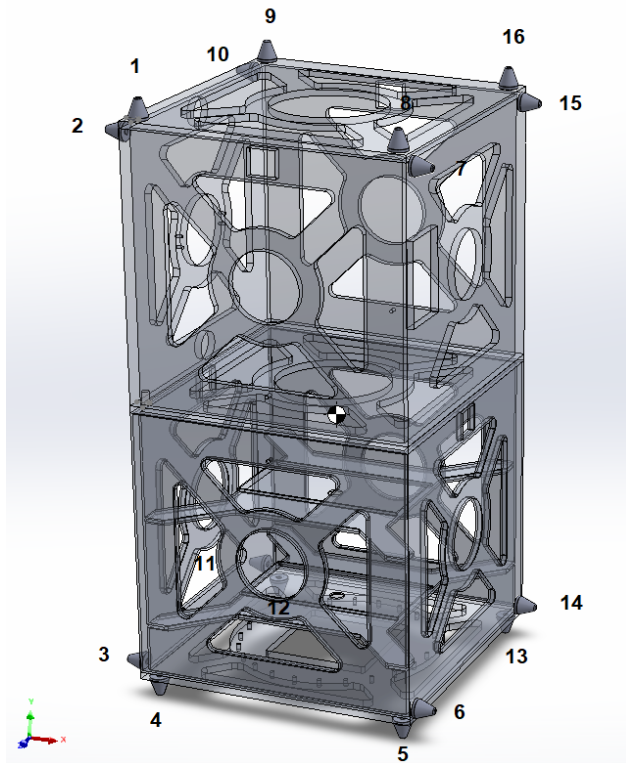


Figure 54. ACS Thruster Integration

Table 16. ACS Thruster pair firing configuration

Axis Rotation	Thruster #
+ x axis	4, 5, 9, 16
- x axis	1, 8, 12, 13
+ y axis	7, 6, 11, 10
- y axis	2, 3, 15, 14
+ z axis	2, 10, 6, 14
- z axis	3, 11, 7, 15

The hydrazine is stored in a cylindrical custom-sized fuel tank with spherical end caps. Designed to hold 3.37 kg of hydrazine at 500 psi, within an internal volume of 0.006 m<sup>3</sup>. The tank is made of Titanium (Ti-6Al-4V) with a tensile strength of 900 Mpa. A safety factor of 2.0 is assumed when calculating the thickness of the spherical endcaps (0.25 mm) and the cylindrical body (0.51 mm).

## 6.3 Control Algorithm

The spacecraft can now determine its current attitude and control its orientation using reaction wheels. The reaction wheels and RCS thrusters are controlled by an on-board computer. Now we must model a control scheme to study the performance of the reaction wheels during the detumbling stage and any reorientation maneuver required. To do so, MATLAB has been used to model both scenarios. A proportional–integral–derivative controller (PID) within a feedback loop system has been used.

### 6.3.1 Detumbling

The detumbling phase commences after the SmallSat has been released from the launch vehicle. The launch vehicle applies a rotation of  $0.5^\circ/\text{s}$  on each axis. To counteract this disturbance, the reaction wheels are actuated enacting a torque and bringing back the angular velocity to zero. The feedback loop system continuously checks the difference between the desired angular velocity and the current angular velocity, the PID controls the amount of torque needed based on this difference.

To properly model the control algorithm, it is necessary to account for the moment of inertia of the spacecraft, that is, the opposition that the SmallSat exhibits to having its angular velocity about an axis altered by the application of a torque. The spacecraft has two mission configurations: launch configuration (folded solar arrays), and mission configuration (deployed solar arrays). The moment of inertia matrix was computed using SolidWorks.

$$J_{launch\ config} = \begin{bmatrix} 23.97 & -0.41 & -0.05 \\ -0.41 & 8.28 & -0.04 \\ -0.05 & -0.43 & 23.40 \end{bmatrix} kgm^2$$

$$J_{mission\ config} = \begin{bmatrix} 51.35 & -0.46 & -0.06 \\ -0.46 & 34.07 & -0.05 \\ -0.06 & -0.48 & 24.38 \end{bmatrix} kgm^2$$

The spacecraft's moment of inertia will influence the settling time of the detumbling analysis. Where the settling time measures the amount of time it takes to detumble all axes of rotation, which coincides with the settling time of the axis with the largest moment. This difference is apparent in Figure 51, where the the x axis takes 18.25 s to detumble.

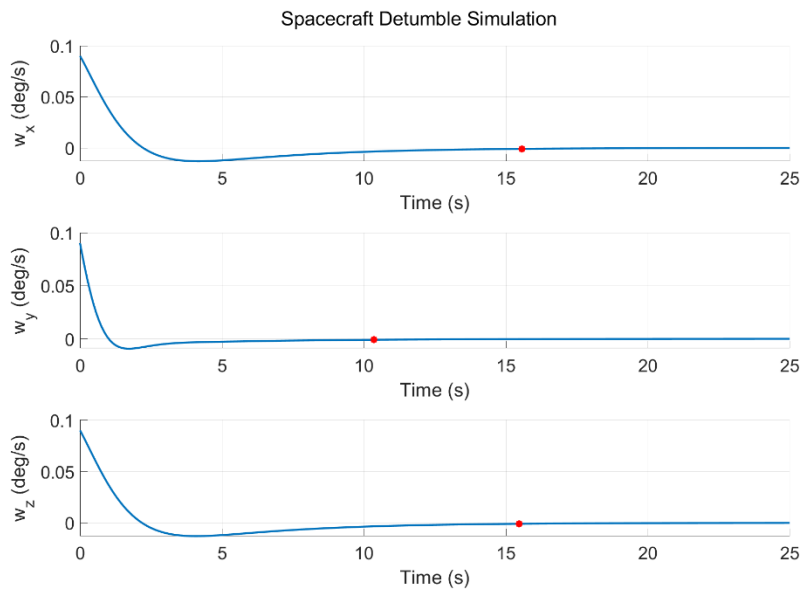


Figure 55. Detumble Simulation (Launch Configuration)



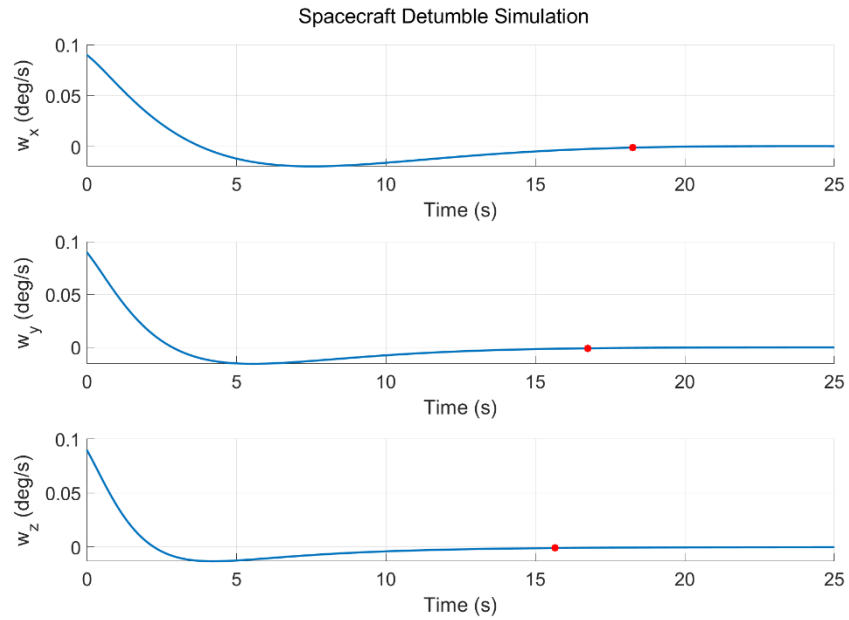


Figure 56. Detumble Simulation (Mission Configuration)

The analysis determines that the detumbling maneuver should take place before solar array deployment. Reducing the settling time from 18.25 s to 15.56 s and minimizing the total reaction wheel saturation from 0.24 Nms to 0.11 Nms. The detumble maneuver is well within the 67.8 Nms saturation constraint. In the next simulation the momentum storage will be tested with larger rotation maneuvers.

### 6.3.2 Slew Maneuver

The reaction wheels have been proven through analysis to be sufficient for stabilization against small perturbations like the initial launch vehicle separation stage. The ADCS control system must also be able to perform larger pointing maneuvers during the mission to properly point to Earth and send data. For this simulation, a worst-case scenario 180-degree turn will be performed on each axis to prove that the spacecraft can rotate freely within the reaction wheel saturation limits. For this case we will assume that the solar arrays are deployed as well as take into consideration the 0.7 Nm maximum torque that the reaction wheels can produce. This is a

rest-to-rest slew maneuver, the spacecraft begins at rest and must also come to a final rest at the desired angle of rotation. The PID algorithm employs a level of anticipation to slow down the spacecraft before it encounters its desired destination, or else it would overshoot. Although, some level of overshoot is acceptable for our application as long as the spacecraft reaches the desired angle.

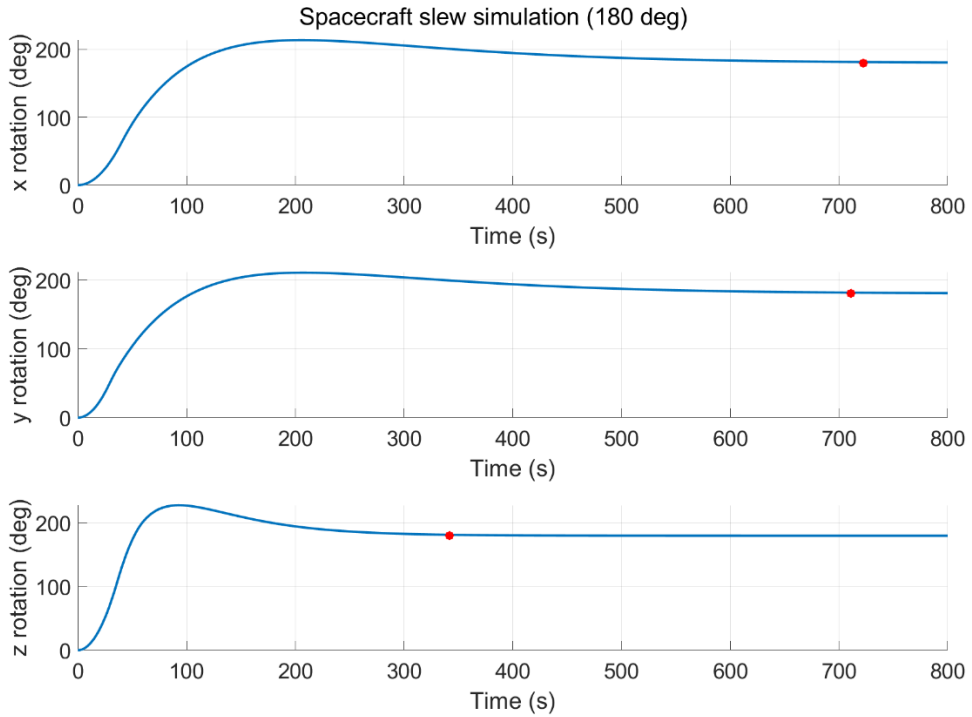


Figure 57. 180 degree Slew Maneuver (Mission Configuration)

## 7 Communications

The communications subsystem involves all communications between the spacecraft and the ground stations on Earth. The communication architecture consists of an on-board computer with flight software, a radio transceiver, and an antenna. The specific ground station that will be communicated with must be determined when designing the communication architecture, as the ground station must be compatible with the radio frequency required for the mission. More specifically, the antenna size must be large enough to receive the incoming signals. This section describes the components chosen for the communication subsystem architecture. This section also presents analysis and simulations of the spacecraft's connection to ground stations, which will be used to calculate the data budget for the spacecraft.

### 7.1 Communications Architecture

A communications architecture is a network of satellites and ground stations interconnected by communication links. Communication links allow a satellite system to function by carrying tracking, telemetry, and command data or mission data between its elements. For the ISS VOPEd, the communication architecture will consist of the ground station, the on-board computer, the radio transceiver, and the antenna. The following sections will provide information about each component of the communication architecture (Larson & Wertz, 1992).

#### 7.1.1 Ground Station

The ground station that will be used for this mission is the Deep Space Network (DSN). The Deep Space Network is operated by NASA's Jet Propulsion Laboratory, The DSN consists of three facilities spaced equidistant from each other – approximately 120 degrees apart in longitude

– around the Earth. These sites are at Goldstone, California; near Madrid, Spain; and near Canberra, Australia. (Monaghan) The strategic placement of these sites permits constant communication with spacecraft as Earth rotates – before a distant spacecraft sinks below the horizon at one DSN site, another site can pick up the signal and carry on communicating. Each facility consists of multiple large antennas, the largest being the 70-meter antenna (Tzini).

Using Systems Toolkit (STK) a simulation of the spacecraft’s access to the ground station can be modeled. Using this model, the duration of a single access window can be determined. Knowing the duration of a single access window will determine the limit to the amount of data that can be uplinked to the ground station in one access window.



Figure 58. Goldstone and Madrid DSN Sites Modeled in STK

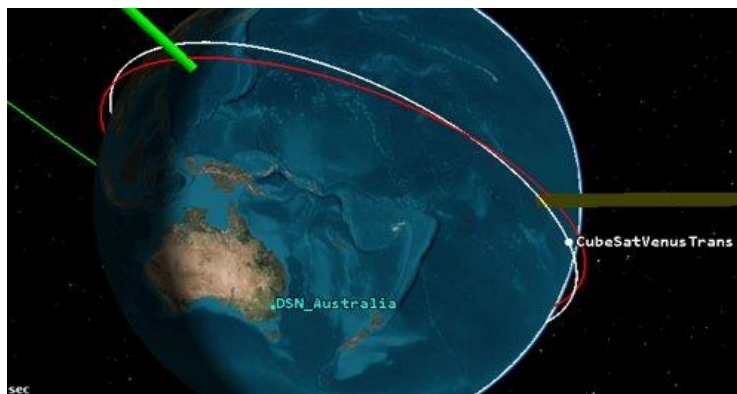


Figure 59. Canberra DSN Site Modeled in STK

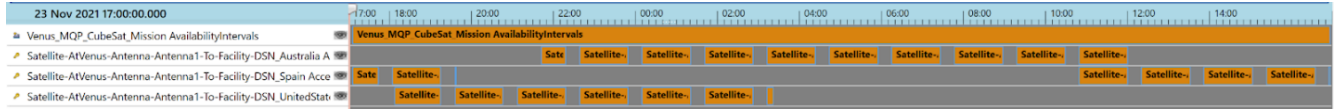


Figure 60. Access Windows from Satellite to DSN Ground Stations

The access windows shown above demonstrate the access windows available to the ISS VOPED when orbiting Venus. When the ISS VOPED is not in an eclipse, it always has access to at least one of the DSN ground Stations. The mean duration for a single access window calculated in STK was 3,715 seconds. The average amount of access windows in a 24 hour period is 15, so the total access window duration in one 24 hour period is 55,725 seconds.

### 7.1.2 On-Board Computer

The on-board computer (OBC) has many functions, namely: Attitude and orbit control, telemetry data management, telecommunication actions, system housekeeping, on-board time synchronization, and failure detection, isolation, and recovery. Mainly, the OBC processes all data coming from the ground station and sends commands to all other subsystems. It comes with flight software installed to manage the spacecraft's trajectory. For the purposes of our mission, a lightweight and low power consuming OBC was desired. The Kryten-M3 OBC from Clyde Space fit the required design specifications, so it was chosen for this mission. Additionally, the previous interplanetary satellite mission design MQP team, where the mission was to design satellite to send to the Iris 7 asteroid, also used this OBC (Mayer et al., 2021). Other options considered for the OBC were the ABACUS 2017 and the CubeSat On-Board Computer from German Orbital Systems. Below is a table comparing some of the specifications of the options considered.

Table 17. On-Board Computer Comparison Matrix (Satsearch, nd.)

<b>OBC</b>	<b>Size Dimensions (mm)</b>	<b>Mass (g)</b>	<b>Flash memory</b>	<b>Power</b>
<b>Kryten-M3</b>	95.89x90.17x23.24	61.9	4 GB	400mW (nominal) – 1 W (max)
<b>ABACUS 2017</b>	90.14x95.86x23.24	62	32 MB	650 mW (max)
<b>German Orbital Systems OBC</b>	90x96x24	64	2GB	1.65 W (max)

Comparable to other OBC, the Kryten M-3 is both light-weight, and power-efficient. It has a mass of 61.9 kg and a maximum power usage for the of 1 Watt. For data storage, it contains 4 GB of SLC flash memory. If additional memory is needed, a microSD card slot is available for memory expansion. The OBC is supplied with a BSP including bare drivers and a FreeRTOS port. The OBC is compatible with Gen1 and software support from Bright Ascension Limited (BAL) is available. Below are the specifications and dimensions of the Kryten-M3 OBC.

## Technical Specifications

### General

Design Life	5 years in LEO
Processor	Smart Fusion 2 SoC including an ARM Cortex-M3 processor delivering 62.5 DMIPS
Processor Clock	50 MHz
SCET	Real time counter (w/40mins. Backup Power)
MRAM	8 MB
Operating Temperature Range	-40°C to +80°C
Boot Image Storage	256 kB eNVM + 8MB MRAM
Radiation (TiD)	20 kRAD
Typical Energy Usage	6.4 mJ/DM
GPS (PLUS model only)	<10m RMS position accuracy <1m/s RMS velocity accuracy

Figure 61. Kryten-M3 Data Sheet Specifications

### Interfaces

I2C		2
SPI	7 Chip Select Lines	1
UART	3.3 V Logic	8
RS422	(can be used as 2xRS485)	1
CAN		1
DTMF		1
	JTAG w/ETM Support + 1 Serial	
Debugging	Debug	1
LVDS	20x Lines, Expansion	1
QSPI	[2x LVDS, 1x 3V3 Logic]	3
GPIO	3.3 V Logic	17

\* Not all interfaces available simultaneously

### Size, Weight and Power

Nominal Power Consumption	400 mW (typ), 1 W max
Mass	61.9 g
Length	95.89 mm
Width	90.17 mm
Height*	5.51 mm

Figure 62. Kryten-M3 Data Sheet Specifications

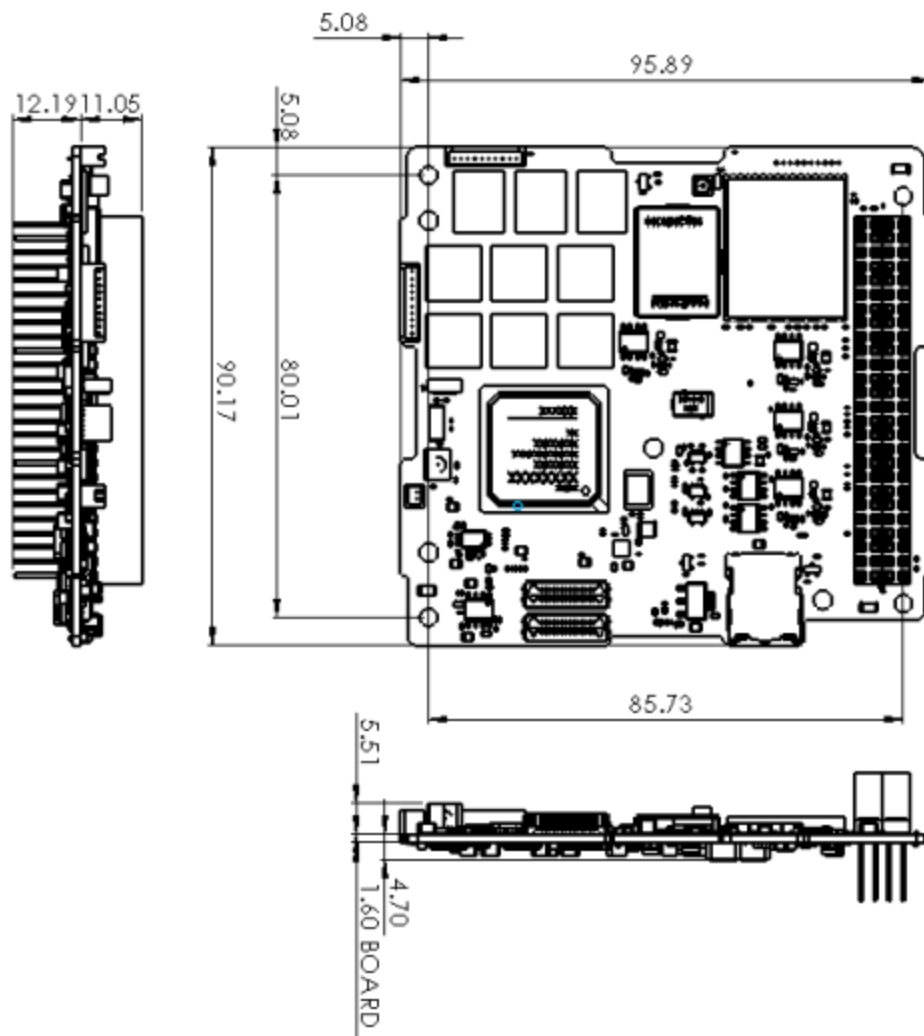


Figure 63. Kryten-M3 Dimensions

### 7.1.3 Radio

On a spacecraft, the radio is used to communicate with the ground stations. It can be composed of many different parts, or the individual parts can come compact together in one device. The components consist of an antenna, a transponder, and a receiver. Often, the transponder and receiver are combined into one device named a transceiver. Communications with spacecraft and ground stations utilize ultra-high frequency radio waves.



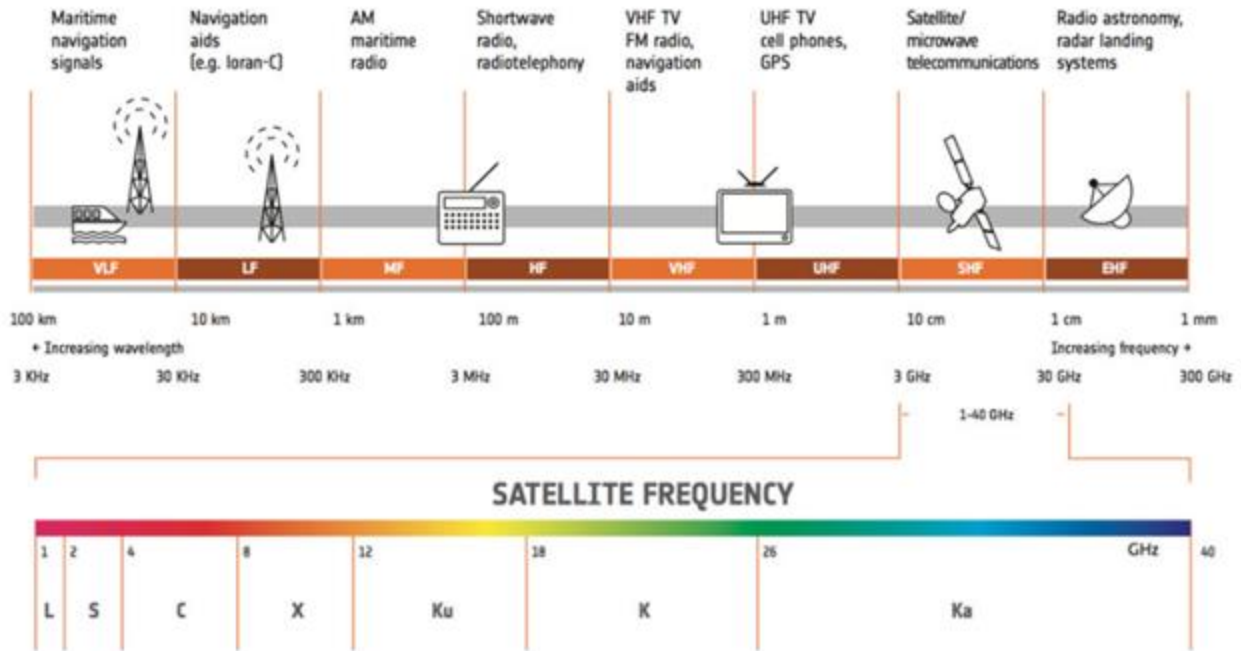


Figure 64. Satellite Frequency Bands

SmallSat and CubeSat radios and antennas are typically S-band, as these types of spacecraft rarely leave Earth orbit. However, most interplanetary missions utilize X-band and even K-band communication for the higher bandwidth. This offsets the large distances that the signal travels, at the cost of more power and more complex radios and antennas. Fortunately, a SmallSat radio capable of X-band communication: the Iris Deep Space Small Satellite Radio. Developed by the Jet Propulsion Laboratory, it utilizes a Solid-State Power Amplifier (SSPA) and a Low Noise Amplifier (LNA) to amplify the received radio frequency signal. The design specifications of the Iris Radio are shown below.

MASS & POWER SPECIFICATIONS		
Transponder Stack Mass	875 g	
LNA Mass	≤125 g	
SSPA Mass	≤230 g	
Transponder Envelope	101 x 101 x 56 mm	
LNA Envelope	114.3 x 46.0 x 15.5 mm	
SSPA Envelope	102.9 x 55.7 x 24.4 mm	
Input Supply Voltage	12–28 VDC	
Input Supply Power	0.5–35 W	
	Mode	DC Input (W)
	Battery Connect	<0.04
	X-Receive Only	10.3
	X-Transmit Only	29.6
X-Transmit/Receive	33.6	



Figure 65. Iris Radio Mass and Power Specifications

TRANSPONDER SPECIFICATIONS	
X-Band Uplink Frequency Range	<ul style="list-style-type: none"> <li>• 7.145–7.190 GHz (channel assignment programmed in firmware)</li> <li>• 7.190–7.235 (near Earth supported)</li> </ul>
X-Band Downlink Frequency Range	<ul style="list-style-type: none"> <li>• 8.400–8.450 GHz (channel assignment programmed in firmware)</li> <li>• 8.450–8.500 (near Earth supported)</li> </ul>
Other Bands	<ul style="list-style-type: none"> <li>• S-band: Deep space<sup>(1)</sup>/near Earth<sup>(1)</sup></li> <li>• Ka-band: Deep space<sup>(1)</sup>/near Earth<sup>(1)</sup></li> <li>• UHF: 390–450 MHz receive, transmit<sup>(1)</sup></li> </ul>
Coherent Turnaround Ratio	<ul style="list-style-type: none"> <li>• X-band: 880/749</li> <li>• Standard S- &amp; Ka-band ratios<sup>(1)</sup>, arbitrary ratios</li> </ul>

RECEIVER SPECIFICATIONS	
Noise Figure	2.2 dB X-band
Carrier Tracking Signal Range	-70 to -130 dBm
Tracking Range	100 MHz

Figure 66. Transponder and Receiver Specification

In addition to the transceiver and amplifiers, the spacecraft radio requires an antenna to receive the radio communications coming from the ground station. CubeSats often utilize patch antennas with small apertures and low gains as this is all that is necessary for communications in Low Earth Orbit. Patch antennas consist of a patch of conductive material that is etched onto a dielectric substrate. This dielectric material is mounted on a ground plate that consists of a metal with high conductivity. For patch antenna, the common material for ground plates is copper, so that will be the material used for the ISS VOPED’s patch antenna. The dielectric substrate that our patch antenna array will use is polytetrafluoroethylene, commonly known as Teflon™. Teflon™ is a common substrate used in patch antennas, with a dielectric constant  $\epsilon_r = 2.1$ .

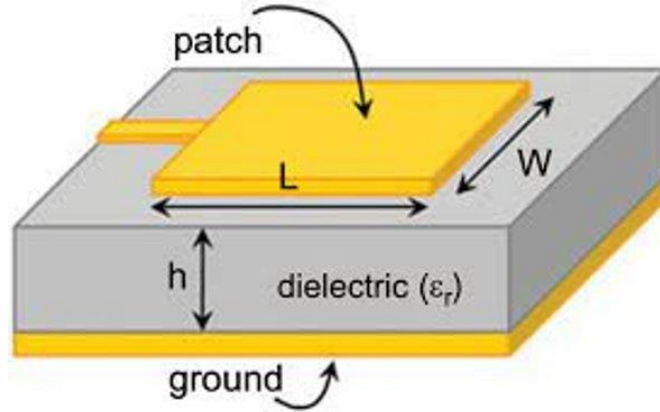


Figure 67. Patch Antenna

As the specifications in figure 65 shows, the frequency that will be used to communicate will be 7.2 GHz for uplink and 8.4 GHz for downlink. To calculate the aperture size for a patch antenna receiving 8.4 GHz, following equations are used to calculate the length and width of the aperture (Pasternack):

$$Width = \frac{c}{2f_o \sqrt{\frac{\epsilon_R + 1}{2}}} \quad \text{Eq. 16}$$

$$\epsilon_{eff} = \frac{\epsilon_R + 1}{2} + \frac{\epsilon_R - 1}{2} \left[ \frac{1}{\sqrt{1 + 12 \left(\frac{h}{W}\right)}} \right] \quad \text{Eq. 17}$$

$$Length = \frac{c}{2f_o \sqrt{\epsilon_{eff}}} - 0.824h \left( \frac{(\epsilon_{eff} + 0.3) \left(\frac{W}{h} + 0.264\right)}{(\epsilon_{eff} - 0.258) \left(\frac{W}{h} + 0.8\right)} \right) \quad \text{Eq. 18}$$

where  $h$  is the dielectric height,  $\epsilon_r$  is the dielectric constant,  $c$  is the speed of light and  $f_o$  is the resonant frequency. A dielectric height of 6 mm and a dielectric constant of 2.1 were used to calculate the width and height of the aperture. The resulting length was 7.8 mm and width of 14.343 mm. To calculate the patch aperture area, the length is multiplied by the width. The final

aperture area for a single patch antenna was  $111.875 \text{ mm}^2$ . With the efficiency of the antenna estimated to be 0.41. The effective aperture can be calculated with the equation:

$$A_e = \mu A \quad \text{Eq. 19}$$

The gain of the antenna, which is calculated in the next section, is too low if just one patch antenna with a length of 7.8 mm and width of 14.34 mm is used. To resolve this issue, an array of 10 of the custom patch antennae can be made. The aperture area of the ten antenna combined into an array is  $1118.75 \text{ mm}^2$ . The efficiency of the antenna is 0.41, so the effective aperture area is  $458.8 \text{ mm}^2$ .

## 7.2 Data and Storage

Storing data on spacecraft is common, as most spacecraft cannot be in constant communication with a ground station due to the satellite's orbit and Earth's rotation. Even in geosynchronous orbit (GEO), it is difficult for spacecraft to maintain constant communication with ground stations. Factors such as position, velocity, and atmospheric inference limit the spacecraft's communication with the ground stations. Because of this, spacecraft must store their data before it can be transmitted to a ground station. The amount of storage space required depends on the rate at which the spacecraft's payload or other sensors produce data, as well as the total amount of data that will be produced. The Kryten-M3 OBC contains 4 GB of flash storage (Kryten-M3). Additionally, some payload instruments also have built-in data storage.

Once a spacecraft enters the access window of a ground station, it must downlink as much data as possible. To calculate the amount of data that can be downlinked and uplinked per second, the equations provided in the following section will be utilized.

### 7.2.1 Data Rate Equations

Calculating the satellites functional data transfer rate requires knowing or calculating the following parameters: Effective aperture of ground and satellite antenna; antenna gain; signal power density; received power; total noise; data size; time to transfer. Using the effective aperture calculated in section 7.13, the gain for the patch antenna is found with

$$G = 4\pi A_e / \lambda^2 \quad \text{Eq. 20}$$

where  $\lambda$  is the wavelength of the communication frequency. The received power density is then calculated with

$$\rho = \frac{P_t G}{4\pi R^2} \quad \text{Eq. 21}$$

where  $P_t$  is the transmitted power from the transceiver and  $R$  is the distance to Venus. The received power is calculated with

$$P_r = \rho A_e \quad \text{Eq. 22}$$

The data rate for a telemetry link is calculated using the Shannon-Hartley Capacity theorem:

$$C = B \log_2 \left( 1 + \frac{S}{N} \right) \quad \text{Eq. 23}$$

The  $S$  in the Shannon-Hartley Capacity theorem is equal to the received power  $P_r$ , which was calculated with Eq. 22, and  $B$  is the bandwidth of the signal (equal to the wavelength used to calculate the gain). The  $N$  in Eq. 23 is the noise in the signal, which is calculated with

$$N = kTB \quad \text{Eq. 24}$$

where  $k$  is the Boltzmann constant ( $1.38064852e - 23 \text{ m}^2 \text{ kg s}^{-2} \text{ K}^{-1}$ ) and  $T$  is the operating temperature of the amplifier in the transceiver.

### 7.2.2 Data Rate Calculations

Using the equations from the previous section, the data transfer rate for uplink and downlink for the spacecraft can be calculated. The following table shows the calculated values as well as the final data transfer rate for uplink and downlink.

Table 18. Data rate calculation values

<b>Property</b>	<b>Downlink (ISS VOPEd to DSN ground stations)</b>	<b>Uplink (DSN ground stations to ISS VOPEd)</b>
Distance (km)	127,437,349	127,437,349
Power density ( $W/m^2$ )	1.289E-20	1.955E-12
Receiving Aperture ( $m^2$ )	3800	0.1735
Receiving Antenna Efficiency	0.67	0.41
Effective Receiving Aperture ( $m^2$ )	2546	4.588E-04
Received Power (W)	3.282E-17	1.388E-13
Amplifier Temperature (K)	28.5 K	273 K
Bandwidth (GHz)	8.4	7.2
Noise (W)	3.30527E-12	2.693E-11
Signal to Noise Ratio	9.930E-06	0.00515
Data Capacity (MB/s)	3.1976E-04	6.3172

From Table 18, the data rate for downlink (ISS VOPED to DSN ground stations) is  $3.1976 \times 10^{-4}$  MB/s. As mentioned in a previous section, by using STK, the average access was found to be 3715 seconds. By multiplying the data transfer rate by the access window duration, it is found that 1.1879 MB of data can be transferred in a single access window. The average amount of access windows in one 24 hour period is 15, so the total access window duration in one 24 hour period is 55,725 seconds. The total data transfer budget for one 24-hour period is 17.8185 MB.

The SPICAV/SOIR has a data volume of 100 - 400 Mbits/day, so the total amount of data for downlink in one 24-hour period is 11.92 MB – 47.6837 MB. If the SPICAV/SOIR produced its maximum capacity every day (47.6837 MB) , and if the maximum data transfer was completed every access window, it would take about 124 days to fill up the 4 GB of storage in the Kryten-M3 OBC. Because our mission duration is greater than 124 days, extra storage is needed. Fortunately, the Kryten-M3 has a microSD port for extra storage capacity. For simplicity reasons, if the mission duration is 5 years, then 55 GB of extra storage is needed. This was calculated by assuming 29.8652 MB/day ( $47.6837 - 17.8185$ ) for 1825 days. Thus, a microSD card with at least 55 GB of storage will be needed. To be safe, a microSD card with 256 GB can be used, as these are affordable and can be purchased easily (*SanDisk*®). With this extra storage, the ISS VOPED will not run out of storage for the SPICAV/SOIR data.

## 8 Thermal Control

The environments the ISS VOPEd will encounter on its mission are vastly different from the environment on earth and change depending on its point in the mission. This presents challenges for controlling the thermal environment of all the components on-board. All spacecraft components have a range of temperatures which they need to be within to continue to function. The thermal control system's objective is to keep all the components within these ranges throughout all phases of the mission. This section covers the thermal control system, including background information, analysis, and component selection.

### 8.1 Thermal Control Background

The environment in space is extremely volatile ranging from temperatures close to absolute zero to hundreds of degrees above freezing. Within the solar system spacecraft are also exposed to radiation from the sun which can be damaging to the spacecraft or any of its components. It is the thermal control systems job to ensure all the components survive and operate in this harsh environment.

Components onboard the SmallSat cannot shed heat as they would on earth because there is no atmosphere in space. The only way to expel, or absorb, heat is through radiation. Radiation is the emission or transmission of energy, as waves, into space through a surface. The sun's radiation is intense, ranging from 1300 to 1400 W/m<sup>2</sup> outside the Earth's atmosphere to almost 2700 W/m<sup>2</sup> outside the atmosphere of Venus. The radiation energy is proportional to the fourth power of the temperature, as described by

$$P = \varepsilon\sigma A (T^4 - T_0^4) \quad \text{Eq. 25}$$

where P is the net heat flow,  $\varepsilon$  is the emissivity,  $\sigma$  is the Stefan-Boltzmann constant, A is the surface area of the object emitting or absorbing the thermal radiation, T is the absolute



temperature of the object emitting or absorbing the thermal radiation, and  $T_0$  is the absolute temperature of the environment.

From the known value of solar flux at Venus, an average of about  $2630 \text{ W/m}^2$ , the temperature the spacecraft will encounter will be over  $200^\circ\text{C}$ . This is only while the satellite is in direct sunlight. When the satellite is out of direct sunlight there will be little radiation changing the satellite's temperature from extreme hot to extreme cold. The temperature of space is about 3 K. These drastic changes in temperature are called thermal shock. Thermal shock is an abrupt change in temperature that can cause materials and components to break if not protected properly.

### 8.1.1 Passive Systems

Small spacecraft usually cannot support complex thermal control systems due to their size, volume, and limited power supply. There are two broad categories of thermal control systems, passive and active. Passive thermal control systems do not require power to operate. SmallSats, generally, only use passive systems because they are relatively low cost, take up less space, have lower mass, and are highly reliable compared to active systems.

Film, coatings, and thermal insulation are some of the simplest passive systems. There are many different kinds of films and coatings to serve different needs of missions. These surface finishes change the emittance and absorbance of the spacecraft or its components without changing the functionality at all. Certain finishes can decrease the absorbance so the surface heats up slower when exposed to solar radiation. White paint for example has a solar absorption value of between 0.05 and 0.2, where black paint can have an absorption rate of up to 0.98. The white coating would increase the emittance of radiation from the spacecraft or its components. The black coating would increase the absorbance of solar radiation which can be useful as a passive heating method for

other components that could require more heating. Figure 68 shows the absorbance and emittance behaviors of different colors by their wavelength.

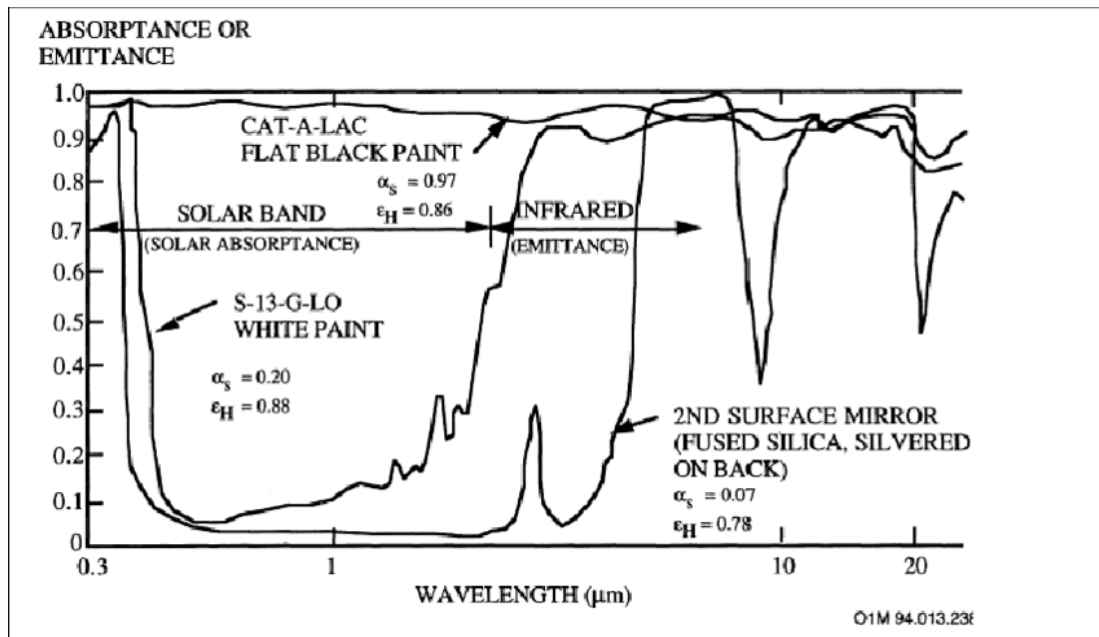


Figure 68. Absorbance and Emittance by Wavelength/Color (L. V. Pisacane, 2016)

Along with different color paints, different materials or finishes can be applied as coatings to the spacecraft or its components to achieve similar results. Gold plating is common on many satellites because it is reflective, malleable, and both electrically and thermally conductive. These help keep the inside components cooler, make it easy to apply to any design and make it easy for it to dissipate heat generated from radiation. Treating bare metal can also provide effective finishes, although not always as good as many external alternatives and generally have a low emittance value. Figure 69 shows the absorption and emittance behaviors of different materials and coatings. Other materials can increase the emittance to emit excess radiation faster.

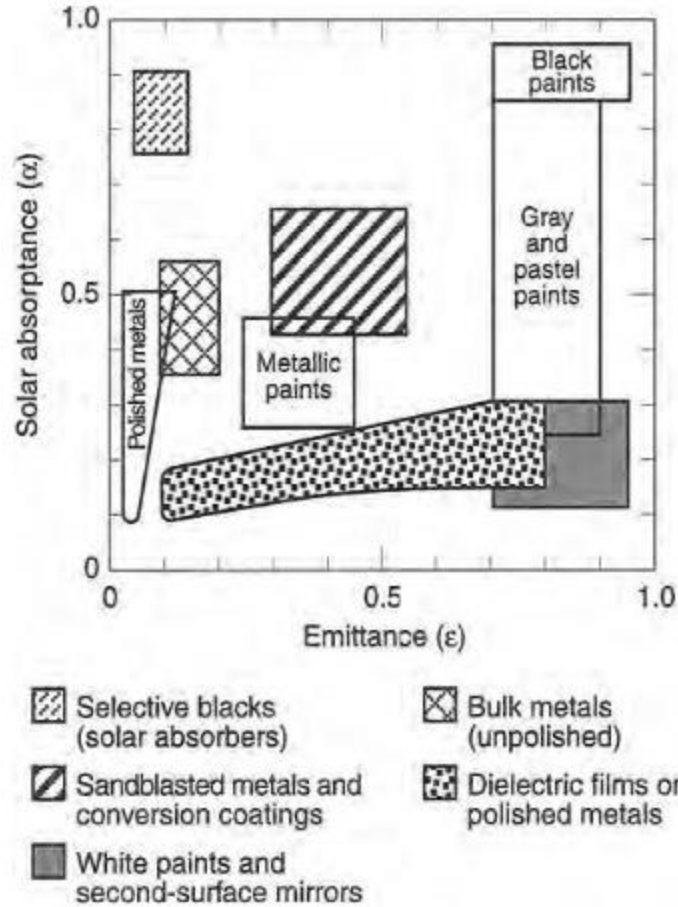


Figure 69. Absorbance and Emittance by Material (D. G. Gilmore, 2002)

Multi-layer insulation (MLI) is another simple passive system. It is used as a radiation barrier from solar and infrared flux. MLI is commonly used to insulate electronics and batteries. MLI is useful in that it can insulate electronics so the heat the components generate can be used to heat itself without relying on an external source. Their efficiency drops as its size decreases, making it less ideal for SmallSats. Surface coatings and film are more commonly used because they are less delicate and better suited for the exterior of the spacecraft.



Figure 70. Flexible Thermal Straps (Felt, 2017)

Other passive thermal systems used in spacecraft include thermal straps, sunshields, thermal louvers, heat pipes, and heat switches. Flexible thermal straps can effectively transfer heat to a heat sink and can be custom made. Sunshields are used to divert or reduce incoming solar radiation to the spacecraft. Thermal louvers use a bimetallic spring to control its flaps by expanding or contracting according to their temperature, modifying the exterior's emissivity. Louvers are often used on larger spacecraft and sometimes are considered an active system, but they require no power. Heat pipes transfer heat using temperature gradients from electronics to a heatsink or

radiator. Heat switches can change between being a conductor or a thermal insulator to help control the temperature of electronics or internal components.



Figure 71. Thermal Louver (“CubeSat Form Factor Thermal Control Louvers)

### 8.1.2 Active Systems

Active thermal control systems use input power to operate and are much more effective than passive control systems at maintaining internal component temperatures. Active systems are generally used on large spacecraft that have ample power budgets and have more sensitive components or payloads. These systems are much more complex and have lower reliability than passive systems. Examples of active thermal control systems include heaters, cryocoolers, and radiators. Heaters are typically electrical resistors that heat up when current is run through them and can maintain electrical components while in cold cycles. Cryocoolers are cooling devices that can cool up to 100 K and used with equipment such as high precision IR sensors. Radiators are used to remove heat but are limited by their size and temperature.

### 8.1.3 Target Temperatures

Thermal control systems are designed to keep internal components within their operating temperature while they are working and their survival temperature while they are not. All components have operating and survival temperature. Operating temperature is the temperature where the components can function properly to achieve its task. Survival temperature is the temperature limit the component can withstand before suffering permanent damage. Electronics and batteries generally have the narrowest range of allowable temperatures, making the thermal control system cater to their temperature requirements. Every component has a different range for their operating and survival temperatures which is identified in Table 19.

Table 19. Component Operating and Survival Temperatures

<b>Components</b>	<b>Operating Temp Minimum (C)</b>	<b>Operating Temp Maximum (C)</b>	<b>Survival Temp Minimum (C)</b>	<b>Survival Temp Maximum (C)</b>
<b>Digital Electronics</b>	0	50	-20	70
<b>Analog Electronics</b>	-30	40	-40	70
<b>Battery</b>	10	20	0	35
<b>Payload</b>	-35	0	-35	35
<b>Reactions Wheels</b>	0	50	-20	70
<b>Solar Panels</b>	-100	125	-100	125
<b>Star Tracker</b>	-40	30	-40	70
<b>Sun Sensor</b>	-45	85	-55	115

#### 8.1.4 Thermal Analysis Tool

Thermal analysis can be complex and often requires the use of computational analysis tool for accurate results. Using the program COMSOL Multiphysics, a finite element analysis and solver software, the thermal control subsystem team can perform thermal analysis of the SmallSat. COMSOL Multiphysics is designed to solve physics-based simulation for fluid, electrical, thermal,

and dynamic structural analysis. The heat transfer and surface-to-surface radiation modules were used to conduct in-depth thermal analysis of the SmallSat.

## 8.2 Thermal Analysis

To conduct thorough and accurate thermal analysis, the environment around the spacecraft must be determined. The next step is to determine the power distribution and thermal properties on all the materials of the spacecraft's components. Once the environment and thermal properties of the spacecraft have been determined thermal analysis can be simulated in COMSOL Multiphysics.

### 8.2.1 Solar Radiation

Incoming solar radiation is the primary source of heat applied to the spacecraft. Especially as the spacecraft moves towards Venus, and closer to the sun, the solar radiation becomes more intense. Solar radiation decreases at an inverse square rate as given by Eq. 26:

$$S = \frac{L}{4\pi r^2} \quad \text{Eq. 26}$$

Where  $S$  is solar flux, in  $\text{W}/\text{m}^2$ , and  $r$  is the distance from the sun, in meters. The average solar flux at Earth is  $1367 \text{ W}/\text{m}^2$  but can range from  $1317 \text{ W}/\text{m}^2$  to  $1419 \text{ W}/\text{m}^2$  depending on where Earth is in its orbit. As Venus is about 0.7 AU from the sun, or about  $1.08 \times 10^{11} \text{ m}$ , the average solar flux at Venus would be  $2624 \text{ W}/\text{m}^2$ . Figure 72 shows the inverse square relationship of solar flux to distance from the sun from 0.3 AU to 1.6 AU, encompassing the planets Mercury to Mars.



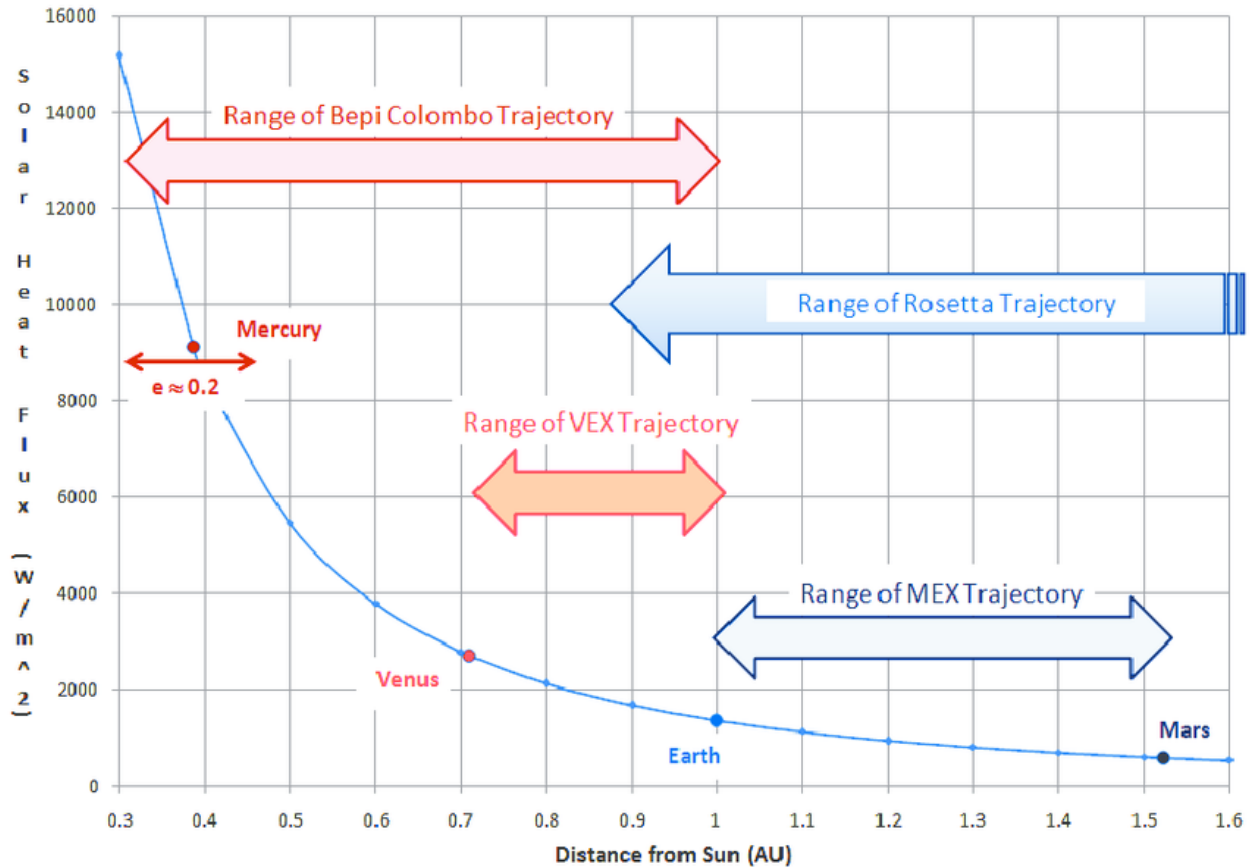


Figure 72. Solar Flux as a Function of Distance (Van der Ha, 2010)

While the solar flux will increase as the spacecraft moves towards Venus, once it reaches Venus orbit it will only be exposed to solar flux while it is between Venus and the sun. While the spacecraft is in eclipse it will receive no radiation and be exposed to the cold temperature of space, about 2.7 K. The thermal analysis will have to account for both phases of orbit on the space.

### 8.3 COMSOL Multiphysics Thermal Analysis

COMSOL Multiphysics was used to create both a 2D and 3D thermal model of the spacecraft to simulate the thermal environment of the spacecraft on its mission to Venus. This software was chosen based on work from previous MQP groups as well as its ease of use with

CAD models from Solidworks and STK. To conduct the thermal analysis two programs were used, Heat Transfer in solids and Surface-to-Surface Radiation. These two modules are best suited to analyze the thermal environment of the spacecraft in route to and orbit of Venus.

### 8.3.1 Set Up

The setup of the COMSOL simulation is critical to maintain continuity throughout the whole simulation, especially using two different modules for analysis. The spacecraft is assumed to be at a 90° angle with the incoming solar radiation with the payload pointed towards the sun. Due to the length of the mission COMSOL analysis is not possible for the entire duration of the mission. To simplify the analysis the spacecraft will be analyzed at two points, at Earth and at Venus. Table 20. shows the distance from the sun and the projected time of Flight.

<b>Analysis Point</b>	<b>Radius (AU)</b>	<b>Time of Flight (days)</b>
GEO Orbit	1	0
Venus Orbit	0.7	121

Table 20. Analysis Points

In the setup of the thermal model in COMSOL some of the spacecraft components were simplified to aid in the simulation speed and mesh of the model. The COMSOL model used was developed by the structural subsystem in SolidWorks and saved as a .STEP file to preserve all the details when transferring to COMSOL. The model is a Time-Dependent Heat Transfer in solids with Surface-to-Surface Radiation to accurately model the incoming radiation as well as transfer of heat from each component to another.

Each component within the spacecraft is complex, but COMSOL must define each as one material to simulate the thermal conductivity throughout the model. Each material was selected from COMSOL’s database of materials, and some properties of each material have to be used

manually, surface emissivity for example. Table 21 lists each component and the material assigned to it.

<b>Component</b>	<b>Material</b>
Spacecraft Structure	6061-T6 Aluminum
Payload	High Density Polyethylene
Battery	LiCoO <sub>2</sub>
On-Board Computer	FR-4 (PWB)

Table 21. COMSOL Material List

The overall geometry of the spacecraft is modeled from assembly as opposed to from union. From assembly means that heat will only transfer if the boundaries are in contact. Identity pair was selected in addition to from assembly after switching from from union to model radiation between the different sides of the cube.

The mesh was created using the physics-controlled sequence type and a fine element size. The mesh size in the spacecraft model is not uniform across the entire body. As seen in Figure 73, the mesh is denser around the hinges of the solar panels and less dense on the solar panels themselves. The thermal analysis will be more detailed in the areas with denser mesh as opposed to the areas with less dense mesh which are expected to have a uniform and simple temperature distribution. The mesh included some thin surfaces that are smaller than the minimum specified temperature side which can cause errors, however, when finer mesh size was selected the simulation did not converge.

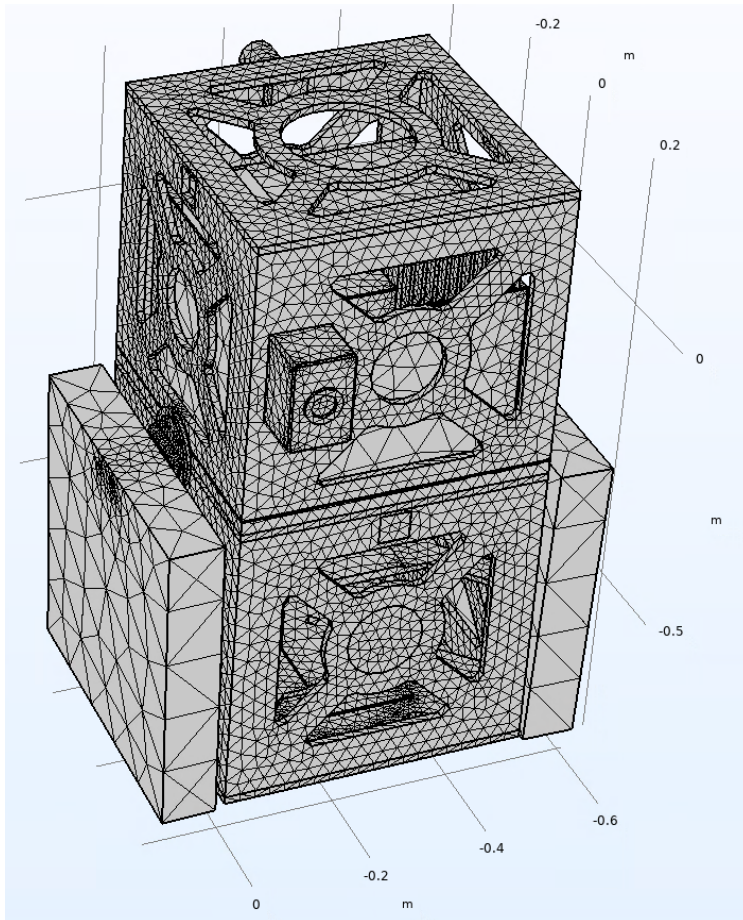


Figure 73. Spacecraft's Thermal Mesh

Both solar radiation and generated heat from internal electronics were considered in the Power usage for each component was given by each corresponding subsystem. Surface-to-Surface-Radiation between faces was selected through the Diffuse Surface module. The incoming solar radiation was modeled as an external radiation source an infinite distance away. The solar flux values used are shown in Table 22 .

Table 22. Solar Radiation

<b>Radiation Source</b>	<b>At Earth</b>	<b>At Venus</b>
<b>Solar Flux (W/m<sup>2</sup>)</b>	1419	2624

The COMSOL model was simulated over a 24 hour period with a time step of one hour. The setup for the analysis of internal components dissipation and Heat Transfer in Solids is shown in Figure 74. The setup for the analysis of Surface-to-Surface Radiation including external radiation is shown in Figure 75.

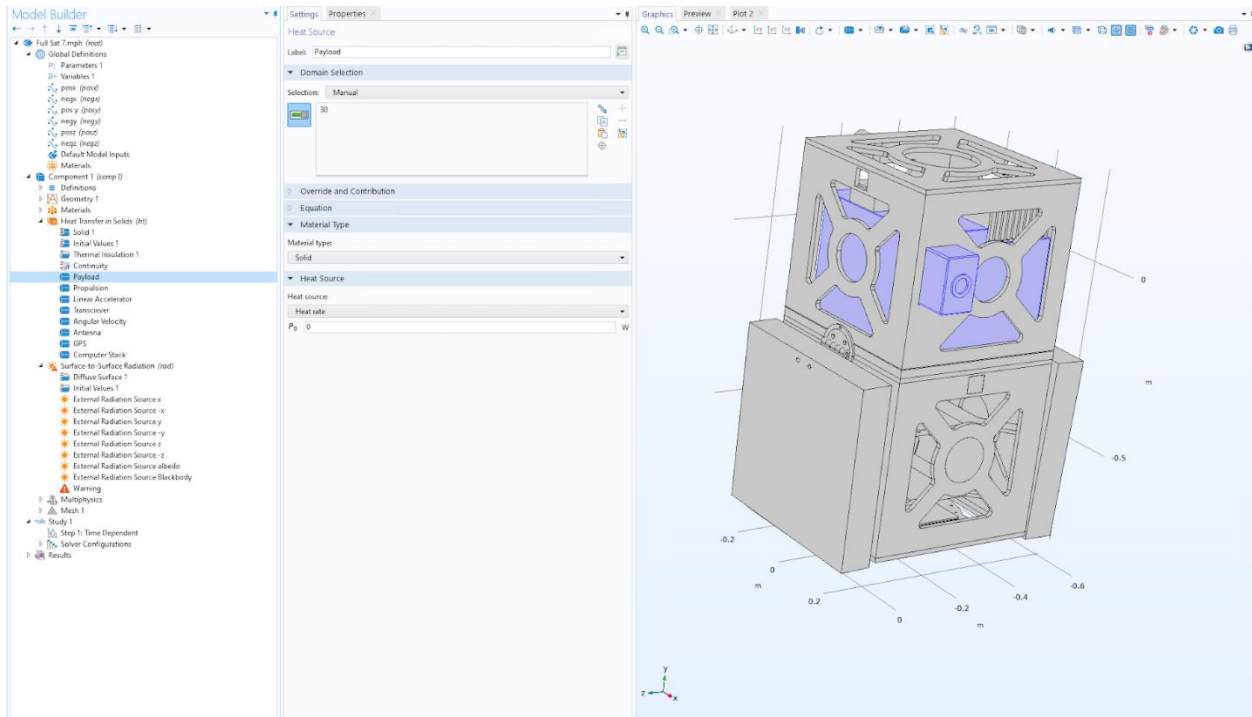


Figure 74. COMSOL Model setup for Heat Transfer in Solids

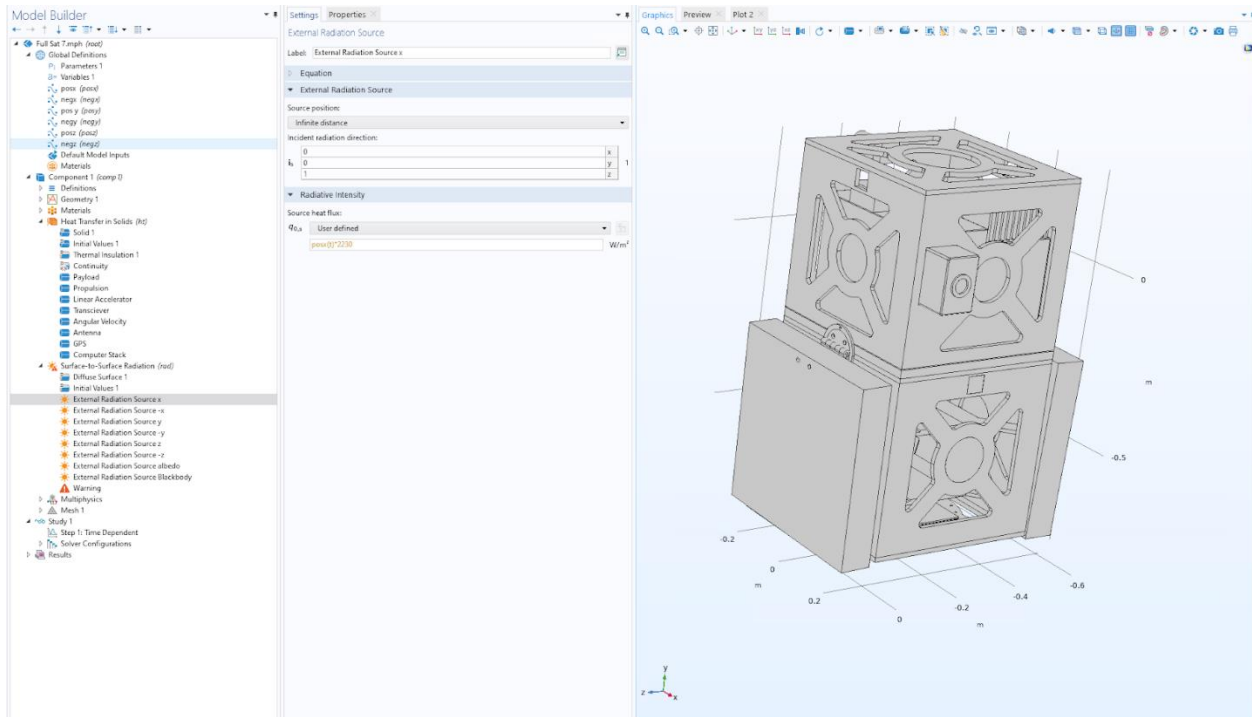


Figure 75. COMSOL Model setup for Surface-to-Surface Radiation

### 8.3.2 Results

A simple 2D model was created to understand the basic model and test different configurations. This model is not representative of the spacecraft or the thermal environment as a whole, it does give good insight into the problem. The 2D model is much more simple than the 3D model making quick analysis easy for both Heat Transfer and Surface-to-Surface Radiation.

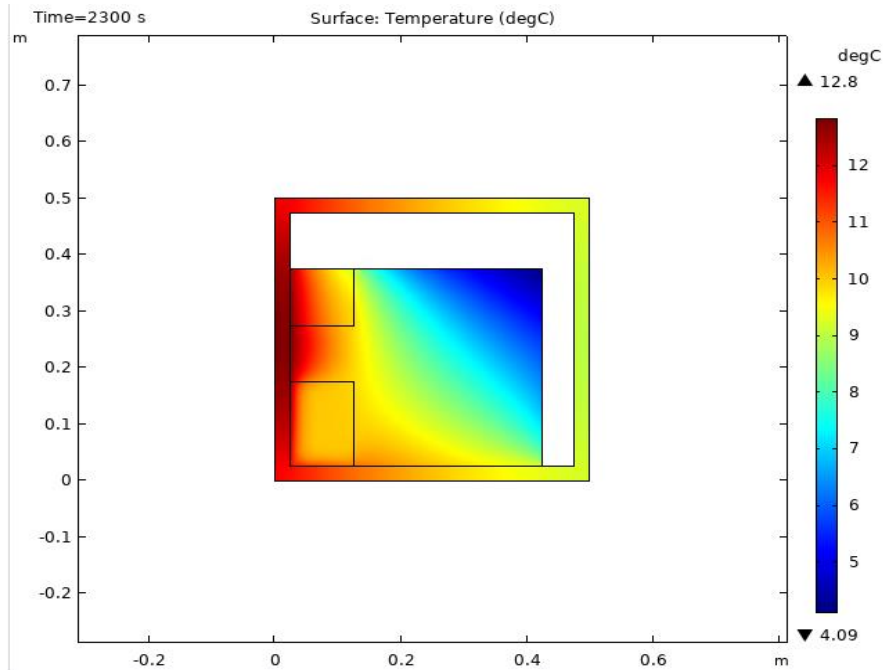


Figure 76. 2D Thermal Model

In the STK SEET simulation the spacecraft was modeled orbiting Venus for a 24 hour period. The results were an average temperature of  $-47.840^{\circ}\text{C}$  with a swing of about  $\pm 0.15^{\circ}\text{C}$ . The temperature peaked early at  $-47.825^{\circ}\text{C}$  and got as low as  $-47.856^{\circ}\text{C}$  by the end as seen in Figure 77. STK SEET Temperature Graph Over 24 Hours. The average temperature of the spacecraft also decreased linearly with each cycle.

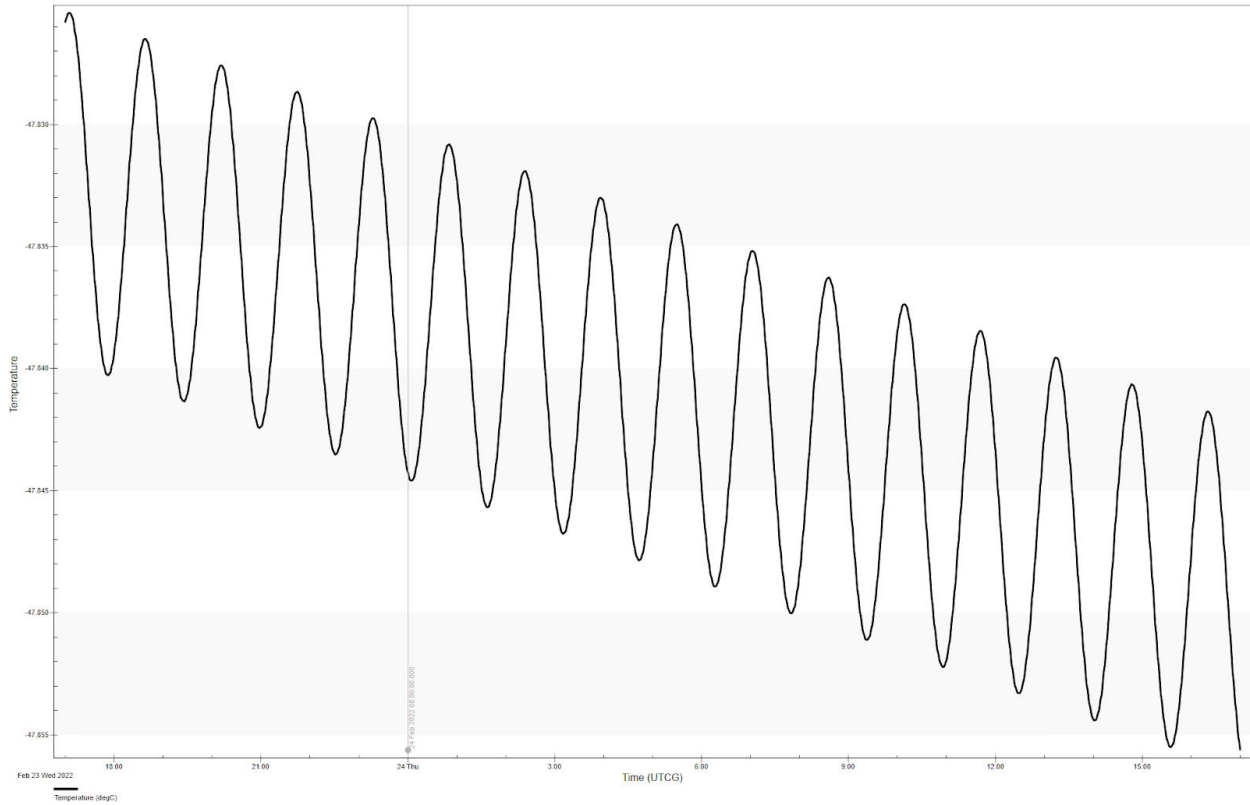


Figure 77. STK SEET Temperature Graph Over 24 Hours

The bulk temperature never reached the survivability temperature of a few of the components on board. However, this model only shows an estimate of the bulk spacecraft temperature and does not account for internal heat sources, model dissipation, or some complex surface conditions. These results were compared to the results of the COMSOL Multiphysics simulation results which offer more in-depth analysis of the spacecraft's thermal environment. The STK SEET simulation also used a simple object to analyze the bulk temperature whereas the COMSOL model analyzed the structure and components of ISS VOPED.



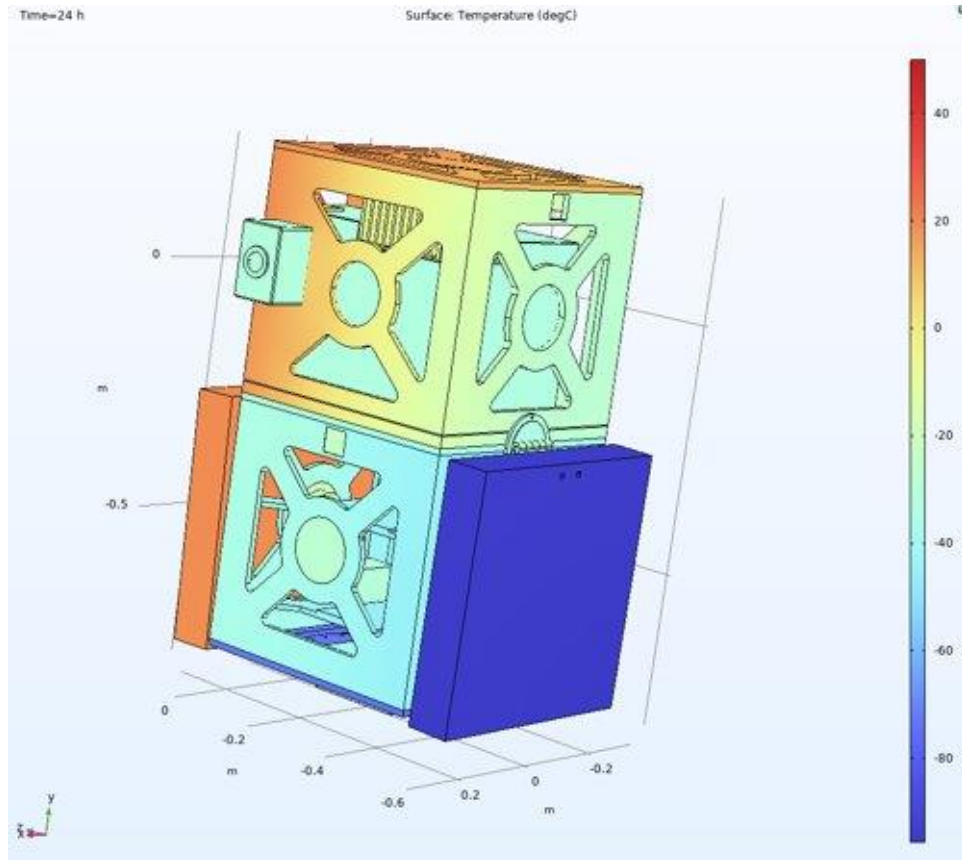


Figure 78. COMSOL Temperature Model at Earth

Table 23. Component Temperatures at Earth

<b>Components</b>	<b>Temperature (°C)</b>	<b>Operating Temperature (°C)</b>	<b>Survival Temperature (°C)</b>
<b>Payload</b>	-29	-20 to 40	-35 to 50
<b>Computer</b>	2	0 to 50	-20 to 70
<b>Battery</b>	1	0 to 55	-20 to 60
<b>Antenna</b>	-20	-30 to 20	-40 to 70
<b>Star Tracker</b>	-2	-40 to 30	-40 to 70
<b>Reaction Wheel</b>	-19	-20 to 50	-30 to 70

Two simulations were run, one of ISS VOPED at Earth and one at Venus. At Earth, the spacecraft temperature ranged from -90°C to 45°C. As shown above in Figure 78 The solar panels were the components with the highest and lowest temperature ranges depending on their orientation towards the oncoming solar radiation. The temperature of all the components was

recorded after 24 hours and is shown in Figure 79. All the components are within the operating temperature ranges except the payload, which is still within its survival temperature. As the payload will not be used till the spacecraft is in orbit around Venus. The emissivity of the spacecraft was different for each component. The payload, computer, battery, star tracker, and solar panels were given a surface coating of 0.8. The rest of the components and spacecraft was given a surface coating of 0.4. When the spacecraft as a whole had the same surface coating with an emittance of 0.8, the payload was colder than its survival temperature. The reaction wheels, computer, and battery all became colder than their operating temperature but still within their survival temperatures.

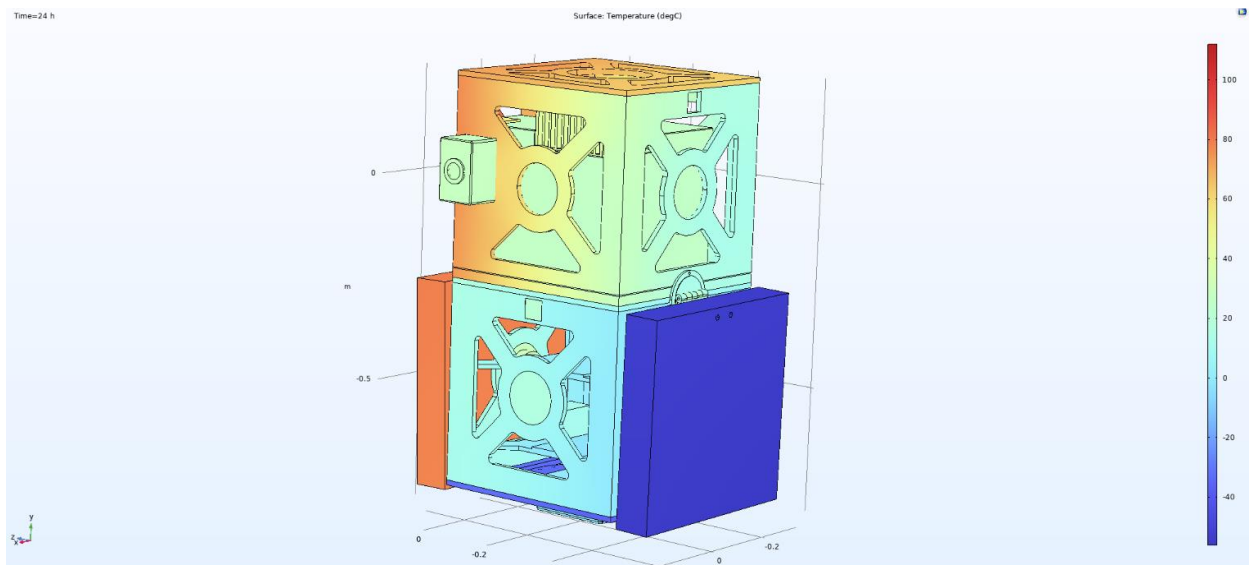


Figure 79. COMSOL Temperature Model at Venus

Table 24. Component Temperatures at Venus

<b>Components</b>	<b>Temperature (°C)</b>	<b>Operating Temperature (°C)</b>	<b>Survival Temperature (°C)</b>
<b>Payload</b>	37	-20 to 40	-35 to 50
<b>Computer</b>	46	0 to 50	-20 to 70
<b>Battery</b>	35	0 to 55	-20 to 60
<b>Antenna</b>	-4	-30 to 20	-40 to 70
<b>Star Tracker</b>	29	-40 to 30	-40 to 70
<b>Reaction Wheel</b>	23	-20 to 50	-30 to 70

At Venus, the ISS VOPED had a temperature range of -55°C to 112°C as seen above in Figure 79. Like with the spacecraft at Earth, at Venus both the hottest and coldest temperatures occurred on both solar panels. All the components were within their operating temperature ranges, as shown in Table 24. The payload, computer, and star tracker are all close to the high end of their operating temperature, but this model was for continuous exposure to solar radiation and not orbiting around Venus. The temperature of the COMSOL model and the STK SEET model was vastly different, off by about 50°C. This may be because the STK simulation is run on a simplified sphere and was modeled orbiting Venus, where the COMSOL model was exposed to solar radiation for the whole 24 hours.

#### 8.4 Conclusion

Based on the COMSOL simulation the payload, computer, battery, star tracker, and solar panels should be given a highly emissive surface coating of 0.8. The rest of the components and spacecraft should be given a more reflective surface coating of 0.4. In both simulated cases with these surface finishes the temperatures stayed within their survival temperatures and, other than the payload at Earth, all the components stayed within their operating temperature ranges. The

payload, computer, battery, star tracker, and solar panels get hot quickly, the increased emissivity helps the components shed radiation to continue to be within their operating temperature range. Having a less emissive coating on the payload could make it warmer at Earth to be within its operating temperature range, but the payload would exceed its temperature range while at Venus. Since the payload is operated at Venus and not at Earth, giving it a highly emissive coating is the best solution for the mission.

The overall thermal analysis process was simplified and might not be accurate to real spacecraft hardware. To create a more accurate thermal analysis a more in-depth model of the components and specify the location of heating within components and not assumed as uniform heating would be needed. A more accurate model of solar radiation should also be considered to create a more accurate model.

## 9 Environment

The environment of space must be considered when designing any spacecraft. Each component of the spacecraft has a survivability factor for the effects of thermal, radiation, space debris and other possible factors. A failure in one of these areas will result in the failure of the entire spacecraft. The goal of the environment subsystem is to anticipate and mitigate the hazards of space.

### 9.1 Environmental Effects

In this section, different types of environmental effects including radiation, thermal loading, space debris, and magnetic interference will be explored. Because the conditions while the ISS VOPED is orbiting Earth differs from the conditions it experiences while it travels between Earth and Venus and while it is orbiting Venus, it will be explored how these differing environments effects the ISS VOPED throughout its mission life.

#### 9.1.1 Magnetic Fields

The effect of the magnetic field of Earth and other bodies poses the most hazard to the ISS VOPED's electronic components. Sensitive electronics such as the attitude control system, the on-board computer, and the payload would normally need to be shielded from magnetic interference so that the spacecraft can accurately deliver and receive information. One significant magnetic field interference is caused by Earth's Van Allen belt.

The Van Allen radiation belt is a zone of energetic charged particles, most of which originate from the solar wind, that are captured by and held around a planet by that planet's magnetosphere. Earth has two such belts, and sometimes others may be temporarily created. Earth's two main belts extend from an altitude of about 640 to 58,000 km above the surface, in

which region radiation levels vary. Because the spacecraft uses electric propulsion, the transfer orbit from Earth to Venus is inside of the Van Allen belt for longer duration compared to a high thrust Hohmann transfer. Thus, the spacecraft will be most affected by the effects of radiation due to Earth's magnetic fields during the beginning of the mission.

### 9.1.2 Space Debris

Satellites and junk orbiting Earth travel at thousands of kilometers per hour, so collisions are catastrophic. When satellites retire or have unintended collisions in space, they leave behind material that continues to orbit Earth. Although some of this material is very small, it still poses a threat if it collides with a satellite. Additionally, as more satellites are placed in orbit, more space debris is added into the already dangerous debris fields orbiting Earth. To protect the ISS VOPED's mission-critical components from a catastrophic impact, these components are placed inside the spacecraft, with additional protective containment.

In addition to space debris, there are certain orbit distances that are common for satellites to utilize, namely Low Earth orbit and Geosynchronous Equatorial orbit (GEO). By virtue of these orbits containing a higher volume of satellites compared to other orbit distances, the probability of a collision increases as the ISS VOPED passes through. When satellite orbits are designed, they purposefully design the orbit to avoid collisions with other satellites, however the chance of impact is still higher in these areas.

### 9.1.3 Thermal Impact

During the ISS VOPED's interplanetary transfer, it will experience longer durations of sun exposure which may warm some surfaces of the spacecraft. On the other hand, surfaces that do not face the sun will be exposed to the cold of deep space which will draw heat away from

components. It is important to regulate the internal temperatures of the spacecraft since the heat can radiate from the outer surfaces towards the inner surfaces. In regard to ways that the ISS VOPED regulates its temperature, in-depth thermal analysis can be found throughout the Thermal Control Section. Each electronic component has an operations temperature, at which the device functions properly, and a survivability temperature, where the properties of the material and circuitry reach their physical limits before failing prematurely. Also, each temperature fluctuation degrades the material properties resulting in brittleness and/or hardening. Additionally, each material in the spacecraft has a unique coefficient of thermal expansion (CTE), meaning each part of the spacecraft will expand or shrink at different rates. Because a metal with a low CTE was chosen for the ISS VOPED (Al 6061-T6), the structure of the spacecraft is stable throughout the mission. Also, when modeling the chassis of the satellite, the extra expansion and contraction was considered.

Because the ISS VOPED orbits Venus for an extended period of its mission life, thermal shock due to the satellite going into and out of eclipse of the sun must be considered. Similar to satellites that orbit Earth, the ISS VOPED will be subject to frequent periods of sun and eclipse. The transition between these two conditions will produce a significant fluctuation in the heat flux on the spacecraft, which over time can cause material degradation. Further discussion on how thermal shock affects the ISS VOPED and what measures are put in place to mitigate its effects can be found in the **8 Thermal Control** section.

## 9.2 Environment Analysis

Utilizing the Systems Tool Kit (STK) Space Environment and Effects Tool (SEET), the impact that the environment of space has on the spacecraft can be simulated. It is possible to graph

the rate at which space debris impacts the ISS VOPED as it travels from Earth to Venus. Below is the graph for particle impacts with the ISS VOPED when on its transfer orbit from Earth to Venus.

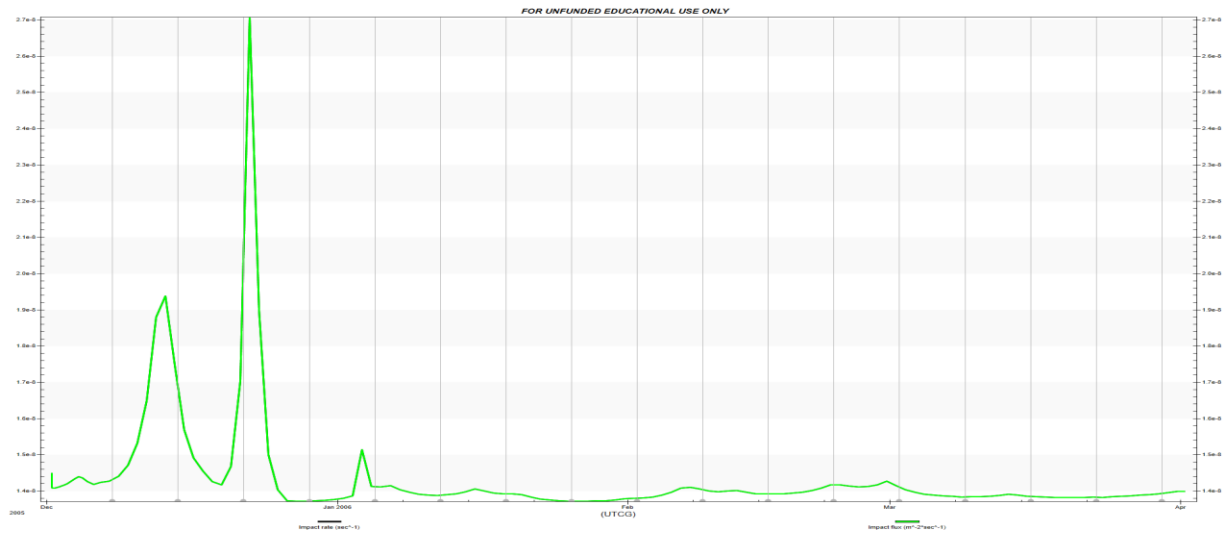


Figure 80. Particle Impact Probability with ISS VOPED

The two spikes in Figure 80. Particle Impact Probability with ISS VOPED correspond to the ISS VOPED passing through Low Earth orbit (LEO) and Geostationary orbit (GEO). Because a high volume of satellites orbit Earth at these distances, the probability of encountering other



satellites in orbit greatly increases. Once the ISS VOPED enters the interplanetary transfer, the probability of an impact decreases.

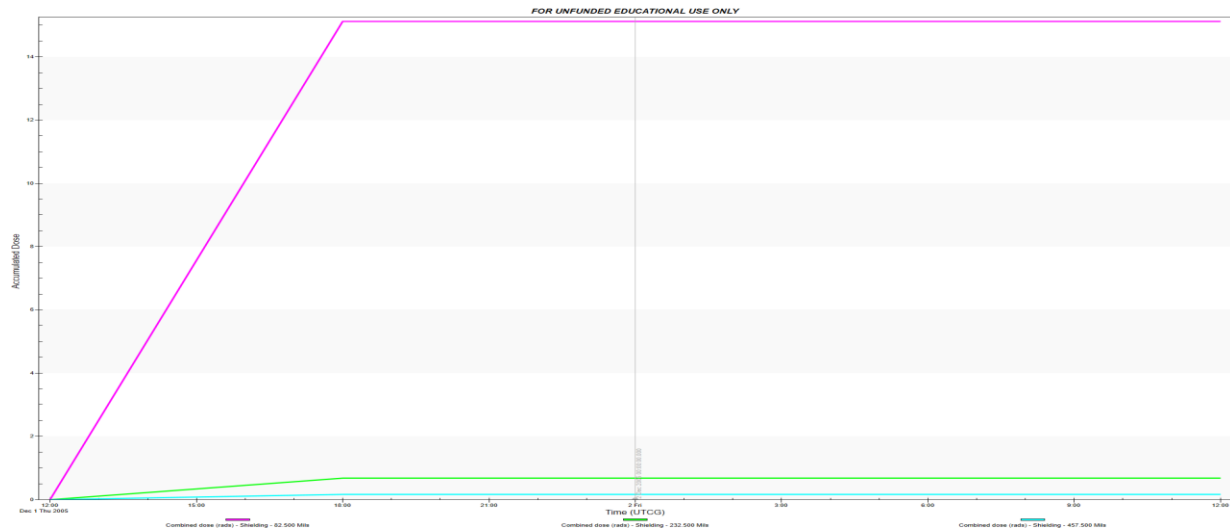


Figure 81. Accumulated Radiation Dose on ISS VOPED

Above is the graph for accumulated radiation dose for the spacecraft. The spacecraft encounters the most radiation when passing through Earth’s Van Allen belts. Therefore, once the spacecraft enters its interplanetary transfer, the radiation accumulated does not show a significant increase. Using this graph and its data, it is necessary to compare the accumulated radiation dose that the ISS VOPED endures to the radiation survivability factor for all of the electronic components on the ISS VOPED. The most critical electronics components are the on-board computer and the SPICAV/SOIR. For the Kryten-M3, the MRAM and Flash memories are protected via an EDAC mechanism to guard against radiation effects. This mechanism provides protection, not only against data modifications, but also against errors in the address decode logic (Kryten-M3, 2021). Additionally, the Total Ionizing Dose (TID) rating for the Kryten-M3 is 20 kRad. As shown in Figure 81. Accumulated Radiation Dose on ISS VOPED, the total accumulated dose does not exceed 20 kRad, so the Kryten- M3 does not have a failure due to the effects of radiation.

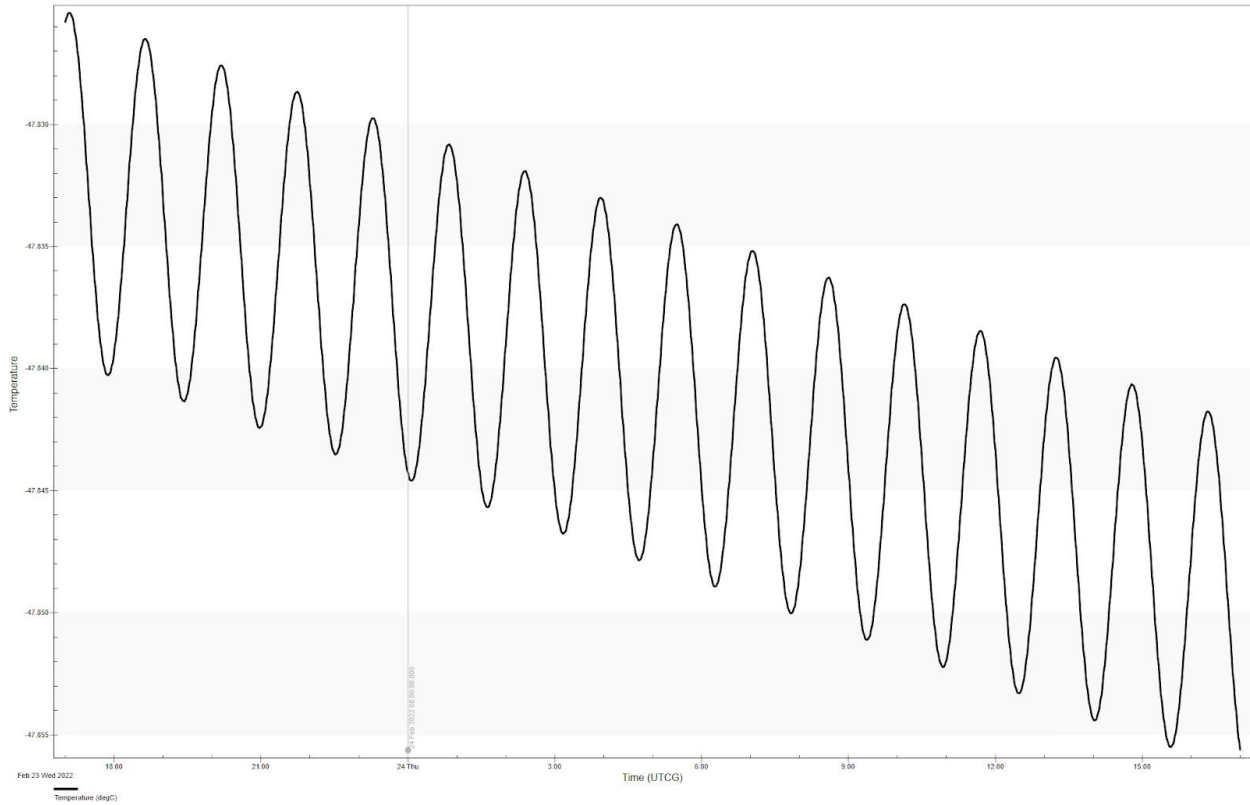


Figure 82. STK SEET Temperature of ISS VOPED in Orbit Around Venus

As shown in Figure 82. STK SEET Temperature of ISS VOPED in Orbit Around Venus, the temperature on the surface if the ISS VOPED reaches an equilibrium temperature of approximately  $-47^{\circ}\text{C}$ . The simulation gathered data from the surface of the ISS VOPED as it orbited Venus over a 24 hour period. The graph may look misleading; however, the scale of the temperature axis is very small. Over the 24 hour period, the temperature did not decrease by more than  $0.01^{\circ}\text{C}$ . As mentioned in the **8 Thermal Control** section, the bulk temperature never reached the survivability temperature of a few of the components on board. The STK SEET model used, however, only shows an estimate of the bulk spacecraft temperature and does not account for complex surface conditions.

## 10 Thermal Vacuum Chamber

To lower the pressure in the vacuum chamber three pumps are used, each in a different pressure regime, ultimately to a pressure representative of space. The useful range of a pump is mainly constrained by the vapor pressures of its components. For example, a pump that operates in the viscous flow region will not operate in the molecular flow region and vice versa. Consequently, vacuum systems generally operate a variety of vacuum pumps at different pressure ranges.

The vacuum system at the WPI Fluids and Plasma Dynamics Lab is no different and it employs the following vacuum pump types. The first pump is the mechanical pump. This oil-sealed rotary pump is the most common. It operates by extracting gas particles from the chamber through an inlet that leads to a one-way valve that compresses the gas forcing it through the exhaust.

The second pump is the Roots Blower pump. Roots blowers work by having two counter-rotating interconnected rotor units rotating within a housing unit. Gas then enters through an inlet flange, perpendicular to the rotating units. This gas is then isolated between the rotating units, to then be expelled through an exhaust.

The third and final pump in the TVAC system is the cryopump. Cryopumps work by exposing a metallic plate inside the chamber. This plate is then cooled to around 20 K. This plate causes the leftover gas in the chamber to condense on it and freeze, effectively removing it from a gaseous state. If the gas in the chamber is Hydrogen, Helium, or Neon, then the plate may not be able to condense the gas. However, the plate can consist of a special porous material to absorb the gas. This is the final stage in the pumping process, as it only works when there is a small amount of gas particles left in the chamber.

## 10.1 TVAC Liquid Nitrogen Assembly & Phase Separator

Once a hard vacuum is reached, all accompanying components can be used. These components consist of the shroud, tests stand, and the liquid Nitrogen (LN2) system.

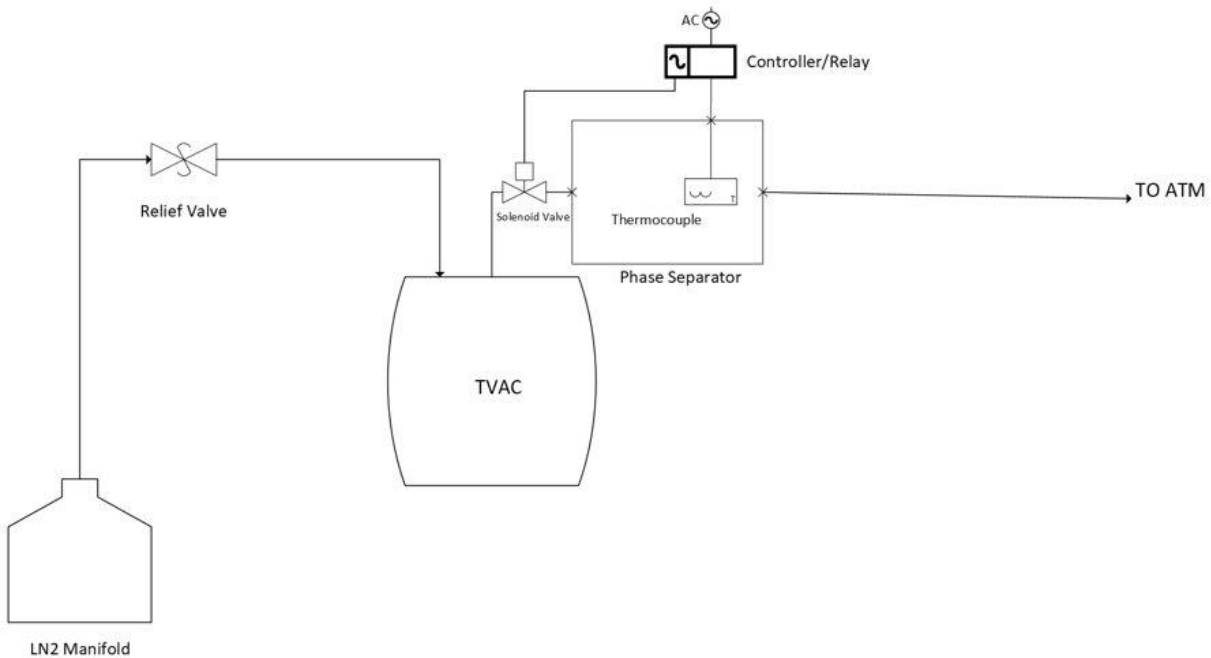


Figure 83. Diagram of the TVAC Liquid Nitrogen System

For proper testing environments, the chamber must reach its lowest vacuum possible. It then must be able to simulate the temperature of space as well. This is where the liquid nitrogen system is useful. LN2 is stored in a pressurized Dewar tank. Once unpressurized, the LN2 will have a temperature of  $-196^{\circ}\text{C}$ . The use of LN2 is the most viable way to reach a temperature near that of space.

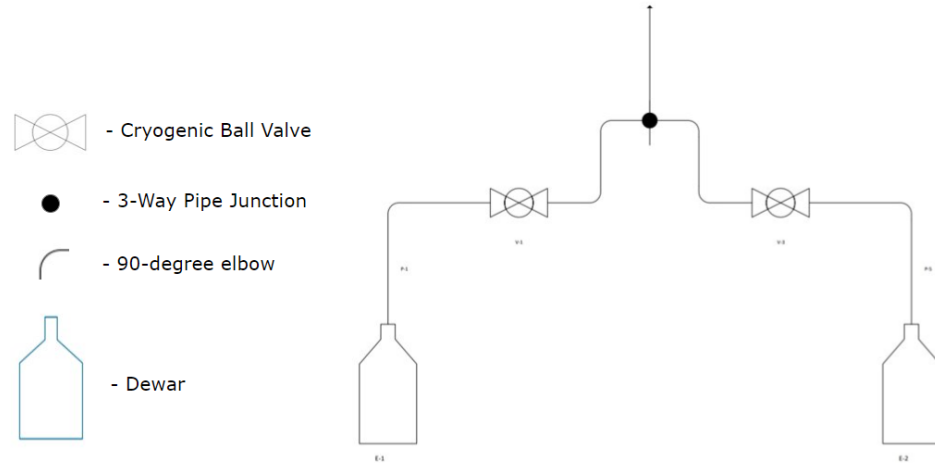


Figure 84. Diagram of the Liquid Nitrogen Manifold

LN2 will be pumped through a manifold, shown in Figure 84. This manifold requires the use of two LN2 dewars, and two cryogenic ball valves. The piping from each tank is connected by a 3-way junction that exits to the vacuum chamber. This system allows for continuous unperturbed flow of LN2 into the vacuum chamber by allowing for one or both tanks to be used simultaneously. The LN2 will then travel through ½ NPT steel piping to one of the entry flanges of the vacuum chamber. The flange allows for the LN2 to enter the chamber, without disrupting the vacuum environment. After entering the flange, the LN2 will flow through the D-tubing of the shroud to cool the chambers environment. The LN2 will heat up as it travels through the shroud, which does not allow the liquid to be reused. This creates an LN2 waste, which needs to be disposed of properly. The LN2 cannot be exhausted out a vent as a liquid, however, if the LN2 is converted into a gas, then it can be vented to the atmosphere, outside the building. This requires the use of a phase separator. The phase separator assembly consists of a cryogenic solenoid valve, storage tank, thermocouple, and controller. The valve chosen for this project is a 304 Stainless Steel solenoid valve, suitable for cryogenic conditions. The controller is a CNiD1633 with two relay outputs that can connect with the valve.

In order to safely release the LN2 to atmosphere, a solenoid valve is to be used to control the flow as the nitrogen leaves the TVac. The valve's on/off status is determined by the temperature inside the exhaust tank. More LN2 inside the tank will lead to cooler temperatures indicating that the flow must be stopped. Temperature data collected by thermocouple is transferred to and analyzed by the controller. The built-in relay gives power to the valve, turning it on and off. This process can be seen from the figure below:

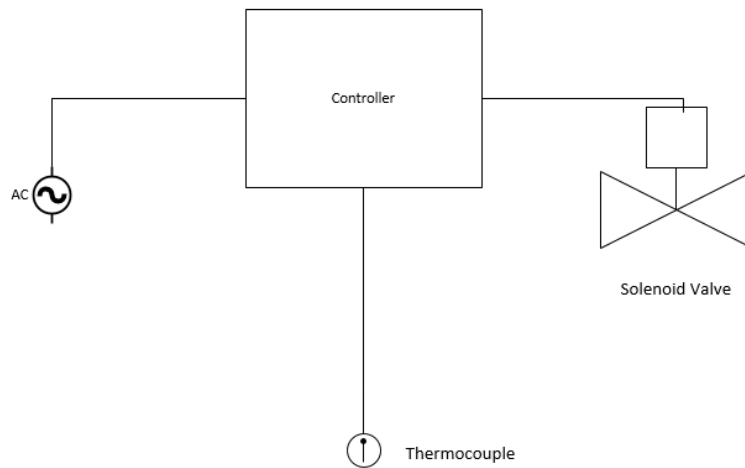


Figure 85. Controller-Valve Configuration

The phase separator consists of a tank, with an entry pipe for liquid to flow in, and an exit exhaust for gas to flow out. Once the LN2 enters the tank, it naturally will evaporate due to the room's ambient temperature being significantly higher than that of the LN2. Figure 86 and Figure 87 shows the design of a basic phase separator.

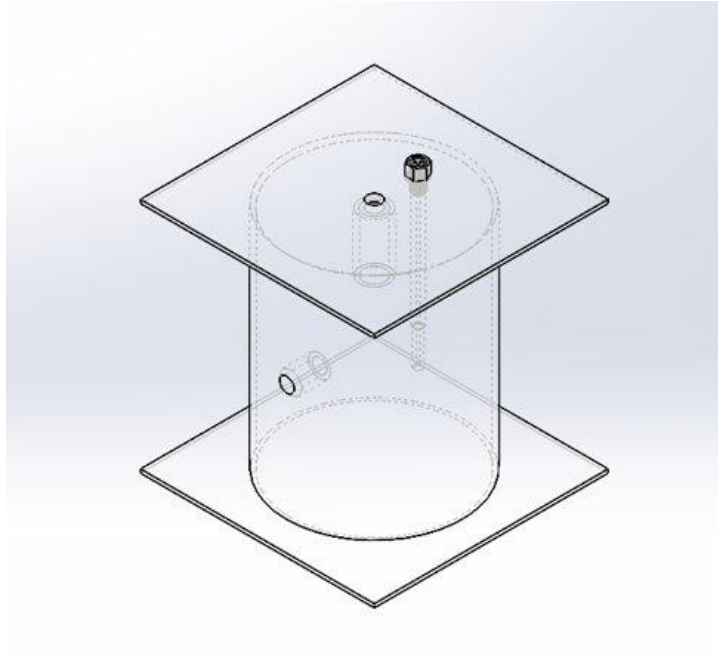


Figure 86. Isometric View of the Phase Separator

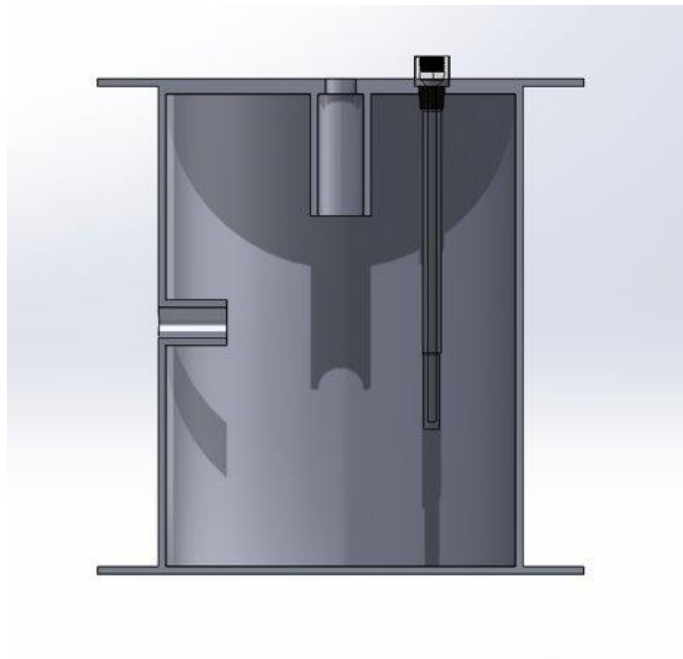


Figure 87. Internal View of the Phase Separator

The 12-inch diameter cylindrical tank sits between two 16x16 inch plates to allow for secure containment of the LN2 and for mounting purposes. The inlet, left side of the cylindrical tank, allows for the LN2 to be dispensed into the tank. Within the tank exists a thermowell, which will protect a thermocouple from the liquid.

## 10.2 TVAC Test Stand

Within the tank exists components such as the shroud, test stand fixture, and the light fixture. The shroud is a 32-inch inner diameter aluminum cylinder that is 0.125 inches thick and has 35 ft of 0.5-inch D-tubing wrapped around it as a cooling coil. This shroud is supported by three 2-inch x 2-inch L-brackets with corresponding arcs cut out to rest the shroud in. These brackets are supported by plastic sliders riding in the vacuum chamber's 1.5-inch T-slot rails. The heating lamps are supported by a T-slot cross brace between the integrated rails and a 19.375-inch vertical T-slot post. The lamp sockets are affixed to a horizontal T-slot attached to this post. The sample will sit on the plate that would be connected to the two upper horizontal beams that were being extended into the shroud, shown in Figure 88.



Figure 88. Specimen Holder within TVAC



The test stand will have an addition of a 24-inch flat plate that will sit on the top two beams where the specimen will be held, as shown in Figure 89.

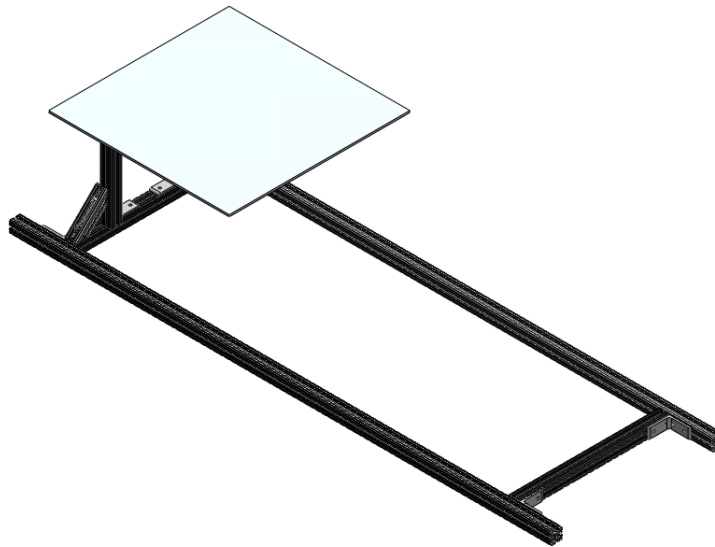


Figure 89. Specimen Holder with Flat Plate

This test stand is comprised of two hollow single four rail (1.5" x 1.5" x 72"), four diagonal braces for single rails (1.5" x 6"), four T-slotted framing brackets (1.5"), two hollow single four rails (1.5" x 1.5" x 16"), and four hollow single four rails (1.5" x 1.5" x 20"), as shown in Figure 90.

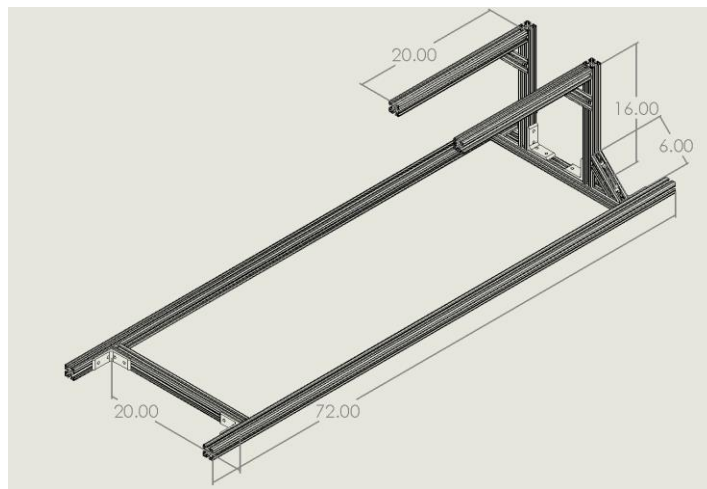


Figure 90. TVACTVAC Test Stand with Dimensions

This setup can be assembled and disassembled in the chamber. The shroud will sit on the bottom plane beams while the upper plane beams will penetrate the center of the shrouds opening, as shown in Figure 91.



Figure 91. Test Stand and Shroud Configurations

This design was chosen to decrease the probability of the shroud suffering damage during the test. Previously, the specimen would sit on a plate that would be touching the bottom of the shroud. This design removes that potential for damage by having the specimen floating within the testing area.

## 11 Conclusions and Recommendations

As the iterative design process progressed, the overall mass and volume of ISS VOPEd matured and increased. This development was expected due to the iterations of propellant mass and the necessity for solar arrays that corresponded with the spacecraft. , shows a complete mass breakdown of the components within each subsystem.

As anticipated, the iodine propellant mass and the external frame are the two largest contributors to the total mass value. The propellant mass is about 26.7% and the frame is about 27.2% of the overall mass. The current dimensions and mass of the spacecraft still lie within the allowable values for the rideshare dispenser ring, making the mission possible.

The components were chosen based on mass, efficiency, contributions, and abilities. Each subsystems hardware was able to be successfully integrated into the spacecraft in order to contribute to a successful rideshare mission to Venus's atmosphere. The protection and placement of the SOIR Spectrometer was crucial to this mission.

Future teams investigating Venus's atmosphere or similar missions, given more time and less setbacks, should focus on expanding theoretical analysis on the spacecraft. Testing alternative environments in COMSOL and ANSYS that are referenced in the Falcon 9 User Guide. As well as focusing more on a hands-on component of the project to validate designs. Physically conducting material analysis using load testing equipment or creating a small-scale model and conducting a vibrational/shock test using a vibrometer.

Table 25. Mass Breakdown of ISS VOPEd

<b>Component</b>	<b>Mass (kg)</b>
<b>Structure/Mechanisms</b>	
Frame	50.42
Hinge(s) [2]	1.32
Rotator(s) [2]	1.38
<b>Payload</b>	
SPICAV/SOIR Spectrometer	13.92
<b>ADCS</b>	
Star Tracker(s) [2]	0.7
Reaction Wheel(s) [3]	31.5
Sun Sensor(s) [5]	0.125
Hydrazine Propellant Tank (Dry/Wet)	0.35/3.72
RCS Thruster(s) [12]	0.12
<b>Propulsion</b>	
Power Propulsion Unit	5.0
Iodine Propellant Tank (Dry/Wet)	3.69/53.17
BHT-1500 Thruster	7.10
<b>Power</b>	
Power Distribution Unit	2.5
Battery	1
Solar Array(s) [2]	11.76
<b>Communications</b>	
Iris Deep Space Transponder	1.23
Kryten-M3 OBC	0.41
Custom-Sized Patch Antenna	0.16
<b>TOTAL</b>	
Spacecraft Dry Mass	<b>132.58</b>
Spacecraft Wet Mass	<b>185.43</b>

## 11.1 Payload

The objective of the payload was to be capable of detecting trace amounts of Phosphine gas in the Venusian atmosphere. This was completed by studying the spectroscopy data of Phosphine gas and determine a payload device that could detect it. Phosphine's spectral absorption bands exist between 0.9 - 3.7  $\mu\text{m}$ . This required the use of a spectrometer capable of detecting infrared sized wavelengths. This spectrometer would also need to detect the atmospheric composition from orbit. The solution to this is the SPICAV/SOIR Spectrometer. This spectrometer has a solar occultation technique that will be capable of detecting the spectroscopy data of solar light passing through the atmosphere. This spectrometer's data collection technique imposes pointing requirements on the ADCS subsystem. These requirements are the need for the spectrometer to be pointed 10 arcmin above the solar center of the Sun through the entire collection process.

The data collection is very reliant on one device, whereas most spacecraft will have multiple payloads. Having more spectroscopy devices could allow for more analysis of the Venusian atmosphere. A secondary issue was the thermal control around the spectrometer. The spectrometer is coincident to the structure facing the Sun at all times. This could cause severe problems for the operation of the spectrometer. Too hot of temperatures can easily disrupt the components inside the spectrometer, rendering them useless.

## 11.2 Structures and Design

The objective of ISS VOPED was to house the subsystems components and carry out a successful mission to Venus's atmosphere. The design of the spacecraft had to meet specific mass and volume constraints. As well as meet a mass to center of gravity set of values that corresponds

with the rideshare dispenser ring. The structural integrity of the craft was determined based on the chosen material of Al 6061 T6. Analysis was conducted on the natural frequencies and random vibration of the system to simulate the fairing environment. The yield strength Al 6061 is greater than any of the deformation that was presented, leading ISS VOPED to not reach failure.

As stated, in order to classify a satellite as a SmallSat, it needs to be no larger than 180 kg. Unfortunately, the overall mass of ISS VOPED is about 185.43 kg, meaning the mass constraint in terms of the definition of SmallSat is broken. Although, the mass is still within an allowable value to be able to participate in rideshare. From the Falcon 9 User's Guide, analysis could be expanded to conducted acoustic, shock, and a variety of PSD G environments. As well another dispenser ring connection test with the populated model to view how the shift in mass allocation affects the stress, strain and deformation of the overall system. As previously stated, conducting a physical test on material and shock would be beneficial to validating simulated results and providing the user with a deeper understanding of structural design.

### 11.3 Propulsion

The objective of the propulsion system was to meet the delta-V requirements imposed by the necessary spacecraft maneuvers to reach the desired final orbit. This was accomplished many steps. The first was to determine which propulsion system type is more viable based off of preliminary delta-V estimations. This became the use of an electric propulsion system, as the preliminary propellant mass calculations were significantly lower than that of chemical propulsion. Next was to determine a thruster and propellant type capable of meeting the restrictions of mass and volume imposed on the propulsion system. This resulted in using the Busek BHT-1500 for its low power requirement and relatively high thrust and  $I_{sp}$  for that power requirement. The BHT-

1500 will run on solid Iodine propellant to increase storage density and decrease volume usage. The next step was to simulate the mission's main propulsion system maneuvers. This was done using STK and Astrogator to determine trip times and Delta-V requirements. This resulted in a total trip time of and a total delta-V requirement of 7.131 km/s.

There are adjustments that could be made for future plans with this project. The first could be a more in-depth simulation with STK. This could involve accurate Earth departure data, including the escape location and escape velocity from the launch vehicle. More analysis on the propellant mass consumption can be used to determine optimal orbit trajectories, launch days, or coast periods. Other future goals for the propulsion subsystem could be more research on thermal control of the propulsion systems. This could prevent any unwanted heating of components near the propulsion system components and provide a more accurate analysis of the spacecraft.

## 11.4 Power

The goals of the power subsystem were to supply the required amount of power to the spacecraft and its components to perform the required tasks at Venus. Much of this was accomplished by generating power through a solar array of size 3.92 m<sup>2</sup> and a 175 W-hr lithium-ion battery. The primary driver of the power subsystem was the propulsion subsystem. Electrical propulsion greatly increased the mass of the solar arrays, but this increase was necessary for the mission. By choosing efficient and mature technologies like multijunction solar cells and lithium batteries, the mass contribution from the power subsystem was kept to a minimum, given the constraints. Barring mass requirements, future interplanetary projects could explore alternate power sources like RTGs which were used in missions like Cassini and Galileo.

## 11.5 ACDS

The Attitude Dynamics and Control System had been tasked with managing and logging the SmallSat's attitude. Both stabilizing and reorienting the spacecraft with precession. To accomplish this objective, the subsystem employed multiple sensors and actuators that work in tandem. The main driving force of the subsystem were the reaction wheels, which require an understanding of control theory as well as the dynamics of the spacecraft to work properly. With both the detumbling and reorientation simulation, the reaction wheels are proven to perform the required maneuvers. There are limitations to the model that can be improved in future versions. The simulation assumes that the reaction wheels can change their torque instantaneously. In most real time applications, reaction wheels take a small amount of time to achieve the desired torques requested by the PID controller. Additionally, ADCS should study and outline every necessary maneuver of each phase to properly estimate the total reaction wheel saturation. A deeper understanding of each mission phase would determine a more accurate estimate of ACS propellant needed for the whole mission.

## 11.6 Communications

The objectives of the communications subsystem are to design a communication architecture for the ISS VOPED, as well as calculate the downlink and uplink data transfer budget. The communication architecture for the ISS VOPED includes the on-board computer, the radio transceiver, the antenna array, and ground stations. The Kyrten-M3 was chosen as the OBC; the IRIS radio was chosen for the radio transceiver; a custom patch-antenna array was designed for the antenna array; and the Deep Space Network was chosen for the ground stations.

The data transfer rate for downlink (ISS VOPED to the DSN ground stations) was calculated to be 0.015 MB/s. Using Systems Tool Kit, the average access window duration from



the DSN ground stations to the ISS VOPED while orbiting Venus was calculated to be 3715 seconds. Therefore, the data transfer budget for a single downlink access window was 1.1879 MB and the maximum capacity for data transfer in one 24-hour period is 17.8185 MB.

Any data that cannot be downlinked during the access window is stored in the OBC storage, which is 4 GB for the Kryten-M3. If the SPICAV/SOIR produces its maximum data volume, it will create 47.687 MB of data per day. Thus, with a 17.8185 MB capacity for data transfer, the amount of untransferable data per day could be 29.8685 MB per day. The 4 GB in the Kryten-M3 as well as the 256 GB of microSD card storage will be used to store this extra data.

If the mission required that the data must be downlinked as soon as it was created, then the need for a greater data transfer rate would arise. Thus, a recommendation for a future/updated design of this mission would be to design a better antenna array to increase the gain of the antenna. Because the ISS VOPED is a SmallSat, a custom microstrip patch antenna array was considered as the best option at the time. However, it is possible to improve on the design of this antenna. For example, changing the substrate material, ground material, substrate thickness, or overall dimensions. The 10-array design was chosen due to size limitations, and to have the ability to affix the antennae array onto one side of the ISS VOPED. Other options such as designing the antenna array to be deployed similar to the solar arrays should be considered to improve the antenna gain.

## 11.7 Thermal

The objective of the thermal control system is to keep all the components of the ISS VOPED within their survival temperatures and operating temperature while working. The environments the spacecraft will encounter on its mission are vastly different from the environment on earth and change depending on its point in the mission. To complete a total

thermal analysis of the ISS VOPED the software applications COMSOL Multiphysics and STK were used.

Based on the COMSOL simulation the payload, computer, battery, star tracker, and solar panels should be given a highly emissive surface coating of 0.8. The rest of the components and spacecraft should be given a more reflective surface coating of 0.4. In both simulated cases with these surface finishes the temperatures stayed within their survival temperatures and, other than the payload at Earth, all the components stayed within their operating temperature ranges. The payload, computer, battery, star tracker, and solar panels get hot quickly, the increased emissivity helps the components shed radiation to continue to be within their operating temperature range.

## 11.8 Environment

The environment of space must be considered when designing any spacecraft. Each component of the spacecraft has a survivability factor for the effects of thermal, radiation, space debris and other possible factors. A failure in one of these areas will result in the failure of the entire spacecraft. The goal of the environment subsystem is to identify hazardous space conditions and their effect on the spacecraft. One of the main hazards that was analyzed is the radiation absorption, as this affects the most critical electronic components of the ISS VOPED such as the SPICAV/SOIR and the Kryten-M3 OBC. A model of the radiation absorption across the lifespan of the mission was done using STK SEET. Additionally, the thermal and debris impact analysis was done using STK SEET. Using the results of the graphs and data created recommendations to Thermal, Communications, and ADC subsystems, were possible.

The spacecraft models used in the STK SEET could be improved upon in the future to get a more detailed model of the spacecraft. For example, the temperature model used a slightly different numbers than the default values as specified by this STK manual:

[https://help.agi.com/stk/11.0.1/Content/seet/Sat\\_Basic\\_Thermal.htm](https://help.agi.com/stk/11.0.1/Content/seet/Sat_Basic_Thermal.htm).

However, even the numbers that were used were not as detailed as possible. To fully model the ISS VOPED's actual temperature model, the values for each area in the manual linked above must be found for the component materials on the ISS VOPED. Similar updates to the radiation and debris impact models can be done to further replicate the actual conditions that the ISS VOPED would encounter in space.

## 11.9 Thermal Vacuum Chamber

The purpose of the TVac experiment was to validate and improve the thermal environment simulation run by the previous MQP (Mayer et al., 2021). Unfortunately, due to the thermal vacuum chamber facing many issues, the experiment was halted. The team focused on improving the specimen test stand and designing a liquid Nitrogen assembly and phase separator. The construction of a new test stand would decrease the potential of damaging the shroud. The implementation of the liquid Nitrogen assembly and phase separator would better simulate a space-like environment, ensuring the results are more realistic.

### 11.9.1 TVac Test Stand

The thermal vacuum test stand has been remodeled to ensure the internal surface of the shroud is not damaged. Previously, the specimen holder within the shroud sat within the shroud. The contact of the legs of the stand to the surface of the shroud had high possibility of scratching

the shroud. The shroud, donated by Dynavac, was an extremely expensive piece of equipment. The design of the new stand is constructed to not make any contact with the internal surface of the test stand. As shown previously in Figure 9/91, the 80/20 rails are floating about the center of the shroud, a flat plate will sit on the penetrating rails. The specimen sits on the plate when the simulation is running.

A potential improvement to the TVac test stand is devising a simpler way of assembly. Since the specimen is on the opposite side of the lights, the stand must be partial constructed within the vacuum chamber, which could lead to injuries. Another improvement is a better system for the lights. Currently they are housed on an 80/20 T-shaped railing system where the hardware is temperamental. More accurate results would be collected if the lights were on an automated system that had the ability to rotate and dim.

### 11.9.2 Liquid Nitrogen Assembly & Phase Separator

The LN2 is pumped to the TVac through a manifold. The manifold consists of two cryogenic ball valves and two dewars to store the LN2. This assembly allows a continuous and unimpeded flow of LN2 through the system. Future teams should at refining this design and purchasing the required equipment to create a functioning LN2 manifold.

The phase separator uses valves, temperature controller, thermocouple, and a stainless-steel tank in combination to safely release LN2 to the atmosphere. Temperature data collected by the thermocouple is used to open and close the solenoid valve, which controls the flow of LN2. Future projects should measure LN2 flow rate, prototype the controller-valve combination, and then proceed to test the complete phase separator.

The final feature that should be developed further is a failsafe feature. The current design employs a pressure relief valve that would release liquid nitrogen into the lab once a certain high-

pressure threshold is reached, ensuring the structural integrity of the liquid nitrogen assembly. This current setup is not enough to ensure the safety of future lab users in the vicinity. There must be an additional system to monitor nitrogen levels in the lab and warn users of any harmful nitrogen levels. Additionally, it would be ideal to automatically close the source that supplies liquid nitrogen if the relief valve is ever actuated.

## Societal Impact

The technology of CubeSats is relatively new as compared to other more established aerospace technology. However, CubeSats are already helping to reduce the cost of launching and building satellites for certain scientific missions. This is due to the CubeSats being smaller in size and the shape being easier to construct. There are currently very few companies able to launch their own satellites because of restrictions including cost and the size of traditional satellites. Smaller more accessible satellites allow for more companies to be able to launch their own satellites and open the potential for what tasks CubeSats can accomplish.

Our project is unique as it is one of a very select few missions to Venus. The technology that would be used on our mission is still relatively untested and would help to validate both the accuracy and precision of the instruments used. Venus being a planet nearly the same shape as Earth but having a vastly different atmosphere and climate offers numerous insights to the study of planets. This can help in the future to identify certain factors that would make other planets suitable or unsuitable for habitation. In addition, our mission deals with being able to detect and measure the presence of specific compounds and gases in a planet's atmosphere. This technology can help scientists attempt to combat climate change or more reliably measure the condition of Earth or other planets.

Our designed mission functions as a means of testing the viability of sending a smaller satellite on an interplanetary mission. Most interplanetary and research missions done by NASA typically use a larger and more costly satellite or spacecraft making them expensive and time consuming. If interplanetary research missions can be conducted with smaller satellites, then other companies could potentially carry out smaller more specific missions. In addition, due to the small size of CubeSats, these satellites do not need to be launched as a primary payload and are able to rideshare. This opens the possibility of adding CubeSats to larger missions and narrowing the focus of larger spacecraft, having the CubeSats take smaller measurements and conducting more rudimentary tasks.

## References

- Abacus 2017. (n.d.). Retrieved October 16, 2021, from <https://satsearch.co/products/gauss-abacus-2017>.
- Bertaux, D. Nevejans, O. Korablev, E. Villard, E. et al. (2007) *SPICAV on Venus Express: Three spectrometers to study the global structure and composition of the Venus atmosphere*, Planetary and Space Science, Volume 55, Issue 12, Pages 1673-1700, ISSN 0032-0633, <https://doi.org/10.1016/j.pss.2007.01.016>.
- Busek. (2021) *BHT-1500 Hall Effect Thruster*, Retrieved March 1, 2022
- CubeSat structural frame. (2022, January 11). Retrieved March 3, 2022, from <https://nanoavionics.com/cubesat-components/cubesat-structural-frame/>
- CubeSat Form Factor Thermal Control Louvers | T2 Portal. (n.d.). Retrieved October 22, 2021, from technology.nasa.gov website: <https://technology.nasa.gov/patent/GSC-TOPS-40>
- Department of Energy. (2021, February 16). What is a radioisotope power system? Retrieved October 15, 2021, from <https://www.energy.gov/ne/articles/what-radioisotope-power-system>
- Department of Energy. (n.d.). Solar Photovoltaic Cell Basics. Retrieved October 15, 2021, from <https://www.energy.gov/eere/solar/solar-photovoltaic-cell-basics>
- D. G. Gilmore, *Spacecraft Thermal Control Handbook Volume 1: Fundamental Technologies*, El Segundo: The Aerospace Press, 2002.
- E. Boslooper, N. Heiden, D. Naron, R. Schmits, J. Velde, and J. Wakeren. (2012). BepiColombo fine sun sensor. International Conference on Space Optics

ESA. (2021). *Venus Express*. Retrieved March 6, 2022, from [https://www.esa.int/Enabling\\_Support/Operations/Venus\\_Express](https://www.esa.int/Enabling_Support/Operations/Venus_Express)

Esa.int. Retrieved October 20, 2021 from [https://www.esa.int/Science\\_Exploration/Space\\_Science/Extreme\\_space/Surviving\\_extreme\\_conditions\\_in\\_space](https://www.esa.int/Science_Exploration/Space_Science/Extreme_space/Surviving_extreme_conditions_in_space)

Felt, Matt; Sinfield, Matt; Thompson, Brian; Munns, Matt; and Lloyd, K., "Thermal Conductance Measurement and Flexibility Enhancement of Flexible Thermal Links" (2017). Space Dynamics Lab Publications. Paper 220. [https://digitalcommons.usu.edu/sdl\\_pubs/220](https://digitalcommons.usu.edu/sdl_pubs/220)

Greaves, J. S., Richards, A. M., Bains, W., Rimmer, P. B., Sagawa, H., Clements, D. L., . . . Hoge, J. (2020). Phosphine gas in the cloud decks of Venus. *Nature Astronomy*, 5(7), 655-664. doi:10.1038/s41550-020-1174-4

Inc, P. (2015). Pumpkin Space Systems. Retrieved March 01, 2022, from <https://www.pumpkinspace.com/>

Kalogirou, S. (2018). *McEvoy's Handbook of Photovoltaics: Fundamentals and Applications*. London: Academic Press an imprint of Elsevier.

Kryten-M3 & Kryten-M3-plus - Satellite Command & Data handling. (2021, November 15). Retrieved October 6, 2021, from <https://www.aac-clyde.space/what-we-do/space-products-components/command-data-handling/kryten-m3>

Kryten-M3. (n.d.). Retrieved March 6, 2022, from <https://satsearch.co/products/aac-clyde-kryten-m3>

L. V. Pisacane, *The Space Environment and Its Effects on Space Systems*, 2nd Ed, AIAA, 2016.

Larson, W. J., & Wertz, J. R. (1992). *Space Mission Analysis and Design*. Torrance, Calif: Microcosm.

Markley, F.L., & Crassidis, J.L. (2014). *Fundamentals of Spacecraft Attitude Determination and Control*.



Mayer, I., Zollinger, P., Lodge-McIntire, G., Edwards, S., Levi, E., Kirejczyk, M., & LaGrasse, B. (2021). *Design and Analysis of an Interplanetary SmallSat*. Worcester Polytechnic Institute.

Metal plating on satellites: The benefits of light reflection: SPC. (2018, April 17). Retrieved October 6, 2021, from <https://www.sharrettsplating.com/blog/metal-plating-satellites-benefits-light-reflection/>

Mit.edu. Retrieved Sep 22, 2021 from: <https://ocw.mit.edu/courses/aeronautics-and-astronautics/16-851-satellite-engineering-fall-2003/lecture-notes/123thermalcontro.pdf>.

Monaghan, H. (2020, March 30). *About the Deep Space Network*. NASA. Retrieved October 16, 2021, from [https://www.nasa.gov/directorates/heo/scan/services/networks/deep\\_space\\_network/about](https://www.nasa.gov/directorates/heo/scan/services/networks/deep_space_network/about).

NASA. (2018, September 25). Radioisotope thermoelectric generators (RTGs). Retrieved October 15, 2021, from <https://solarsystem.nasa.gov/missions/cassini/radioisotope-thermoelectric-generator/>

NASA. (2020). Electromagnetic spectrum. Retrieved March 6, 2022, from <https://imagine.gsfc.nasa.gov/science/toolbox/emspectrum1.html>

NASA. (2021, August 03). In depth: Venus. Retrieved March 6, 2022, from <https://solarsystem.nasa.gov/planets/venus/in-depth/#:~:text=The%20atmosphere%20is%20mostly%20carbon,behaves%20in%20a%20corrosive%20fashion.>

NASA. (2021, December). General Environmental Verification Standard (GEVS) for GSFC Flight Programs and projects. Retrieved March 3, 2022, from <https://standards.nasa.gov/standard/gsf/gsf-std-7000>

NASA. (2021, June 01). Chemical Propulsion Systems - Glenn Research Center. Retrieved March 6, 2022,

NASA. (2022, February 10). Venus Retrieved March 6, 2022, from <https://solarsystem.nasa.gov/planets/venus/overview/#:~:text=The%20Latest&text=Venus%20has%20a%20thick%2C%20toxic,is%20closer%20to%20the%20Sun.>

Nasa.gov. Retrieved Oct 3, 2021 from <https://www.nasa.gov/SmallSat-institute/sst-soa-2020/thermal-control>

Nasa.gov. Retrieved Sep 12, 2021 from <https://www.nasa.gov/SmallSat-institute/sst-soa/thermal-control>.

Norman, K., & Leonard, K. (2000). Gas chromatography–mass spectrometry determination of ... Retrieved March 6, 2022, from <https://pubs.acs.org/doi/full/10.1021/jf991221v>

On board computer. (n.d.). Retrieved October 6, 2021, from <https://satsearch.co/products/german-orbital-systems-on-board-computer>

Rafalskyi, D., Martínez, J.M., Habl, L. *et al.* *In-orbit demonstration of an iodine electric propulsion system. Nature* 599, 411–415 (2021). <https://doi.org/10.1038/s41586-021-04015-y>

SanDisk® high endurance microsd™ card class 10, Dash Cam Memory Card. (n.d.). Retrieved October 6, 2021, from <https://www.westerndigital.com/products/memory-cards/sandisk-high-endurance-uhs-i-microsd#SDSQQR-256G-AN6IA>

Saville BP. Comfort. In: *Physical Testing of Textiles*. Elsevier; 1999. p. 209–43.\

SpaceX. (2009). Falcon 9 launch vehicle payload user's ... - spaceflight now. Retrieved March 3, 2022, from <https://spaceflightnow.com/falcon9/001/f9guide.pdf>

SpaceX. (2020, January). Rideshare Payloads User's Guide. Retrieved March 3, 2022, from <https://www.spacex.com/vehicles/falcon-9/>

SpaceX. (2021, September). User's Guide - SpaceX. Retrieved March 3, 2022, from [https://www.spacex.com/media/falcon\\_users\\_guide\\_042020.pdf](https://www.spacex.com/media/falcon_users_guide_042020.pdf)

Standard products. (n.d.). Retrieved October 15, 2021, from <https://www.ibeos.com/standard-products>

STAR T3. Retrieved October 15, 2021 from <https://space-inventor.com/star-t3/>

STK Seet Thermal Model. (n.d.). Retrieved October 6, 2021, from [https://help.agi.com/stk/11.0.1/Content/seet/Sat\\_Basic\\_Thermal.htm](https://help.agi.com/stk/11.0.1/Content/seet/Sat_Basic_Thermal.htm)

Szabo, J. (2017). Measurements of a Krypton Fed 1.5 kW ... - electricrocket.org. Retrieved March 6, 2022, from [http://electricrocket.org/IEPC/IEPC\\_2017\\_26.pdf](http://electricrocket.org/IEPC/IEPC_2017_26.pdf)

*The Online Materials Information Resource*. ASM material data sheet. (n.d.). Retrieved October 15, 2021, from <http://asm.matweb.com/search/SpecificMaterial.asp?bassnum=ma7075t6>.

Titov DV, Bullock MA, Crisp D, Renno NO, Taylor FW, Zasova LV. Radiation in the atmosphere of Venus. In: *Exploring Venus as a Terrestrial Planet*. Washington, D. C.: American Geophysical Union; 2007. p. 121–38.

Tzinis, I. (2020, March 30). *70-meter antenna*. NASA. Retrieved October 16, 2021, from [https://www.nasa.gov/directorates/heo/scan/services/networks/deep\\_space\\_network/complexes/70-meter](https://www.nasa.gov/directorates/heo/scan/services/networks/deep_space_network/complexes/70-meter).

Tzinis, I. (2020, March 30). *DSN complexes*. NASA. Retrieved October 16, 2021, from [https://www.nasa.gov/directorates/heo/scan/services/networks/deep\\_space\\_network/complexes](https://www.nasa.gov/directorates/heo/scan/services/networks/deep_space_network/complexes).

Vacuum Chamber. (n.d.). Retrieved March 3, 2022, from <https://www.sciencedirect.com/topics/chemistry/vacuum-chamber>

Van der Ha, Jozef & Stramaccioni, Daniele. (2010). Thermal Radiation Effects on Deep-Space Trajectories. *Advances in the Astronautical Sciences*. 136. 1861-1880.

Welle, R. (2007). Propellant storage considerations. Retrieved March 6, 2022, from <http://electricrocket.org/IEPC/IEPC1991-107.pdf>

Yao, P., & Sands, T. (2021). Micro Satellite Orbital Boost by Electrodynamic Tethers. *Micromachines*, 12(8), 916. MDPI AG. Retrieved from <http://dx.doi.org/10.3390/mi12080916>

## Appendix

A,

```
clc;clear all;

T = readtable('Satellite1_Solar_Panel_Power.xlsx');
time = table2array(T(:,1));
time = datetime(time,'InputFormat','ddMMyyyy HH:mm:ss.SSS');
power_gen = table2array(T(:,2));
bat = zeros(1,length(power_gen));
bat(1) = 175; %w-hr

Net_power = (power_gen - 150);
dt = 10/60;
for i = 1:length(time)

    if i == 1
        bat(1) = 175; %w-hr
    else
        bat(i) = bat(i-1)+(Net_power(i)* (dt/60));
        check(i)=(Net_power(i)* (dt/60));
    end

    if bat(i)<0
        bat(i) = 0;
    end

    if bat(i)>175
        bat(i) = 175;
    end

end

plot(time,bat)
title('Battery Capacity vs Time','interpreter','latex')
ylabel('Capacity (w-hr)','interpreter','latex')
print -depsc2 batterycharge.eps
print('-r1000','batterycharge','-djpeg')
```

